Glass Capillary X-ray Waveguides
Scott M. LaBrake
December, \thisyear

Dedication:

To my wife Sandra and my daughter Alexandra.

Acknowledgments:

First and foremost I would like to thank my beautiful wife Sandra for all of her love and support over the last eight years. I could not have completed this without you. There are not enough words to express how I feel about you. You are my best friend and the love of my life. I am so grateful to have you by my side. I love you!

To my daughter Alexandra: Daddy finished this for you! Daddy loves his Doots!

I would also like to thank my advisor Ariel Caticha for his support, guidance and patience during my years at the University at Albany. Thanks are also due to the other members of my thesis committee, John Kimball, Bill Lanford, Carolyn MacDonald, and Walter Gibson.

I am also indebted to my parents Kathleen LaBrake and Arthur LaBrake, Jr., and my in-laws Massimo and Linda Spezzaferro for all of their support and belief in me during this long process.

I would also like to acknowledge my brothers Kevin and Dennis, my sister-in-law Deanne and my nephews Brian and Michael. Thank you for your support.

To my brother-in-law John: Thank you for everything that you've done for me. May the IPA never run dry.

Thank you to my late grandfather Dominic Malivindi. Your encouragement an support meant the world to me. I wish you could have been here to see this.

Of course, I could not have done this without the support of Michelle Donegan over these many years of graduate school. Thank you so much for all you have done for me and for being here for my defense and for being such a great friend.

To Steve Amadon: Thanks for being a great friend and for the many scotch nights. Our tastes are definately improving. Some year we are going to see and get turkey during turkey season and deer during deer season.

I also owe a sincere thank you to the faculty and staff of the Union College Physics Department for their support, knowledge and patience while I finished this work. You all have been a source of inspiration for me.

Finally, thank you to the inventor of purple ink. Most of this work has been was researched and written in this color.

\maketitleabstract

INSERT ABSTRACT HERE. \clearpage (required for 1-page abstract)

\mainmatter

Introduction

What is a Waveguide?

A waveguide is a structure that is used to direct the propagation of energy in the form of an electromagnetic wave along a specified path. Typical waveguides have been developed to guide the propagation of radio waves, microwaves, visible light, and recently x rays. The simplest type of waveguide, the planar metallic

waveguide, is generally constructed from two semi-infinite planar metallic sheets separated by a vacuum gap. In the standard optical waveguide terminology, the vacuum gap is usually called the core and has an index of refraction denoted by n_{core}, and the two metallic plates comprise the cladding with index of refraction denoted by $n_{cladding}$. One could replace the metallic sheets with two dielectric plates constructed from, for example, borosilicate glass shown in figure 1.1 below. Of course other guiding structures are possible. One could use instead of the planar geometry, a cylindrical geometry in the form of a metallic rod, dielectric rod or hollow glass cylinder. The hollow glass cylinder is shown in figure 1.2 below.

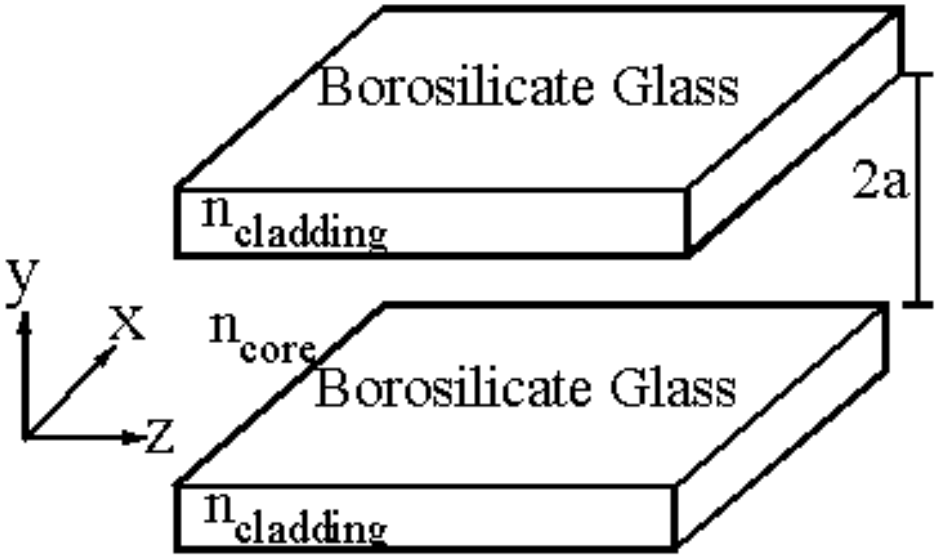

Semi-infinite planar dielectric waveguide of width *2a*, where *a* is the half-thickness of the guide, oriented in the *y*-direction. The guide is constructed of borosilicate glass with index of refraction n_{glass}. Between the glass is a vacuum with index of refraction $n_{vacuum\ channel}$.

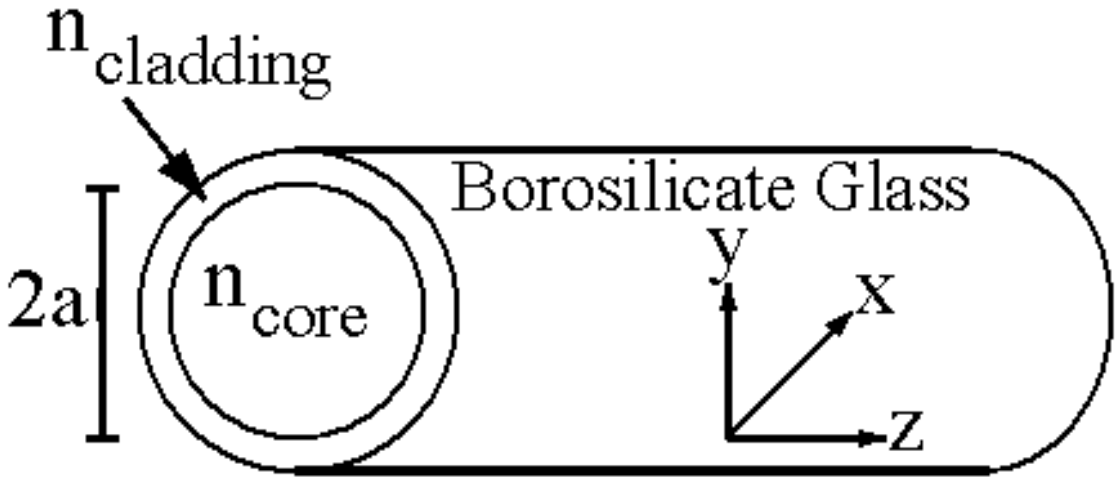

Cylindrical dielectric waveguide of internal diameter *2a*. The typical construction for an optical fiber waveguide made out of borosilicate glass has index of refraction, for the glass, $n_{cladding}$.

The operating principle of most optical waveguides is based on the idea of total internal reflection. In order for total internal reflection to occur, $n_{cladding} < n_{core}$, and the waveguide is called a step-indexed waveguide. An electromagnetic wave is guided by total internal reflection within the fiber core if its angle of incidence on the core-cladding boundary is less than the critical angle, θ_c, of the waveguide. θ_c, is defined from Snell's law and is given by

$$\theta_c = \sin^{-1}\left(\frac{n_{core}}{n_{cladding}}\right).$$

Most dielectric fibers, such as optical fibers and x-ray waveguides, are fabricated from fused silica glass (SiO_2) of a high chemical purity. Slight changes in the refractive index are achieved by adding low concentrations of doping materials such as boron [Saleh]. For an x-ray waveguide hollow glass fibers made from borosilicate glass are usually used and the operating principle behind these waveguides is total external reflection. For an x-ray to be guided by total external reflection within the fiber core, for an x-ray waveguide termed the vacuum channel, its angle of incidence on the vacuum channel-glass boundary must be less than the critical angle, θ_c, of the waveguide. The critical angle, θ_c, is defined from Snell's law and is given by equation

$$\theta_c = \sin^{-1}\left(\frac{n_{vacuum\ channel}}{n_{glass}}\right).$$

In an ideal waveguide the propagation of energy would be done with no losses to the surrounding medium, the glass capillary. Real waveguides, of course, are only approximations to the ideal.

History of the Waveguide

Probably the most widely known and used cylindrical waveguide today is the optical fiber. The development of the optical fiber spans a little more than a century. It might be said that the optical fiber is one of the important technological advances of the twentieth century.

Waveguides were first studied at the turn of the twentieth century by Lord Rayleigh [Rayleigh] Thomson [Thomson], and Sommerfeld [Saleh]. They studied guided electromagnetic waves within perfectly conducting cylinders. The first theoretical description of mode propagation along a dielectric waveguide was apparently that of Hadros and Debye [Hadros and Debye] in 1910. In 1936, Southworth [Southworth] discovered the transmission of radio waves in hollow conducting waveguides. His report was accompanied by an article detailing the mathematical theory of waveguides by Carson, Mead, and Schelkunoff [Carson]. This eventually paved the way for dielectric rods as waveguides for microwaves, utilized by Chandler and Elsasse [Chandler].

The first dielectric waveguide studied at optical frequencies were glass coated fibers packed into assemblies

each a few microns in diameter with the adjacent fibers less than one micron apart [Kapany and Burke]. The glass fibers rely, as before, on total internal reflection of the light inside of the core of the fiber. In 1961, Snitzer investigated the types of modes carried on a cylindrical dielectric waveguide. It was found that one could limit the number of modes which are supported by a guide by using a step-indexed fiber, where the

fractional refractive index change Δ defined by the relation

$$\Delta = \frac{n_{core} - n_{cladding}}{n_{core}} \ll 1$$

is small. In 1971, Gloge [Gloge] tried to simplify the theory of the cylindrical dielectric waveguide in the limit of optical frequencies. For a comprehensive treatment of optical fibers the reader is referred to the excellent book by Marcuse [Marcuse].
Soon after researchers began to comment on the possibility of using waveguides to guide x rays. The dimensions of the waveguide would need to be very small and the most common configuration for these x-ray waveguides is the planar thin-film waveguide. These attempts have met with varying amounts of success.

Capillary Optics

The field of capillary optics uses glass capillary tubes to take advantage an x-ray having an index of refraction less than unity in glass. The small difference between the indices of refraction produces a step-indexed fiber and ensures total external reflection at the vacuum channel-glass interface. These bundles of capillary tubes are typically 0.5 millimeters in diameter and 120 millimeters in length. Each single capillary channel is approximately 5-50 microns in diameter and is constructed of mainly borosilicate glass, which is a high purity silica glass that has been doped with boron. The critical angle for total external reflection from borosilicate glass is on the order of a few milliradians. These x-ray optics, as they are now called, were first suggested by Kumakhov [Kumakhov] as a means of controlling the size and shape of an x-ray beam and are being studied for a wide variety of applications, including x-ray lens systems for use in x-ray astronomy, the production of collimated x-ray sources for materials analysis, and in industrial and medical radiography. Studies and analysis of polycapillary optics have be performed for hard x-rays (see for example the paper by Lei Wang, *et al* [Wang]) whose energies are in the range of 10 to 80 keV. Extensive experimental studies of the effects of roughness of the glass surface as well as some curvature (or bending) of the waveguide have been carried out. The experimental results were used to assign values to the various parameters involving the roughness and curvature of the waveguide model. A theoretical roughness model was proposed by Kimball and Bittel [Kimball and Bittel], based on the work of Vinogradov, *et al* [Vinogradov] , was used to determine whether the effects of surface roughness was causing lower transmission rates at higher energies. It was found that the roughness was not the cause, but rather waviness of the surface on much larger scales was at least partially to blame.
These present studies, however, do not include waveguide effects, such as diffraction. The computer simulations in use at the present time are based on "geometrical optical (ray tracing) methods." Since the diameter of the capillary is much larger than the wavelength of the x rays being used, geometric optics proves quite accurate. Older experiments involving capillary optics use incoherent incident beams with large angular spreads. In such cases, calculations that involve geometrical optics give results that are essentially identical to those found with wave methods. As the waveguide diameter shrinks and with future experiments utilizing second and third generation x-ray sources, waveguide effects may become observable and useful.

The highly collimated x-ray sources and the small fiber size may allow one the opportunity to view some interesting waveguide effects such as diffraction.

The incident wave has associated with it a wave vector, $\vec{k}$, where $\left|\vec{k}\right| = \frac{2\pi}{\lambda}$. λ is the wavelength of the incident wave and the direction of wave propagation defines the direction of $\vec{k}$. If the incident wave makes an angle θ with respect to the symmetry axis of the waveguide, one can imagine the wavelength to have longitudinal and transverse "components", where the transverse component $\lambda_t = \frac{\lambda}{\sin\theta}$. As the angle that the incident beam makes with respect to the symmetry axis of the waveguide becomes shallower, the transverse "component" of the wavelength would become larger. Even though the wavelength of the wave may be much smaller than the dimensions of the waveguide, the transverse "components" of the wavelength may become comparable to the dimensions of the waveguide and wave effects such as diffraction may become evident.

X-ray Waveguides

There are groups working on the design and implementation of x-ray waveguides. Most of the work in the last ten to fifteen years has been in the study of primarily planar metallic and dielectric waveguides. In the late 1980's and early 1990's, Feng, Sinha, *et al* [Feng and Sinha] - [Feng and Fullerton] have developed planar waveguides made out of SiO_2/polyimide/Si. Their method was to start with an optically flat silicon wafer, deposit a roughly 1230Å polyimide film on the top of the silicon wafer,and then evaporate a roughly 380Å thick layer of SiO_2 on the top of the polyimide film. Feng, Sinha, *et al* were able to obtain an increase in the photon flux at certain energies by a factor of 20. They also determined the probability of mode mixing, which they attributed to rough surface scattering. In addition, they studied the Fraunhoffer diffraction pattern for individually excited modes that exited the waveguide along a cleaved crystallographic axis of the silicon. They found that the angular divergence of the beam was on the order of 10 μrad and that the modes were separated by roughly 60 μrad allowing for single mode excitation.

There have been many modifications on this basic approach. Zheludeva, Kovalchuk, *et al* [Zheludeva] investigated planar waveguides constructed out of mainly alternating carbon and nickel layers and glass using the carbon as a guiding layer because of its low absorption coefficient. Zheludeva, *et al* used ultra-thin metal layers to measure the excitation of different waveguide modes as a function of the angle of incidence of the x-ray beam. Jark, Di Fonzo, *et al* [Jark], [Jark1], used a similar structure of alternating nickel and carbon layers and SiO_2. Jark, *et al* used an incident beam with an angular divergence approximately 8 μrad and produced a 13 keV exit beam with one dimension as small as 0.137 microns. There are problems associated with these waveguides. While carbon (or any organic material) may have a low absorption coefficient, the absorption coefficients are not low enough to prevent large losses in x-ray intensity. These waveguides are on the order of 1 cm long; for many practical applications, the waveguides would need to be longer.

Liu and Golovchenko [Golovchenko], [Golovchenko1] have been studying x-ray waveguides of another variety, namely x rays that undergo repeated reflections from a single curved surface. These are called whispering galley modes and were first investigated for acoustic waves by Lord Rayleigh [Rayleigh1] more

than a century ago. Whispering-galley optics relies on the ability of a concave surface (a mirror) to act as a waveguide. In essence the x rays undergo many small grazing incidence reflections but the net result is to deflect the x-ray beam through a large total angle. Liu and Golovchenko using an incident beam (with angular divergence of about 16 μrad) were able to measure the transmittance as a function of curvature. Here they have the fundamental mode being detectable over the length of the waveguide and the higher order modes are attenuated by tunneling of the mode into the mirror. This type of arrangement has been suggested for the construction of resonant cavities for x rays [Braud] - [Vinogradov1].
The theory for scalar waves was studied in the thesis of Barcomb [Barcomb]. In his doctoral thesis Barcomb showed that he could use the approximation that the x rays could be treated as scalar waves, since the susceptibility for x rays incident in borosilicate glass was small ($\chi_0 \sim 10^{-5}$). He found that absorption effects are nearly nonexistent since the x-ray modes penetrate very little into the glass and thus propagate distances of tens of kilometers. Barcomb also studied the excitation of various modes as a function of incident angle of an externally directed plane wave. He found that for plane waves incident with energy 8 keV on a planar waveguide (with a gap of 10 microns) as much as 80% of the incident energy appears as the fundamental mode, while for a cylindrical waveguide (with diameter 10 microns) the excitation was on the order of 70%. Thus a single mode fiber can be studied provided a sufficiently collimated incident x-ray beam can be used.

Outline

In this thesis, the vector nature of x rays is incorporated into a waveguide model. The goal of this work is to provide a theoretical description for the propagation of x rays along a glass capillary waveguide. The objectives are four-fold:

- to understand the individual modes, how modes are excited at the waveguide entrance, and how modes emerge at the waveguide exit,
- to understand the distribution of fields and polarizations of the various modes,
- to understand the effects of photoelectric absorption and surface roughness on the propagation of the x rays in the waveguide,
- to understand whether it is possible and how to accomplish selective excitation of individual modes.

To accomplish the above objectives, a detailed description for the launching of the various modes that the waveguide can support will be given. Chapter 2 gives the background on the interaction of x rays and matter, the laws of reflection and refraction and the Fresnel equations.
In chapter 3 the modes of the electromagnetic field that are sustained within a straight cylindrical dielectric x-ray waveguide are investigated. Maxwell's equations are the basis for calculation of the electric and magnetic fields that constitute the transverse distributions, or modes, in the guiding region of the waveguide. These modes are the eigenfunctions of the waveguide, and the corresponding eigenvalues could be characterized by the propagation constant in the z-direction, the longitudinal component of the incident wave vector, k_z. Exploiting the cylindrical geometry, the hollow glass capillary will be shown to support many circular hybrid modes of propagation for the x rays. Modes in metallic microwave guides are transverse magnetic or transverse electric, but in dielectric waveguides this is not the case. In a dielectric

waveguide the modes are hybrid in the sense of resembling superpositions of transverse magnetic and transverse magnetic modes. These hybrid circular modes will be combined to form a new set of linearly polarized modes. These linearly polarized modes will be studied in great detail, including the study of such effects as energy loss mechanisms due to photoelectric absorption and due to surface roughness on the propagation of the x-ray down the waveguide.
Chapter 4 explores excitation at the waveguide entrance. Here an externally directed plane-polarized wave will be used to excite a set of linearly polarized modes that propagate down the longitudinal axis of the waveguide. One will see that it is very possible to launch a single mode in the waveguide. This same approach could be used for other types of incident waves, namely a circularly polarized mode incident at the waveguide entrance.
In chapter 5 how the x rays exit the waveguide will be studied. The problem is similar to the Fraunhofer diffraction by a circular aperture, except that instead of an incident plane or spherical wave the incident fields are the linearly polarized modes propagating along the waveguide. The standard calculation of the vector diffracted fields is based on the vector analogue of the Kirchhoff diffraction formula and is very difficult to apply except in all but the simplest geometries. The interested reader may wish to consult, for example Jackson[Jackson] and Born and Wolf[Born and Wolf], for the standard way of calculating these vector diffracted fields. This difficulty has inspired one to seek an alternative approach to diffraction. In this chapter, a new approach to vector diffraction theory is proposed. It is inspired by an asymptotic form of the reciprocity theorem (ART) that has been found useful in a variety of other x-ray emission, diffraction and scattering problems ([Caticha].)
In chapter 6 the effects of surface roughness on the propagation of modes is studied. Since the effect of roughness is to scatter x rays away from the guided modes, it is a loss mechanism. A simple way to take this loss into account is by including it, just as other loss mechanisms such as photoelectric absorption, into an effective imaginary part for the dielectric susceptibility. The resulting model is compared to and shown to agree with the results of Kimball and Bittel [Kimball and Bittel].
Chapter 7 includes some concluding remarks on this thesis, as well as some ideas for future directions of research for glass capillary x-ray waveguides. Some future directions will include studies involving curving and/or tapering of the waveguide as well as the possibility of a non-diffracting Bessel beam.

The Reflection of X rays

Introduction

In this chapter the interactions of x rays and matter will be investigated. It will be shown how the dielectric susceptibility for borosilicate glass is calculated on the basis of fractional atomic weights of the constituent elements that make up the glass fiber. The phenomena of total internal and total external reflection will be explained. The idea of Transverse Electric and Transverse Magnetic Modes of a waveguide will be briefly introduced.

Susceptibility for X rays

The wave properties of all electromagnetic phenomena are obtained from Maxwell's equations:

$$\vec{\nabla} \cdot \vec{B}(\vec{r},t) = 0$$

$$\vec{\nabla} \cdot \vec{D}(\vec{r},t) = 4\pi\rho$$

$$\vec{\nabla} \times \vec{E}(\vec{r},t) + \frac{1}{c}\frac{\partial \vec{B}(\vec{r},t)}{\partial t} = 0$$

$$\vec{\nabla} \times \vec{H}(\vec{r},t) - \frac{1}{c}\frac{\partial \vec{D}(\vec{r},t)}{\partial t} = \frac{4\pi}{c}\vec{J}(\vec{r},t)$$

The waveguide will be made out of low atomic density borosilicate glass, which is assumed to be source free ($\rho = 0$ and $J(\vec{r},t) = 0$) and non-magnetic ($\mu = 1$). Since the borosilicate glass is source free one can write:

$$\vec{D}(\vec{r},t) = \varepsilon\vec{E}(\vec{r},t)$$

$$\vec{H}(\vec{r},t) = \frac{1}{\mu}\vec{B}(\vec{r},t) = \vec{B}(\vec{r},t),$$

where ε is the dielectric constant and may be written in terms of the susceptibility of the material, χ_0 as follows:

$$\varepsilon = 1 + \chi_0.$$

Assuming electric and magnetic fields are monochromatic waves of frequency ω, they can be expressed in the following form:

$$\vec{E}(\vec{r},t) = \vec{E}(\vec{r})e^{-i\omega t}$$

$$\vec{B}(\vec{r},t) = \vec{B}(\vec{r})e^{-i\omega t}$$

where r is a position vector. Maxwell's equations thus become:

$$\vec{\nabla} \cdot \vec{B}(\vec{r}) = 0$$

$$\vec{\nabla} \cdot \vec{E}(\vec{r}) = 0$$

$$\vec{\nabla} \times \vec{E}(\vec{r}) - \frac{i\omega}{c}\vec{B}(\vec{r}) = 0$$

$$\vec{\nabla} \times \vec{B}(\vec{r}) + \frac{i\varepsilon\omega}{c}\vec{E}(\vec{r}) = 0$$

Wave equations on $\vec{E}(\vec{r})$ and $\vec{B}(\vec{r})$ can be found by taking the curl of equation . With the help of equation one finds:

$$\nabla^2\vec{E}(\vec{r}) + \frac{i\omega}{c}\vec{\nabla} \times \vec{B}(\vec{r}) = 0$$

where the vector identity

$$\vec{\nabla} \times (\vec{\nabla} \times \vec{A}) = \vec{\nabla}(\vec{\nabla} \cdot \vec{A}) - \nabla^2\vec{A}$$

has been used. An analogous expression for the magnetic field is obtained by taking the curl of equation with the help of equation .

$$\nabla^2\vec{B}(\vec{r}) - \frac{i\varepsilon\omega}{c}\vec{\nabla} \times \vec{E}(\vec{r}) = 0$$

The operator ∇^2 in equations and is defined in the usual way. Substituting equation into equation for $\vec{\nabla} \times \vec{E}(\vec{r})$ produces a wave equation governing $\vec{B}(\vec{r})$ namely

$$\nabla^2\vec{B}(\vec{r}) + \varepsilon k^2\vec{B}(\vec{r}) = 0$$

In an analogous manner, substitution of equation in to equation for $\vec{\nabla} \times \vec{B}(\vec{r})$ yields a wave equation governing $\vec{E}(\vec{r})$.

$$\nabla^2 E(\vec{r}) + \varepsilon k^2 E(\vec{r}) = 0$$

For x rays (as well as any electromagnetic radiation), the wave number $k_0 = \frac{\omega}{c}$ is the magnitude of the wave vector in vacuum. In the borosilicate glass, the wave vector can be related to the wave vector in vacuum through:

$$\vec{k} = n_i\vec{k}_0$$

where n_i is the index of refraction of the medium (in this case the borosilicate glass) through which the x rays travel. When the frequency of an electromagnetic wave is much higher than the highest resonant frequency of a given material, as is the case for an x-ray, the dielectric constant ε of the material becomes easy to calculate. From Jackson [Jackson] :

$$\varepsilon \approx 1 - \frac{(\hbar\omega_p)^2}{(\hbar\omega)^2}$$

ω is the wave frequency and ω_p is the plasma frequency, given by:

$$\omega_p^2 = \frac{4\pi NZe^2}{m}$$

and NZ is the electron density of the material. Combining equations , , and , one finds that the susceptibility may be written as

$$\chi_0 \approx -\frac{(\hbar\omega_p)^2}{(\hbar\omega)^2} \approx -\frac{\hbar^2 4\pi NZe^2}{m(\hbar\omega)^2}$$

The susceptibility is thus proportional to the electron density of the material, where the electron density may be found by taking the weighted average over all of the constituent molecules of the borosilicate glass. This produces susceptibilities that are negative and generally on the order of 10^{-4} to 10^{-6}. To calculate the approximate susceptibility for borosilicate glass, commonly known as Pyrex, consider the weight fractions of the various components as shown in table 2.1 above.

Component	Weight Fraction
Boron	0.040066
Oxygen	0.539559
Sodium	0.028191
Aluminum	0.011644
Silicon	0.377220
Potassium	0.003321

\caption{Weight fracitons by constituent elements for borosilicate glass.\label{key} } The density of borosilicate glass is $2.23\frac{g}{cm^3}$ so that $\hbar\omega_p = 35.1$ eV. For Cu K_α x rays, $\hbar\omega = 8.04$ keV; the susceptibility of the Cu K_α x rays in borosilicate glass, is calculated to be $\chi = -1.9 \times 10^{-5}$. Therefore, one can see that the dielectric constant very nearly equals unity.

Reflectivity and Polarization

When an electromagnetic wave travels through vacuum, nothing much spectacular happens. However, when that same electromagnetic wave travels through matter, it may interact with the material through which it is propagating. Consider an electromagnetic wave that travels from one non-magnetic dielectric region, with dielectric constant ε_1 and permittivity $\mu_1 = 1$, to another non-magnetic dielectric region, with dielectric constant ε_2 and permittivity $\mu_2 = 1$, as shown in figure 2.1 below. In material one the electromagnetic wave has wave vector k_1 and in material two, the electromagnetic wave has wave vector k_2. At the boundary between the two dielectric materials, part of the wave is reflected and part of the wave propagates into the second dielectric material, but with a different wave vector, due to the change in dielectric constants of the material. One uses Maxwell's equations to determine the relative amounts of the electromagnetic wave that are reflected and refracted at the interface. As seen in figure 2.1 below, wave vector k_{inc} has magnitude

$\frac{\omega}{c}\sqrt{\varepsilon_1}$ and makes and angle θ_1 with respect to the normal to the interface. The incident electric field is given as:

$$\vec{E}_{\text{inc}}(\vec{r},t) = \vec{E}_{\text{inc}} e^{i\left(\vec{k}_{\text{inc}}\cdot\vec{r}-\omega t\right)}$$

The second wave is the refracted wave, traveling in the second non-magnetic dielectric material. Wave vector k_{ref} has magnitude $\frac{\omega}{c}\sqrt{\varepsilon_2}$ and makes and angle θ_2 with respect to the normal to the interface. The refracted electric field is given as:

$$\vec{E}_{\text{ref}}(\vec{r},t) = \vec{E}_{\text{ref}} e^{i\left(\vec{k}_{\text{ref}}\cdot\vec{r}-\omega t\right)}$$

The third wave is the reflected wave, traveling in the original non-magnetic dielectric material. Wave vector k_{refl} has magnitude $\frac{\omega}{c}\sqrt{\varepsilon_1}$ and makes and angle θ_3 with respect to the normal to the interface. The reflected electric field is given as:

$$\vec{E}_{\text{refl}}(\vec{r},t) = \vec{E}_{\text{refl}} e^{i\left(\vec{k}_{\text{refl}}\cdot\vec{r}-\omega t\right)}$$

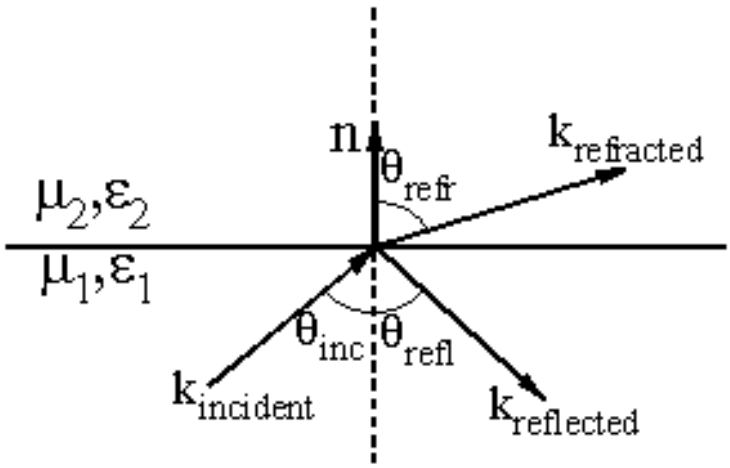

Diagram showing the boundary between two dielectric media, with indicies of refraction $n_1 = \sqrt{\varepsilon_1}$ and $n_2 = \sqrt{\varepsilon_2}$ respectively. Wave vector k_{inc} is incident on the boundary of medium 2 from medium 1. The reflected and refracted wave vectors, k_{refl} and k_{ref} are also shown.

The associated magnetic fields may be found using:

$$\vec{B}_i(\vec{r},t) = \sqrt{\varepsilon_i}\,\frac{\vec{k}_i \times \vec{E}_i(\vec{r},t)}{k_i}$$

where i =(inc, ref,refl), and $j = 1,2$. Suppose that the normal to the interface is the $y-$direction and let the $y-$coordinate of the interface be located at $y = 0$. Since the boundary conditions have to be satisfied at all points on the interface and for all times, the phases of the waves must be equal at all points on the interface where the waves meet. Thus at $y = 0$:

$$\vec{k}_{\text{inc}} \cdot \vec{r} = \vec{k}_{\text{ref}} \cdot \vec{r} = \vec{k}_{\text{refl}} \cdot \vec{r}$$

Therefore these three wave vectors must be coplanar, or their respective dot products would never be equal. From equation and figure 2.1, one finds that

$$k_{\text{inc}} \sin\theta_1 = k_{\text{ref}} \sin\theta_2 = k_{\text{refl}} \sin\theta_3$$

Since the incident wave is partially reflected at the interface,

$$k_{\text{inc}} = k_{\text{refl}}.$$

and therefore it follows that

$$\sin\theta_1 = \sin\theta_3.$$

This result is called the law of reflection, and states that the angle of incidence equals the angle of reflection. Further, from equation ,

$$k_{\text{inc}} \sin\theta_1 = k_{\text{ref}} \sin\theta_2$$

or

$$n_1 \sin\theta_1 = n_2 \sin\theta_2$$

which is called Snell's law. The index of refraction, n_i is related to the dielectric constant of the material through:

$$n_i = \sqrt{\varepsilon_i}$$

Next, as a consequence of Snell's law, there is an angle, θ_c, called the critical angle such that:

$$\sin\theta_c = \frac{n_2}{n_1}$$

In terms of the susceptibility of the material,

for $\chi_0 \ll 1$. Since χ is negative, $n_1 > n_2$. This condition is satisfied for this step-indexed fiber, so equation is precisely the case for total internal reflection.

In order to determine that relative amplitudes of the refracted and reflected waves, $\vec{E}_{\text{refracted}}$ and $\vec{E}_{\text{reflected}}$

respectively, boundary conditions must be imposed on $\vec{E}(\vec{r},t)$ and $\vec{B}(\vec{r},t)$. The boundary conditions are continuity of the normal components of $\vec{D}(\vec{r},t)\left(=\varepsilon\vec{E}(\vec{r},t)\right)$ and $\vec{B}(\vec{r},t)$, and the tangential components of $\vec{E}(\vec{r},t)$ and $\vec{H}(\vec{r},t)\left(=\vec{B}(\vec{r},t)\right)$. These boundary conditions are most easily handled by considering two separate polarizations of the wave, one parallel to the plane of incidence and one perpendicular to the plane of incidence (the plane that contains k_{inc}, k_{ref}, and k_{refl}.) The plane of polarization, by convention , is taken to be defined by the incident electric field vector. The orthogonal polarization, or perpendicular polarization, is termed the Transverse Electric (TE) polarization. [Saleh] Conversely, the parallel polarization is termed the Transverse Magnetic (TM) polarization, since the magnetic field is orthogonal to the plane of incidence, while the electric field is parallel to the plane of incidence. The results of applying the boundary conditions in these two cases are:For $\vec{E}_{\text{inc}}(\vec{r},t)$ parallel to the plane of incidence (TM polarization):

$$\frac{E_{\text{ref}}}{E_{\text{inc}}} = \frac{2\sqrt{\varepsilon_1\varepsilon_2}\cos(\theta_1)}{\varepsilon_2\cos(\theta_1)+\sqrt{\varepsilon_1}\sqrt{\varepsilon_2-\varepsilon_1\sin^2(\theta_1)}}$$

and

$$\frac{E_{\text{refl}}}{E_{\text{inc}}} = \frac{\varepsilon_2\cos(\theta_1)-\sqrt{\varepsilon_1}\sqrt{\varepsilon_2-\varepsilon_1\sin^2(\theta_1)}}{\varepsilon_2\cos(\theta_1)+\sqrt{\varepsilon_1}\sqrt{\varepsilon_2-\varepsilon_1\sin^2(\theta_1)}}$$

For $\vec{E}_{\text{inc}}(\vec{r},t)$ perpendicular to the plane of incidence (TE) polarization:

$$\frac{E_{\text{ref}}}{E_{\text{inc}}} = \frac{2\sqrt{\varepsilon_1}\cos(\theta_1)}{\varepsilon_1\cos(\theta_1)+\sqrt{\varepsilon_2-\varepsilon_1\sin^2(\theta_1)}}$$

and

$$\frac{E_{\text{refl}}}{E_{\text{inc}}} = \frac{\sqrt{\varepsilon_1}\cos(\theta_1)-\sqrt{\varepsilon_2-\varepsilon_1\sin^2(\theta_1)}}{\varepsilon_2\cos(\theta_1)+\sqrt{\varepsilon_1}\sqrt{\varepsilon_2-\varepsilon_1\sin^2(\theta_1)}}$$

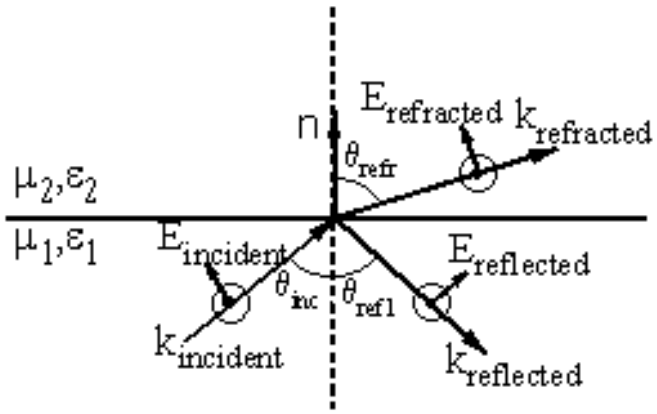

Diagram showing the incident electric field, $\vec{E}_{\text{incident}}$, parallel to the incident wave vector k_{incident}. The reflected and refracted electric fields, $\vec{E}_{\text{reflected}}$ and $\vec{E}_{\text{refracted}}$, are shown after interaction with the dielectric interface. The associated magnetic fields, directed out of the page, are also shown.

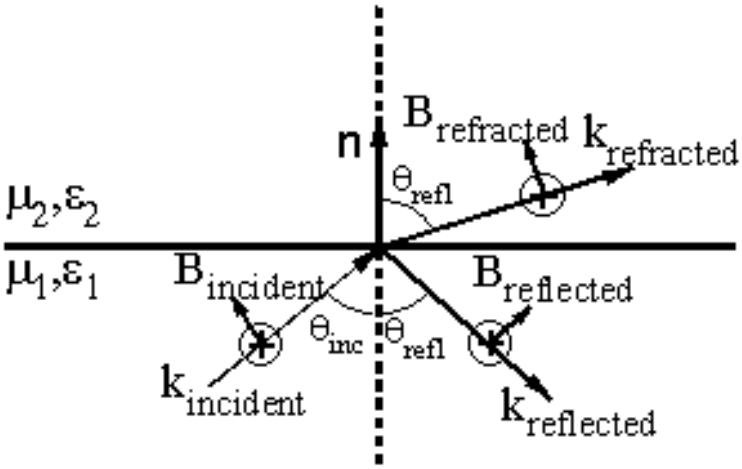

Diagram showing the incident magnetic field, $\vec{B}_{\text{incident}}$, perpendicular to the incident wave vector k_{incident}. The reflected and refracted electric fields, $\vec{B}_{\text{reflected}}$ and $\vec{B}_{\text{refracted}}$, are shown after interaction with the dielectric interface. The associated electric fields, directed into the page, are also shown.

For x rays in vacuum, $(\varepsilon_1 = 1)$ incident on the borosilicate glass surface $(\varepsilon_2 = 1 + \chi)$, where the susceptibility, χ, is negative. Since χ is small $\left(\sim 10^{-5}\right)$ total external reflection will only occur for grazing incidence; that is, for angles of incidence near $\frac{\pi}{2}$. Thus, equation can alternately be expressed in an

equivalent form:

$$n_1 \cos\theta_1' = n_2 \cos\theta_2'$$

where θ_1' and θ_2' refer to the angles that the incident and refracted rays make with the interface. The critical angle for total external reflection is then given by:

$$\cos\theta_c' = \frac{n_2}{n_1}.$$

In terms of the susceptibility, the critical angle is thus:

$$\cos\theta_c' = \frac{\sqrt{\varepsilon_1}}{\sqrt{\varepsilon_2}} = \frac{\sqrt{1+\chi_0}}{\sqrt{1}}.$$

Which for $\chi_0 \ll 1$, can be approximated as:

$$\cos\theta_c' \approx 1 + \frac{\chi_0}{2}.$$

The cosine term on the left hand side of equation can be expanded in a power series.

$$\cos\theta_c' = 1 - \frac{\theta_c'^2}{2} + \ldots$$

Which for grazing angles of incidence may be approximated as:

$$\cos\theta_c' \approx 1 - \frac{\theta_c'^2}{2}.$$

Comparing equations and , one finds that the critical angle for total external reflection in terms of the x-ray susceptibility of borosilicate glass.

$$\theta_c' \approx \sqrt{-\chi_0} \approx 4.4 \text{ mrad}$$

where χ_0 found for Cu K_α x rays incident in borosilicate glass has been used. Returning to equations for TE polarization,

$$\frac{E_{\text{refl}}}{E_{\text{inc}}} = \frac{\cos\theta_1 - \sqrt{1+\chi_0-\sin^2\theta_1}}{\cos\theta_1 + \sqrt{1+\chi_0-\sin^2\theta_1}}$$

and to equation for TM polarization,

$$\frac{E_{\text{refl}}}{E_{\text{inc}}} = \frac{(1+\chi_0)\cos\theta_1 - \sqrt{1+\chi_0-\sin^2\theta_1}}{(1+\chi_0)\cos\theta_1 + \sqrt{1+\chi_0-\sin^2\theta_1}}$$

Equations and are known as the Fresnel equations. For χ_0 equal to zero, there is no difference in the reflected amplitudes for the two polarizations. However, for χ_0 small but different from zero, there is a

small difference between the reflected amplitudes.

Propagation of X rays in Cylindrical Waveguides

Introduction

Our study will be focused on three main areas. First, the waveguide modes will be derived and the manner in which these modes propagate along the longitudinal axis of the guide will be shown. The transverse electric and magnetic fields will be expressed in terms of the longitudinal electric and magnetic fields. Wave equations for the longitudinal electric and magnetic fields will be derived and solved by the technique of separation of variables. Next boundary conditions on the wave equation solutions will be imposed and the characteristic equation for the modes will be derived. It will be found for cylindrical waveguides that the modes have a radial dependence given by a Bessel function and an azimuthal dependence given by $e^{im\varphi}$, where m is the order number of the mode. For lowest order modes, the $m = 0$ case, the modes will be found to resemble the so called *TE* (transverse electric) and *TM* (transverse magnetic) modes in the limit of small angles of incidence and χ_o much smaller than unity. The higher order modes ($m \neq 0$) will be termed hybrid and be denoted by either *EH* (electric magnetic) or *HE* (magnetic electric) modes. Here it should be noted that the results obtained from the cylindrical model of the dielectric waveguide will mirror those of Gloge[Gloge] and Marcuse[Marcuse]. Marcuse and Gloge were primarily concerned with optical and microwave fibers. In dealing with x-ray guides, considerable simplifications will arise because all indices of refraction are close to unity.

The second problem to be tackled is the transformation of the hybrid circularly polarized modes. These circularly polarized hybrid *EH* and *HE* modes will be superposed to form a set of linearly polarized or *LP* modes.

Third, photoelectric absorption of the x rays by the waveguide will be studied. Losses due to photoelectric absorption will be calculated using the imaginary part of the dielectric susceptibility. The imaginary part of the wave vector will then be calculated and subsequently be used to calculate the $\frac{1}{e}$ decay lengths for the x-rays as they travel down the fiber. It will be found that the lowest order modes (the $LP_{0,p}$) propagate on the order of 10 kilometers for higher energy x-rays, while for lower energy x rays, the modes will propagate hundreds of meters. This applies to guides with perfectly smooth walls. Surface roughness has an important contribution to loss in the waveguide. Surface roughness will be studied in chapter 6.

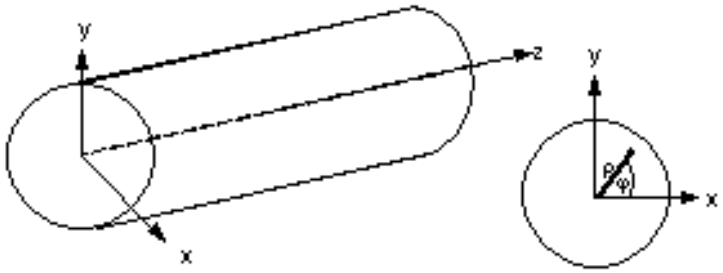

Cylindrical dielectric waveguide with diameter *2a*. The waveguide is constructed out of borosilicate glass where the axis of the guide is usually taken as the z-axis, or the longitudinal axis. In a cylindrically symmetric coordinate system, the radial direction, ρ, has its origin on the z-axis and extends outward from the center of the guide to the glass that forms the boundary of the waveguide, and the angular direction, φ, wraps around the z-axis.

A cylindrical dielectric waveguide is constructed of non-magnetic material, usually borosilicate glass. The waveguide has a hollow vacuum channel on the order of 5 microns in diameter, and the glass capillary extends radially to infinity. The axis of the guide is usually taken as the z-axis, or the longitudinal axis, and has a finite length on the order of say 10 centimeters. In a cylindrically symmetric coordinate system, the radial direction has its origin on the z-axis and extends outward from the core to the glass that forms the boundary of the waveguide, and the angular direction wraps around the z-axis. The various directions may be seen in figure 3.1 below.

Derivation of the Waveguide Modes

The starting point in the analysis of the modes contained in any arbitrary electromagnetic guiding structure for example, a cylindrical dielectric x-ray waveguide, are Maxwell's equations given by equations through :

Assuming that the material composition of the waveguide will be such that it is both source free ($\rho = 0$ and $J(\vec{r},t) = 0$) and non-magnetic ($\mu = 1$). Thus $\vec{D}(\vec{r},t)$ and $\vec{H}(\vec{r},t)$ assume particularly simple expressions, namely

$$\vec{D}(\vec{r},t) = \varepsilon\vec{E}(\vec{r},t) \qquad \text{and} \qquad \vec{H}(\vec{r},t) = \frac{1}{\mu}\vec{B}(\vec{r},t) = \vec{B}(\vec{r},t)$$

where the ε is the dielectric constant and may be written in the form

$$\varepsilon = 1 + \chi_0$$

where χ_o is the susceptibility of the material. Let:

$$\vec{E}(\vec{r},t) = \vec{E}(\rho,\varphi,z)e^{-i\omega t} = (E_\rho\hat{\rho} + E_\varphi\hat{\varphi} + E_z\hat{z})e^{-i\omega t}$$

$$\vec{B}(\vec{r},t) = \vec{B}(\rho,\varphi,z)e^{-i\omega t} = (B_\rho\hat{\rho} + B_\varphi\hat{\varphi} + B_z\hat{z})e^{-i\omega t}.$$

Maxwell's equations thus become after cancelling the common $e^{-i\omega t}$ term:

$$\vec{\nabla} \cdot \vec{B}(\rho,\varphi,z) = 0$$

$$\vec{\nabla} \cdot \vec{E}(\rho,\varphi,z) = 0$$

$$\vec{\nabla} \times \vec{E}(\rho,\varphi,z) - \frac{i\omega}{c}\vec{B}(\rho,\varphi,z) = 0$$

$$\vec{\nabla} \times \vec{B}(\rho,\varphi,z) + \frac{i\omega\varepsilon}{c}\vec{E}(\rho,\varphi,z) = 0,$$

The z-dependence of the E and B fields

The next step is to derive a wave equation that governs the electric and magnetic fields in equations and . This will be done in several steps. The first one will be to use the technique of separation of variables to

determine the form of the z-dependence of the electric and magnetic fields. Then the transverse components of the electric (magnetic) field will be expressed in terms of the longitudinal component of the electric (magnetic) field. Lastly a wave equation on the longitudinal electric (magnetic) field will be developed and continuing to use the separation of variables technique, solved for the final form of the longitudinal electric (magnetic) field. To search for solutions to equations through start by assuming that the electric and

magnetic fields are separable and for brevity the electric field has the form: $\vec{E}(\rho,\varphi,z) = \vec{E}(\rho,\varphi)Z(z)$. Taking the curl of equation and using equations and produces

$$\left(\frac{\partial^2}{\partial\rho^2} + \frac{1}{\rho}\frac{\partial}{\partial\rho} + \frac{1}{\rho^2}\frac{\partial^2}{\partial\varphi^2} + \frac{\partial^2}{\partial z^2} + \frac{\omega^2\varepsilon}{c^2}\right)\vec{E}(\rho,\varphi,z) = 0$$

Substituting the form of $\vec{E}$ into equation produces after some algebra

$$\left(\frac{1}{\rho^2}\frac{\partial^2}{\partial\rho^2} + \frac{1}{\rho}\frac{\partial}{\partial\rho} + \frac{1}{\rho^2}\frac{\partial^2}{\partial\varphi^2}\right)\frac{\vec{E}(\rho,\varphi)}{E(\rho,\varphi)} = -\frac{1}{Z}\frac{\partial^2 Z}{\partial z^2} - k^2\varepsilon$$

where $\frac{\omega}{c} = k$ has been used. Noticing that the right hand side of equation is a constant independent of ρ

and φ, the left hand side must also be a constant. Therefore, the z-dependence of the electric and magnetic fields, is found to be

$$Z(z) = e^{ik_z z}.$$

Thus the electric and magnetic fields look like after inserting the z-dependence

$$\vec{E}(\rho,\varphi,z,t) = \vec{E}(\rho,\varphi)e^{i(k_z z-\omega t)}$$

$$\vec{B}(\rho,\varphi,z,t) = \vec{B}(\rho,\varphi)e^{i(k_z z-\omega t)}.$$

The Wave Equations for E_z and B_z

Again, to derive wave equations that govern the longitudinal electric and magnetic fields, one must write the transverse fields in terms of the longitudinal fields. It will be easily shown from Maxwell's equations that the transverse electric fields may be expressed in terms of the longitudinal electric field. Analogously, expressions for the transverse magnetic fields will be shown to depend only on the longitudinal magnetic field. Maxwell's curl equations and become in component form:For the ρ-direction:

$$\frac{1}{\rho}\frac{\partial E_z}{\partial \varphi} - ik_z E_\varphi - \frac{i\omega}{c}B_\rho = 0$$

$$\frac{1}{\rho}\frac{\partial B_z}{\partial \varphi} - ik_z B_\varphi + \frac{i\varepsilon\omega}{c}E_\rho = 0.$$

For the φ-direction:

$$ik_z E_\rho - \frac{\partial E_z}{\partial \rho} - \frac{i\omega}{c}B_\varphi = 0$$

$$ik_z B_\rho - \frac{\partial B_z}{\partial \rho} + \frac{i\varepsilon\omega}{c}E_\varphi = 0.$$

For the z-direction:

$$\frac{1}{\rho}\frac{\partial}{\partial \rho}(\rho E_\varphi) - \frac{1}{\rho}\frac{\partial E_\rho}{\partial \varphi} - \frac{i\omega}{c}B_z = 0$$

$$\frac{1}{\rho}\frac{\partial}{\partial \rho}(\rho B_\varphi) - \frac{1}{\rho}\frac{\partial B_\rho}{\partial \varphi} + \frac{i\varepsilon\omega}{c}E_z = 0.$$

The magnitude of the wave vector, in vacuum, is given in the usual way as $k = \frac{\omega}{c}$.
Further, the index of refraction may be related to the dielectric constant in the vacuum and in the glass as follows:

$$n^2_{\text{vacuum}} = \varepsilon_{\text{vacuum}} = 1$$

$$n_{glass}^2 = \varepsilon_{glass} = 1 + \chi_0.$$

Thus the transverse components may be solved for simultaneously from equations through . After some simple algebra the results are:

$$E_\rho(\rho,\varphi,z) = \frac{ik_z}{\left(n^2k^2 - k_z^2\right)}\frac{\partial E_z}{\partial \rho} + \frac{ik}{\left(n^2k^2 - k_z^2\right)\rho}\frac{\partial B_z}{\partial \varphi}$$

$$E_\varphi(\rho,\varphi,z) = \frac{ik_z}{\left(n^2k^2 - k_z^2\right)\rho}\frac{\partial E_z}{\partial \varphi} - \frac{ik}{\left(n^2k^2 - k_z^2\right)}\frac{\partial B_z}{\partial \rho}$$

$$B_\rho(\rho,\varphi,z) = \frac{-in^2k}{\left(n^2k^2 - k_z^2\right)\rho}\frac{\partial E_z}{\partial \varphi} + \frac{ik_z}{\left(n^2k^2 - k_z^2\right)}\frac{\partial B_z}{\partial \rho}$$

$$B_\varphi(\rho,\varphi,z) = \frac{in^2k}{\left(n^2k^2 - k_z^2\right)}\frac{\partial E_z}{\partial \rho} + \frac{ik_z}{\left(n^2k^2 - k_z^2\right)\rho}\frac{\partial B_z}{\partial \varphi}.$$

In order to find the longitudinal components, one returns to Maxwell's divergence equations, equations and . Utilizing equations and found above and after some simple algebra, the divergence of the electric field is:

$$\vec{\nabla} \cdot \vec{E}(\rho,\varphi,z) = \frac{ik_z}{\left(n^2k^2 - k_z^2\right)}\frac{\partial^2 E_z}{\partial \rho^2} + \frac{ik_z}{\left(n^2k^2 - k_z^2\right)\rho}\frac{\partial E_z}{\partial \rho} + \frac{ik_z}{\left(n^2k^2 - k_z^2\right)\rho^2}\frac{\partial^2 E_z}{\partial \varphi^2} + ik_z E_z = 0$$

Multiplying equation by the factor $\left(n^2k^2 - k_z^2\right)$ and dividing by ik_z, produces:

$$\frac{\partial^2 E_z}{\partial \rho^2} + \frac{1}{\rho}\frac{\partial E_z}{\partial \rho} + \frac{1}{\rho^2}\frac{\partial^2 E_z}{\partial \varphi^2} + \left(n^2k^2 - k_z^2\right)E_z = 0,$$

Comparing equation and equation , one can see that:

$$\vec{\nabla}_t^2 E_z(\rho,\varphi,z) + (n^2k^2 - k_z^2)E_z(\rho,\varphi,z) = 0$$

$$\vec{\nabla}_t^2 B_z(\rho,\varphi,z) + (n^2k^2 - k_z^2)B_z(\rho,\varphi,z) = 0,$$

where ∇_t^2 is the transverse Laplacian operator defined by

$$\nabla_t^2 = \nabla^2 - \frac{\partial^2}{\partial z^2},$$

and an analogous expression for B_z has been derived on the basis of equations and . Equations and represent

the wave equations that govern the longitudinal electric and magnetic fields.

The φ-dependence of the E and B fields

Next, to determine the form of the solutions for the electric and magnetic fields, one needs to know the azimuthal (φ-dependence) and the radial (ρ-dependence) of the fields. To determine the form of the solutions for the longitudinal fields, one continues to use separation of variables. Thus to find solutions for equations and one lets the longitudinal components of E_z and B_z be given as

$$E_z = R(\rho)\Phi(\varphi)e^{i(k_z z-\omega t)}$$

$$B_z = R'(\rho)\Phi'(\varphi)e^{i(k_z z-\omega t)},$$

where E_z and B_z are assumed to be separable. Substituting equation into the wave equations yields

$$\Phi(\varphi)e^{ik_z z}\left[\frac{1}{\rho}\frac{\partial}{\partial\rho}\left(\rho\frac{\partial R(\rho)}{\partial\rho}\right)\right]+\frac{R(\rho)e^{ik_z z}}{\rho^2}\left[\frac{\partial^2\Phi(\varphi)}{\partial\varphi^2}\right]+$$
$$(n^2k^2-k_z^2)R(\rho)\Phi(\varphi)e^{ik_z z}=0,$$

with a similar expression for B_z. Rearranging,

$$\frac{\rho}{R(\rho)}\frac{\partial}{\partial\rho}\left(\rho\frac{\partial R(\rho)}{\partial\rho}\right)+(n^2k^2-k_z^2)\rho^2=-\frac{1}{\Phi(\varphi)}\frac{\partial^2\Phi(\varphi)}{\partial\varphi^2}.$$

Noticing that the left hand side of equation is a function of ρ only while the right hand side is a function of φ only, it must be the case that equation is a constant, let it be defined as m^2. Thus,

$$-\frac{1}{\Phi(\varphi)}\frac{\partial^2\Phi(\varphi)}{\partial\varphi^2}=m^2,$$

or,

$$\Phi(\varphi)=e^{im\varphi}.$$

Since $\Phi(\varphi)$ is the azimuthal dependence of the electric and magnetic fields, the solution has to be periodic with periodicity 2π. Thus $\Phi(\varphi+2\pi)=\Phi(\varphi)$, and therefore m is any positive or negative integer, including zero. Thus the electric and magnetic fields have an angular dependence given by equation .

The ρ-dependence of the E and B fields

To determine the radial dependence of the field solutions, one returns to equation . Since equation was found to be constant, one may rewrite equation in terms of that same constant m^2. Thus equation becomes

$$\frac{1}{\rho}\frac{\partial}{\partial\rho}\left(\rho\frac{\partial R(\rho)}{\partial\rho}\right)+\left[(n^2k^2-k_z^2)-\frac{m^2}{\rho^2}\right]R(\rho)=0,$$

Inside of the guide, in the vacuum channel, one can define a dimensionless quantity, $\frac{u^2}{a^2}$ through

$$u^2=a^2\left(n_{\text{vac}}^2k^2-k_z^2\right)=a^2\left(k^2-k_z^2\right)=a^2k^2\sin^2\theta$$

where a is the waveguide radius. Since $\sin\theta\approx\theta$ for small incident angles, this makes u in equation an effective angle of incidence. Further, within the glass walls of the guide, one can define a dimensionless quantity, $\frac{w^2}{a^2}$ through

$$w^2=a^2\left(k_z^2-n_{\text{glass}}^2k^2\right)=a^2\left(k_z^2-(1+\chi_0)k^2\right),$$

where w is proportional to an effective angle of refraction and the waves that $\frac{w^2}{a^2}$ describes in the glass are evanescent waves. This implies that w^2 will be positive when the angle of incidence with the glass is less than the critical angle. Thus inside of the vacuum channel, for $\rho<a$ equation becomes

$$\frac{1}{\rho}\frac{\partial}{\partial\rho}\left(\rho\frac{\partial R(\rho)}{\partial\rho}\right)-\left[\frac{m^2}{\rho^2}-\frac{u^2}{a^2}\right]R(\rho)=0.$$

This is Bessel's differential equation. The solutions are Bessel functions of the first kind $J_m(\frac{u}{a}\rho)$ of order m, or Bessel functions of the second kind $N_m(\frac{u}{a}\rho)$, of order m, also called Neumann functions. Bessel functions exhibit the asymptotic behavior of a cosine function with a phase shift and an amplitude that decreases as $\rho^{-\frac{1}{2}}$. Additionally, $J_m(0)=0$, at $\rho=0$, except for the $m=0$ case, where $J_0(0)=1$. The first few Bessel functions are given in figure 3.2 above.

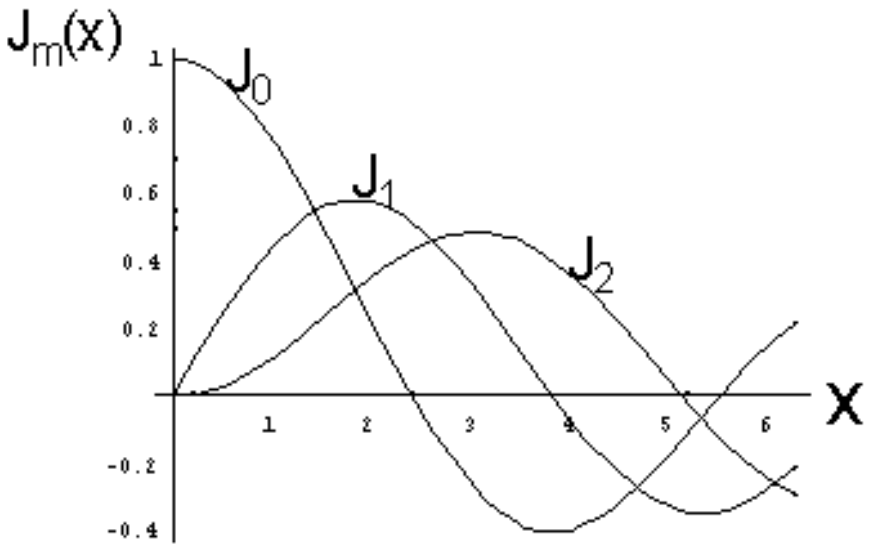

Plot of the Bessel Functions of the first kind, for orders $m = 0, 1,$ and 2.

The Neumann functions exhibit the asymptotic behavior of a sine function with a phase shift and an amplitude that decreases as $\rho^{-\frac{1}{2}}$. As $\rho \to 0$, the solutions diverge. The first few Neumann functions are listed in figure 3.3 below. Thus for physically meaningful solutions, Neumann functions are rejected in favor of Bessel functions, and

$$R(\rho) = J_m\left(\frac{u}{a}\rho\right)$$

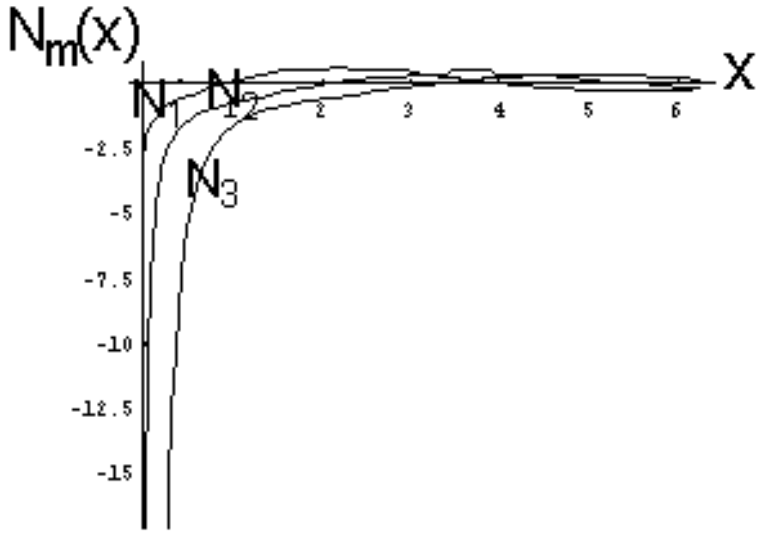

Plot of the Neumann Functions for the orders $m = 0, 1,$ and 2.

Therefore it follows that solutions to the longitudinal components are obtained by joining the solutions for R (ρ), $\Phi(\varphi)$, and Z(z) as follows for $\rho < a$

$$E_z(\rho,\varphi,z,t) = E_{\text{in}} J_m\left(\frac{u}{a}\rho\right) e^{im\varphi} e^{i(k_z z - \omega t)}$$

$$B_z(\rho,\varphi,z,t) = B_{\text{in}} J_m\left(\frac{u}{a}\rho\right) e^{im\varphi} e^{i(k_z z - \omega t)}.$$

In the glass $(\rho > a)$, one has:

$$\frac{1}{\rho}\frac{\partial}{\partial\rho}\left(\rho\frac{\partial R(\rho)}{\partial\rho}\right) - \left[\frac{m^2}{\rho^2} + \frac{w^2}{a^2}\right] R(\rho) = 0,$$

which is the modified Bessel differential equation. Its solutions are given by $I_m(\frac{w}{a}\rho)$, which are modified Bessel functions of the first kind of order m, or $K_m(\frac{w}{a}\rho)$, which are modified Bessel functions of the second kind of order m. Modified Bessel functions of the first kind, $I_m(\frac{w}{a}\rho)$, exhibit the asymptotic behavior $e^{+\rho}\rho^{-\frac{1}{2}}$ and grow without bound (or diverge) as $\rho \to \infty$, while modified Bessel functions of the second kind, $K_m(\frac{w}{a}\rho)$, exhibit the asymptotic behavior $e^{-\rho}\rho^{-\frac{1}{2}}$ and tend to zero as $\rho \to \infty$. A couple of the modified Bessel functions of the first and second kinds are shown in figure 3.4 below. In search of physically meaningful solutions inside of the glass capillary, one does not want the solutions to grow without bound, and therefore the solutions $I_m(\frac{w}{a}\rho)$ are rejected.

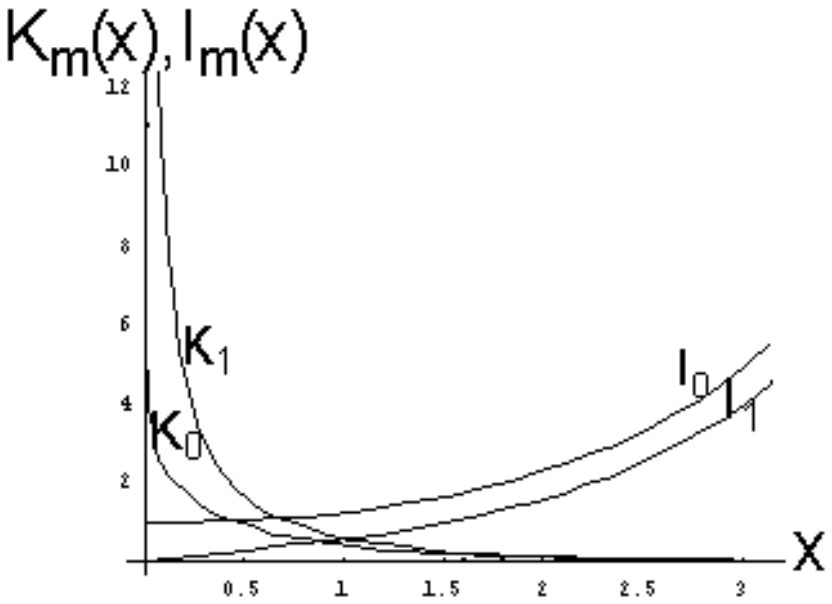

Plot of the modified Bessel Functions of the first and second kind of orders $m = 0$ and $m = 1$.

It therefore follows that the solutions to the longitudinal components are as follows for $\rho > a$:

$$E_z(\rho,\varphi,z,t) = E_{\text{out}} K_m\left(\frac{w}{a}\rho\right) e^{im\varphi} e^{i(k_z z-\omega t)}$$

$$B_z(\rho,\varphi,z,t) = B_{\text{out}} K_m\left(\frac{w}{a}\rho\right) e^{im\varphi} e^{i(k_z z-\omega t)}.$$

Equations and along with and represent the longitudinal form of the electric and magnetic fields respectively in the vacuum gap and in the glass fiber. The coefficients E_{in}, E_{out}, B_{in}, and B_{out} are as yet undetermined amplitudes of the electric and magnetic fields. The amplitudes E_{out}, B_{in}, and B_{out} will be expressed in terms of the amplitude E_{in}. Next boundary conditions must be imposed on the solutions found in order to determine the allowed modes that the capillary can support.

Boundary Conditions at $\rho = a$

Boundary conditions need to be imposed at $\rho = a$. Applying boundary conditions at the vacuum-glass interface imposes restrictions on the undetermined amplitudes (E_{in}, B_{in}, E_{out}, and B_{out}) that appear, and in turn the allowed modes that the fiber can support, as will be shown. The applicable electromagnetic boundary conditions require that the tangential components of the electric field, (E_z, E_φ), and magnetic field, $\left(H_z = B_z, \text{ and } H_\varphi = B_\varphi\right)$, be continuous across the boundary. In addition, the normal components of the displacement ($D_\rho = \varepsilon E_\rho$) and the magnetic field (B_ρ) must be continuous across the boundary. The components of the electric and magnetic field are found from equations through . Evaluating the components one obtains:For $\rho < a$, in the vacuum channel:

$$E_z = E_{\text{in}} J_m\left(\frac{u}{a}\rho\right) e^{im\varphi}$$

$$B_z = B_{\text{in}} J_m\left(\frac{u}{a}\rho\right) e^{im\varphi}$$

$$E_\rho = \frac{ik_z a}{u} E_{\text{in}} J_m'\left(\frac{u}{a}\rho\right) e^{im\varphi} - \frac{kam}{u^2} B_{\text{in}} J_m\left(\frac{u}{a}\rho\right) e^{im\varphi}$$

$$B_\rho = \frac{kam}{u^2} E_{\text{in}} J_m\left(\frac{u}{a}\rho\right) e^{im\varphi} - \frac{ik_z a}{u} B_{\text{in}} J_m'\left(\frac{u}{a}\rho\right) e^{im\varphi}$$

$$E_\varphi = \frac{-k_z a m}{u^2} E_{\text{in}} J_m\left(\frac{u}{a}\rho\right) e^{im\varphi} - \frac{ika}{u} B_{\text{in}} J_m'\left(\frac{u}{a}\rho\right) e^{im\varphi}$$

$$B_\varphi = \frac{ika}{u} E_{\text{in}} J_m'\left(\frac{u}{a}\rho\right) e^{im\varphi} - \frac{k_z a m}{u^2} B_{\text{in}} J_m\left(\frac{u}{a}\rho\right) e^{im\varphi}.$$

For $\rho > a$, in the glass:

$$E_z = E_{\text{out}} K_m\left(\frac{w}{a}\rho\right) e^{im\varphi}$$

$$B_z = B_{\text{out}} K_m\left(\frac{w}{a}\rho\right) e^{im\varphi}$$

$$E_\rho = \frac{-ik_z a}{w} E_{\text{out}} K_m'\left(\frac{w}{a}\rho\right) e^{im\varphi} + \frac{kam}{w^2} B_{\text{out}} K_m\left(\frac{w}{a}\rho\right) e^{im\varphi}$$

$$B_\rho = \frac{-(1+\chi_0)kam}{w^2} E_{\text{out}} K_m\left(\frac{w}{a}\rho\right) e^{im\varphi} - \frac{ik_z a}{w} B_{\text{out}} K_m'\left(\frac{w}{a}\rho\right) e^{im\varphi}$$

$$E_\varphi = \frac{k_z a m}{w^2} E_{\text{out}} K_m\left(\frac{w}{a}\rho\right) e^{im\varphi} + \frac{ika}{w} B_{\text{out}} K_m'\left(\frac{w}{a}\rho\right) e^{im\varphi}$$

$$B_\varphi = \frac{-(1+\chi_0)ika}{w} E_{\text{out}} K_m'\left(\frac{w}{a}\rho\right) e^{im\varphi} + \frac{k_z a m}{w^2} B_{\text{out}} K_m\left(\frac{w}{a}\rho\right) e^{im\varphi}.$$

Next, applying the boundary conditions at $\rho = a$, produces the following coupled equations:

$$E_{\text{in}} J_m(u) = E_{\text{out}} K_m(w)$$

$$B_{\text{in}} J_m(u) = B_{\text{out}} K_m(w)$$

$$\frac{-k_z a m}{u^2} E_{\text{in}} J_m(u) - \frac{ika}{u} B_{\text{in}} J_m'(u) = \frac{k_z a m}{w^2} E_{\text{out}} K_m(w) + \frac{ika}{w} B_{\text{out}} K_m'(w)$$

$$\frac{ika}{u} E_{\text{in}} J_m'(u) - \frac{k_z a m}{u^2} B_{\text{in}} J_m(u) = \frac{-(1+\chi_0)ika}{w} E_{\text{out}} K_m'(w) + \frac{k_z a m}{w^2} B_{\text{out}} K_m(w).$$

These boundary conditions allow one to express the undetermined amplitudes of the electric and magnetic

fields in the glass in terms of the still undetermined amplitudes in the vacuum channel. From equations and , one finds that:

$$E_{\text{out}} = E_{\text{in}} \frac{J_m(u)}{K_m(w)}$$

$$B_{\text{out}} = B_{\text{in}} \frac{J_m(u)}{K_m(w)}.$$

Substitution into equations and produces, in matrix form, the relations:

$$\begin{bmatrix} k_z m\left(\frac{1}{u^2} + \frac{1}{w^2}\right) & ik(\eta_1 + \eta_2) \\ ik(\eta_1 + (1+\chi_0)\eta_2) & -k_z m\left(\frac{1}{u^2} + \frac{1}{w^2}\right) \end{bmatrix} \begin{bmatrix} E_{\text{in}} \\ B_{\text{in}} \end{bmatrix} = \begin{bmatrix} 0 \\ 0 \end{bmatrix}.$$

Where

$$\eta_1 \overset{\text{def}}{=} \frac{J_m'(u)}{uJ_m(u)} \qquad \textit{and} \qquad \eta_2 \overset{\text{def}}{=} \frac{K_m'(w)}{wK_m(w)}$$

Equation is a linear homogeneous system of equations. In order for non trivial solutions to exist, the determinant of equation must vanish identically. Thus,

$$k^2(\eta_1 + \eta_2)(\eta_1 + (1+\chi_o)\eta_2) = k_z^2 m^2 \left(\frac{1}{u^2} + \frac{1}{w^2}\right)^2.$$

Notice that in equation for $m \neq 0$ there are no pure TE or TM modes. Equation is the characteristic equation for the modes in the waveguide. Equation determines the allowed values of k_z and of the transverse components of k, for a given frequency ω and index m. This accomplishes our first task of deriving the modes. Next, one may elicit some of the interesting features of the characteristic equation.

TE and *TM* Modes for x rays

Recall that the index, m, in the characteristic equation for the modes, equation , is allowed to assume all values in the range $0, \pm 1, \pm 2, \ldots$ Here one can investigate what happens to the modes as m is allowed to assume different indices. Suppose that $m = 0$. The characteristic equation that describes the modes becomes:

$$(\eta_1 + \eta_2)(\eta_1 + (1+\chi_0)\eta_2) = 0.$$

Therefore, either $(\eta_1 + \eta_2) = 0$ or $(\eta_1 + (1+\chi_0)\eta_2) = 0$. Here the modes naturally split themselves into two families. One family will have the characteristics of the transverse electric (*TE*) modes while the other has characteristics of the transverse magnetic (*TM*) modes. In the following sections it will be shown that the electric and magnetic fields naturally split themselves up into two families, the *TE* modes which

depend on the amplitude B_{in} and the *TM* modes which depend on the amplitude E_{in}.

TE modes

The *TE* modes are described by the amplitude B_{in}, which is directly proportional to the longitudinal magnetic field B_z. Here one will derive the characteristic equation for the *TE* modes and then examine the resulting electric and magnetic fields. For the case that $(\eta_1 + \eta_2) = 0$ one has

$$\eta_1 = -\eta_2,$$

or

$$\frac{J_0'(u)}{uJ_0(u)} = -\frac{K_0'(w)}{wK_0(w)}.$$

Utilizing the recurrence relations for Bessel and Modified Bessel functions of the first kind, namely,

$$J_m'(x) = \frac{J_{m-1}(x) - J_{m+1}(x)}{2}$$

$$K_m'(x) = -\frac{(K_{m-1}(x) + K_{m+1}(x))}{2},$$

one can express the derivatives of the Bessel and Modified Bessel functions appearing in equation in terms of the functions themselves. Thus, equation becomes

$$\frac{J_1(u)}{uJ_0(u)} = -\frac{K_1(w)}{wK_0(w)}.$$

This is the characteristic equation for the *TE* modes. This agrees with the usual treatment for visible and microwave radiation. (See for example the work by Gloge[Gloge] and Marcuse[Marcuse].) In order for a mode to be transverse electric, the longitudinal component E_z of the electric field, must be identically zero. This can only happen if E_{in} (and thus E_{out}) were identically zero. Thus the *TE* modes only have a longitudinal magnetic field. What does this mean in terms of the electric and magnetic fields? To see what this means, recall equations through . Inserting $m = 0$ into equations through and using equation for E_{out}, for B_{out}, and equations and for the derivatives of the Bessel and modified Bessel functions, one arrives at the fields that depend on amplitude B_{in} (and thus B_z), namely

$$B_z = B_{in} J_0\left(\frac{u}{a}\rho\right)$$

$$E_\varphi = i\frac{ka}{u}B_{\text{in}}J_1\left(\frac{u}{a}\rho\right)$$

$$B_\rho = i\frac{k_z a}{u}B_{\text{in}}J_1\left(\frac{u}{a}\rho\right),$$

where $E_z = E_\rho = B_\varphi = 0$.

TM modes

The *TM* modes are described by the amplitude E_{in}, which is directly proportional to the longitudinal electric field E_z. Here one will derive the characteristic equation for the *TM* modes and then examine the resulting electric and magnetic fields. For the case that $\eta_1 + (1+\chi_0)\eta_2 = 0$ one also has the relation:.

$$\eta_1 = -(1+\chi_0)\eta_2.$$

Rewriting equation in terms of the representations of η_1 and η_2, and again using the recurrence relations for the Bessel and Modified Bessel Functions one finds:

$$\frac{J_1(u)}{uJ_0(u)} = -(1+\chi_0)\frac{K_1(w)}{wK_0(w)}.$$

Equation is valid for any χ_0. This is also in agreement with the usual treatment for visible and microwave radiation. (See for example the work by Gloge [Gloge] and Marcuse [Marcuse].)

Inserting $m = 0$ into equations through and using equation for E_{out}, for B_{out}, and equations and for the derivatives of the Bessel and Modified Bessel functions, one arrives at the fields that depend on amplitude

E_{in} (and thus E_z), namely

$$E_z = E_{\text{in}}J_0\left(\frac{u}{a}\rho\right)$$

$$E_\rho = -i\frac{k_z a}{u}E_{\text{in}}J_1\left(\frac{u}{a}\rho\right)$$

$$B_\varphi = -i\frac{ka}{u}E_{\text{in}}J_1\left(\frac{u}{a}\rho\right),$$

where $B_z = B_\rho = E_\varphi = 0$. Further it is instructive to note that for x rays in the limit that χ_0 is much less than unity, the characteristic equation for the *TM* modes, equation is identical to the characteristic equation for the *TE* modes, equation for dielectric waveguides. The *TE* and *TM* modes are not degenerate in general. However when $\chi_0 \to 0$, the boundary conditions do not distinguish between $\vec{E}$, $\vec{D}$ and $\vec{B}$, $\vec{H}$. Therefore as

$\chi_0 \to 0$ the *TE* and *TM* modes become degenerate. In fact the two modes are polarized at right angle to one another (thus one being transverse electric and the other transverse magnetic). This is also obvious by examining the electric and magnetic fields for the two modes, if further the angle of incidence is also small. This allows one to conclude that $k = k_z \cos\theta$, which for small angles of incidence gives $k \sim k_z$. Thus for example, from equations and (as well as from equations and), $E_\rho \propto E_\varphi$ (and $B_\rho \propto B_\varphi$) and from the *TE* modes a ninety degree rotation gives the *TM* modes for small χ_0 and small angles of incidence.

The Hybrid modes for x rays

Next, one examines the case where $m \neq 0$. Here one will find that the modes do not split themselves naturally into two families. Both sets of modes will depend on the longitudinal electric and magnetic fields. These modes will be termed hybrid since they contain both a longitudinal electric and magnetic field. Recall that the characteristic equation for the modes is given again by equation

$$k^2(\eta_1 + \eta_2)(\eta_1 + (1+\chi_0)\eta_2) = k_z^2 m^2 \left(\frac{1}{u^2} + \frac{1}{w^2}\right)^2,$$

where the definitions of η_1 and η_2 are given by equation . Further, recall that no limitations as of yet have been placed on χ_0. Therefore the characteristic equation is valid for all forms of electromagnetic radiation as well as for all χ_0. Dividing equation by k^2 and utilizing the definition of u^2 given by equation and using the dimensionless parameter, $V^2 = -a^2k^2\chi_o$ produces a characteristic equation explicitly involving the susceptibility.

$$(\eta_1 + \eta_2)(\eta_1 + (1+\chi_0)\eta_2) = m^2\left(1 + \frac{u^2}{V^2}\chi_0\right)\left(\frac{1}{u^2} + \frac{1}{w^2}\right)^2,$$

The quantities u (equation) and w (equation) are proportional to the transverse components of the wave vector within the vacuum channel and the glass walls respectively, V is proportional to the critical angle, $\sqrt{-\chi_0}$ (equation), and the dimensionless quantities u, w, and V are related by

$$V^2 = u^2 + w^2 = -a^2k^2\chi_0$$

Here it is instructive to give some values to the parameters u, V, and w. For a waveguide of radius $a = 5 \times 10^{-6}$m, $k = 4.07 \times 10^{10}\text{m}^{-1}$ (for copper K_α x rays) and $\chi_0 = -1.9 \times 10^{-5}$ (for copper K_α x rays in borosilicate glass), one finds $V \approx 887$. Using the definition of u given by equation , one finds $u \sim 2$, and thus by equation , with $V^2 \gg u^2$, $w \sim 887$. The characteristic equation, equation is exact and is valid for all frequencies of electromagnetic radiation. Further, this form of the characteristic equation is quite complex to work with. Considerable simplifications arise, in the case of x rays, for the susceptibility

being much less than unity. Since $\chi_0 \ll 1$, along with the condition that $V^2 \gg u^2$, one can neglect the terms involving χ_0 to first order in equation . Thus,

$$(\eta_1 + \eta_2)^2 \approx m^2\left(\frac{1}{u^2} + \frac{1}{w^2}\right)^2,$$

or taking the square root

$$(\eta_1 + \eta_2) \approx \pm m\left(\frac{1}{u^2} + \frac{1}{w^2}\right) = \pm m\left(\frac{V^2}{u^2 w^2}\right).$$

Replacing η_1 and η_2 by their definitions, one arrives at the simplified characteristic equation for x rays:

$$\frac{J_m'(u)}{uJ_m(u)} + \frac{K_m'(w)}{wK_m(w)} \approx \pm m\left(\frac{1}{u^2}\right).$$

Equation is valid for all integer values of m including zero. Here one can assign a physical meaning to this integer m, namely that of total angular momentum. This is the angular momentum of the x rays about the longitudinal axis of the waveguide as the electric and magnetic fields of the x rays rotate in the φ-direction and propagate in the z-direction. If $m > 0$, the angular momentum vector points along $+z$. When the mode is viewed looking down the waveguide at the mode, as the mode approaches the observer, the mode would appear to spiral clockwise. If $m < 0$, the angular momentum vector points along $-z$. When the mode is viewed looking down the waveguide at the mode as the mode approaches the observer, the mode would appear to spiral to the counterclockwise.

Modes obtained using the + sign in equation (for any positive or negative value of m) are termed EH_m, while the modes obtained using the − sign (for any positive or negative value of m) are termed HE_m, in the terminology of fiber optics. Clearly the modes EH_m and HE_{-m} are degenerate and will be treated later. The + or − sign will turn out to be the spin angular momentum of the mode, and the total angular momentum, m, of the mode will be the sum of the orbital and spin angular momenta. Next, one will explore and analyze these two hybrid modes for the case of x rays in the glass capillary.

The EH_m modes

Notice that the characteristic equation, equation , contains derivatives of Bessel and Modified Bessel function. It can be rewritten using only the Bessel and Modified Bessel functions themselves, rather than their derivatives. Equation may be simplified through the use of the recurrence relations for the Bessel and Modified Bessel functions. From Abramowitz and Stegun,

$$J_m'(u) = \mp\frac{mJ_m(u)}{u} \pm J_{m\mp1}(u)$$

$$K_m'(w) = \mp\frac{mK_m(w)}{w} - K_{m\mp1}(w)$$

Using the $(+)$ sign in equation and the lower signs from the recurrence relation equations and above produces

$$\frac{J_{m+1}(u)}{uJ_m(u)} + \frac{K_{m+1}(w)}{wK_m(w)} = 0.$$

Equation is the characteristic (or eigenvalue) equation and can in principle be solved for the allowed values of u. Once the allowed values of u are known, one can use equation to determine the allowed values of the longitudinal propagation constant k_z.

Circular Polarization of the Transverse Field Components

The transverse field components are circularly polarized with some interesting implications. The continuity of the electric and magnetic fields at the glass interface puts restrictions on the amplitudes of the allowed fields E_{in} and B_{in}. First one will determine the relation between the amplitudes of the fields. Second, one will show the circularly polarized nature of the fields. Lastly, one will explore the implications of the results obtained.

To demonstrate the relation between the amplitudes of the electric and magnetic fields in the vacuum channel, continuity of the tangential components of the electric and magnetic fields (E_φ (equation) and B_φ (equation)). Using equations and along with equations and , one can relate the amplitudes of the electric and magnetic fields. From equation , the EH_m modes are given by

$$\frac{-k_z am}{u^2}E_{\text{in}}J_m(u) - \frac{ika}{u}B_{\text{in}}J_m'(u) = \frac{k_z am}{w^2}E_{\text{out}}K_m(w) + \frac{ika}{w}B_{\text{out}}K_m'(w),$$

which reduces to

$$k_z amE_{\text{in}}\left(\frac{1}{u^2} + \frac{1}{w^2}\right) = ikaB_{\text{in}}\left(\frac{J_m'(u)}{uJ_m(u)} + \frac{K_m'(w)}{wK_m(w)}\right),$$

where E_{out} and B_{out} have been replaced by equations and respectively. Thus the ratio of the amplitudes of the electric to magnetic fields is given by

$$\frac{E_{\text{in}}}{B_{\text{in}}} = \frac{-ik}{k_z m}\left(\frac{u^2w^2}{V^2}\right)\left(\frac{J_m'(u)}{uJ_m(u)} + \frac{K_m'(w)}{wK_m(w)}\right).$$

Using the recurrence relations for the Bessel and Modified Bessel functions, along with equations and , one is able to simplify equation for the EH_m modes. Thus the ratio of the amplitudes of the electric to magnetic field reduces to

$$\frac{E_{\text{in}}}{B_{\text{in}}} = -i\frac{k_z}{k}$$

for $\chi_0 \ll 1$. Further, by the triangle formed by the incident wave vector with respect to the z-axis, the longitudinal component of the incident wave vector may be expressed as $k_z = k\cos(\theta)$, which for small angles of incidence gives $\cos(\theta) \approx 1$. This produces for the EH_m modes

$$\frac{E_{\text{in}}}{B_{\text{in}}} = -i.$$

This shows that the longitudinal electric and magnetic field amplitudes are out of phase by $\frac{\pi}{2}$.

To show the circularly polarized nature of the EH_m modes, one can calculate the radial and azimuthal components of the electric and magnetic fields $(E_\rho, E_\varphi, B_\rho, B_\varphi)$ directly, by means of the longitudinal components E_z and B_z. For the amplitude ratios for the fields of the EH_m modes given by equation , equations through produce for $\rho < a$,

$$E_\rho = \left[\frac{ik_z a}{u}J_m'\left(\frac{u}{a}\rho\right) - \frac{ika^2 m}{u^2\rho}J_m\left(\frac{u}{a}\rho\right)\right]E_{\text{in}}e^{im\varphi}e^{ik_z z}$$

$$E_\varphi = \left[-\frac{k_z a^2 m}{u^2\rho}J_m\left(\frac{u}{a}\rho\right) + \frac{ka}{u}J_m'\left(\frac{u}{a}\rho\right)\right]E_{\text{in}}e^{im\varphi}e^{ik_z z}$$

$$B_\rho = \left[\frac{ka^2 m}{u^2\rho}J_m\left(\frac{u}{a}\rho\right) - \frac{k_z a}{u}J_m'\left(\frac{u}{a}\rho\right)\right]E_{\text{in}}e^{im\varphi}e^{ik_z z}$$

$$B_\varphi = \left[\frac{ika}{u}J_m'\left(\frac{u}{a}\rho\right) - \frac{ik_z a^2 m}{u^2\rho}J_m\left(\frac{u}{a}\rho\right)\right]E_{\text{in}}e^{im\varphi}e^{ik_z z}.$$

The above set of equations for the EH_m modes contain derivatives of Bessel functions. One would like to eliminate the derivatives in favor of the Bessel functions themselves. The derivatives that appear in equations through may be simplified for the EH_m modes with the help of a recurrence relation for Bessel functions:

$$J_m'(x) = \frac{m}{x}J_m(x) - J_{m+1}(x)$$

Therefore for the EH_m modes,

$$E_z = E_{in} J_m\left(\frac{u}{a}\rho\right) e^{im\varphi} e^{ik_z z}$$

$$E_\rho = -\frac{ik_z a}{u} J_{m+1}\left(\frac{u}{a}\rho\right) E_{\text{in}} e^{im\varphi} e^{ik_z z}$$

$$E_\varphi = -\frac{ka}{u} J_{m+1}\left(\frac{u}{a}\rho\right) E_{\text{in}} e^{im\varphi} e^{ik_z z}$$

$$B_z = iE_{in} J_m\left(\frac{u}{a}\rho\right) e^{im\varphi} e^{ik_z z}$$

$$B_\rho = \frac{k_z a}{u} J_{m+1}\left(\frac{u}{a}\rho\right) E_{\text{in}} e^{im\varphi} e^{ik_z z}$$

$$B_\varphi = -\frac{ika}{u} J_{m+1}\left(\frac{u}{a}\rho\right) E_{\text{in}} e^{im\varphi} e^{ik_z z}$$

where again, for grazing angles of incidence, $k_z = k\cos(\theta) \approx k$. Therefore,

$$E_\rho = +iE_\varphi \qquad \text{and} \qquad B_\rho = +iB_\varphi.$$

This is precisely the condition for circular polarization. Here one has for the transverse electric field

$$\vec{E}^{\text{LCP}}_{\text{transverse}} = E_\rho \hat{\rho} - iE_\rho \hat{\varphi} = E_\rho(\hat{\rho} - i\hat{\varphi}),$$

where an analogous expression for the transverse magnetic field could also be written. Here the rotation of the transverse electric field vector is defined to be clockwise when looking into the wave, and is termed left circularly polarized (LCP) and has positive helicity.

Equation is used to describe the transverse electric field of the fields in the vacuum channel. Examining figure 3.5, at a fixed point in space, say point A with coordinates (ρ, φ, z), the transverse electric field vectors sweep around in a circle at a frequency ω. For the EH_m^{LCP} modes the magnitude of the transverse electric field vector is not constant, but varies with ρ and the direction varies with φ as shown in figure 3.5 for the case $m = 0$. In other words there appears to be no φ-dependence to the electric field vectors. However, the full transverse electric field vector (equation) depends on $\hat{\varphi}$, even if the fields do not. As time passes the electric field rotates clockwise. This is spin and has a value of $+1$ along $\hat{z}$. The φ-dependence of the fields is the orbital angular momentum of the mode about the z-axis. For the case $m = 1$, the electric field vectors all rotate in phase at frequency ω.

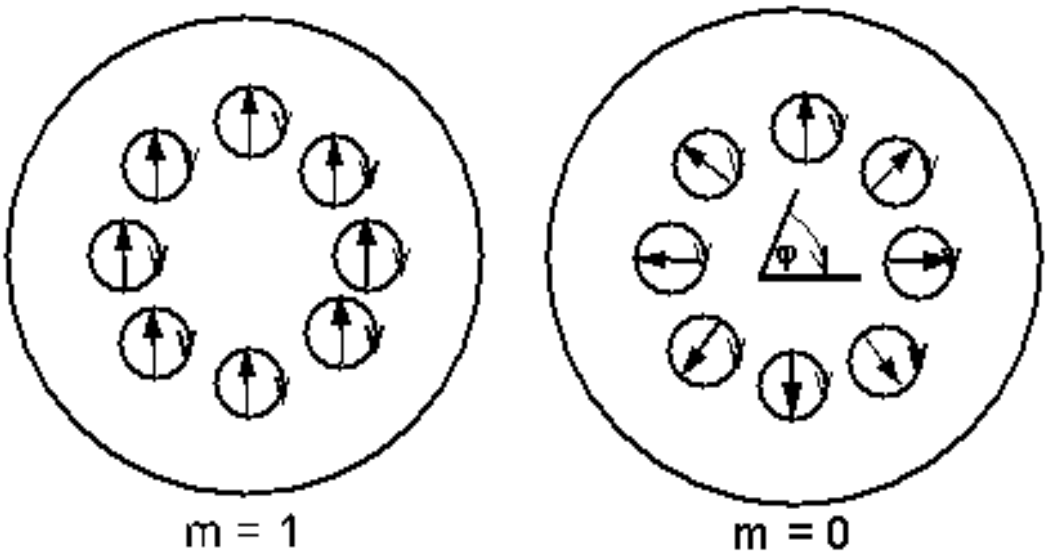

Schematic of the electric field vectors for the two cases $m = 0$ and $m = 1$. In the left picture one has *EH* $_1$ mode. The electric field vectors are all in phase and rotate clockwise when viewed from a fixed point in space, have an orbital angular momentum about the z-axis and have total angular momentum $+1$. In the right picture one has the *TM* mode case. Here the modes have no φ-dependence but do have an associated orbital angular momentum about the z-axis and a total angular momentum of 0.

The *HE* $_m$ modes

In an analogous fashion to the development of the *EH* $_m$ modes, the *HE* $_m$ modes will now be treated. As was done before, the characteristic equation will be expressed in terms of the Bessel and modified Bessel functions themselves, rather than their derivatives. Equation may be simplified through the use of the recurrence relations for the Bessel and Modified Bessel functions, equations and . Using the $(-)$ sign in equation and the upper signs from the recurrence relation equations and above produces:

$$\frac{J_{m-1}(u)}{uJ_m(u)} - \frac{K_{m-1}(w)}{wK_m(w)} = 0$$

Equation is the characteristic (or eigenvalue) equation and can in principle be solved for the allowed values of u. Once the allowed values of u are known, one can use equation to determine the allowed values of the longitudinal propagation constant k_z.

Circular Polarization of the Transverse Field Components

By virtue of the circular symmetry, it will be shown that the transverse field components for the *HE* modes are polarized and that the polarization is circular. The circular polarization of the transverse field components will have some interesting implications. By using the continuity of the electric and magnetic

fields at the glass interface, this put restrictions on the amplitudes of the allowed fields E_{in} and B_{in}. . First one will determine the relation between the amplitudes of the fields. Second, one will show the circularly polarized nature of the fields.
To demonstrate the relation between the amplitudes of the electric and magnetic fields in the vacuum channel, recall the continuity of the tangential components of E_φ (equation) and B_φ (equation). Using equations and along with equations and , one can relate the amplitudes of the electric and magnetic fields. From equation , the *HE* modes are given by:

$$\frac{ika}{u}E_{in}J_m'(u) - \frac{k_z am}{u^2}B_{in}J_m(u) = \frac{-(1+\chi_0)ika}{w}E_{out}K_m'(w) + \frac{k_z am}{w^2}B_{out}K_m(w)$$

which reduces to:

$$-k_z amB_{in}\left(\frac{1}{u^2}+\frac{1}{w^2}\right) = ikaE_{in}\left(\frac{J_m'(u)}{uJ_m(u)} + (1+\chi_0)\frac{K_m'(w)}{wK_m(w)}\right),$$

where E_{out} and B_{out} have been replaced by equations and respectively. Thus the ratio of the amplitudes of the electric to magnetic fields is given by:

$$\frac{B_{in}}{E_{in}} = \frac{ik}{k_z m}\left(\frac{u^2w^2}{v^2}\right)\left(\frac{J_m'(u)}{uJ_m(u)} + (1+\chi_0)\frac{K_m'(w)}{wK_m(w)}\right)$$

for the *HE* modes. Using the recurrence relations for the Bessel and Modified Bessel functions, along with equations and , one is able to simplify equation for the *HE* modes. Thus the ratio of the amplitudes of the electric to magnetic field reduces to:

$$\frac{E_{in}}{B_{in}} = +i\frac{k_z}{k}.$$

Equation is valid for the limit in which χ_o small compared to unity. Further, by the triangle formed by the incident wave vector with respect to the z-axis, the longitudinal component of the incident wave vector may be expressed as $k_z = k\cos(\theta)$, which for small angles of incidence gives $\cos(\theta) \approx 1$. Thus for the *HE* modes:

$$\frac{E_{in}}{B_{in}} = +i.$$

This shows that the electric and magnetic field amplitudes are out of phase by $\frac{\pi}{2}$.
To show the circularly polarized nature of the *EH* modes, one can calculate the radial and azimuthal components of the electric and magnetic fields $(E_\rho, E_\varphi, B_\rho, B_\varphi)$ directly, by means of the longitudinal components E_z and B_z. For the amplitude ratios for the fields of the *HE* modes given by equation ,

equations through produce for $\rho < a$,

$$E_\rho = \left[\frac{ik_z a}{u} J_m'\left(\frac{u}{a}\rho\right) + \frac{ika^2 m}{u^2 \rho} J_m\left(\frac{u}{a}\rho\right) \right] E_{\text{in}} e^{im\varphi} e^{ik_z z}$$

$$E_\varphi = \left[-\frac{k_z a^2 m}{u^2 \rho} J_m\left(\frac{u}{a}\rho\right) - \frac{ka}{u} J_m'\left(\frac{u}{a}\rho\right) \right] E_{\text{in}} e^{im\varphi} e^{ik_z z}$$

$$B_\rho = \left[\frac{ka^2 m}{u^2 \rho} J_m\left(\frac{u}{a}\rho\right) + \frac{k_z a}{u} J_m'\left(\frac{u}{a}\rho\right) \right] E_{\text{in}} e^{im\varphi} e^{ik_z z}$$

$$B_\varphi = \left[\frac{ika}{u} J_m'\left(\frac{u}{a}\rho\right) + \frac{ik_z a^2 m}{u^2 \rho} J_m\left(\frac{u}{a}\rho\right) \right] E_{\text{in}} e^{im\varphi} e^{ik_z z}.$$

The above set of equations for the HE_m modes contain derivatives of Bessel functions. One would like to eliminate the derivatives in favor of the Bessel functions themselves. The derivatives that appear in

equations through may be simplified for the HE_m modes with the help of a recurrence relation for Bessel functions

$$J_m'(x) = -\frac{m}{x} J_m(x) + J_{m-1}(x).$$

For the HE_m modes then,

$$E_z = E_{in} J_m\left(\frac{u}{a}\rho\right) e^{im\varphi} e^{ik_z z}$$

$$E_\rho = \frac{ik_z a}{u}\left[J_{m-1}\left(\frac{u}{a}\rho\right) \right] E_{\text{in}} e^{im\varphi} e^{ik_z z}$$

$$E_\varphi = -\frac{k_z a}{u}\left[J_{m-1}\left(\frac{u}{a}\rho\right) \right] E_{\text{in}} e^{im\varphi} e^{ik_z z}$$

$$B_z = -iE_{in} J_m\left(\frac{u}{a}\rho\right) e^{im\varphi} e^{ik_z z}$$

$$B_\rho = \frac{k_z a}{u}\left[J_{m-1}\left(\frac{u}{a}\rho\right) \right] E_{\text{in}} e^{im\varphi} e^{ik_z z}$$

$$B_\varphi = \frac{ika}{u}\left[J_{m-1}\left(\frac{u}{a}\rho\right) \right] E_{\text{in}} e^{im\varphi} e^{ik_z z}$$

where, for grazing angles of incidence, $k_z = k\cos(\theta) \approx k$. Therefore,

$$E_\rho = -iE_\varphi \qquad \text{and} \qquad B_\rho = -iB_\varphi.$$

This is precisely the condition for circular polarization. Here one has for the transverse electric field

$$\vec{E}^{\text{RCP}}_{\text{transverse}} = E_\rho\hat{\rho} + iE_\rho\hat{\varphi} = E_\rho(\hat{\rho} + i\hat{\varphi}),$$

where an analogous expression for the transverse magnetic field could also be written. Here the rotation of the transverse electric field vector is defined to be counterclockwise when looking into the wave and is termed right circularly polarized (RCP) and has negative helicity.
Equation is used to describe the transverse electric field of the modes at a fixed point in space, say point A with coordinates (ρ, φ, z). The transverse electric field vector sweeps around in a circle at a frequency ω, while the magnitude varies with ρ and the direction varies with φ. For the $m = 0$ case, the φ-dependence is the orbital angular momentum associated with the electric field which makes the electric field vectors rotate out of phase with each other. The spin of the electric field vectors is counterclockwise and has a value of -1 and points along $\hat{z}$ as shown in figure 3.6.

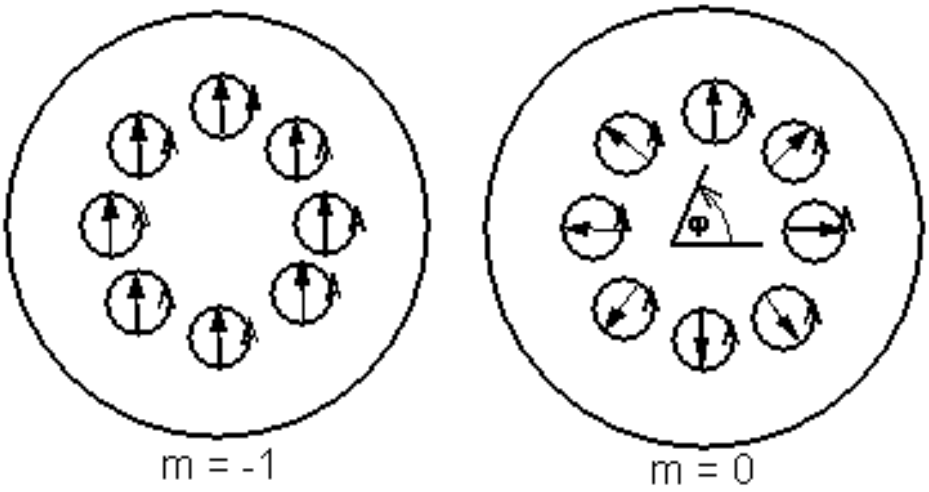

Schematic of the electric field vectors for the two cases $m = 0$ and $m = -1$. In the left picture one has *HE* $_1$ mode. The electric field vectors are all in phase and rotate counterclockwise when viewed from a fixed point in space, have an orbital angular momentum about the z-axis and have total angular momentum -1. In the right picture one has the *TM* mode case. Here the modes have no φ-dependence but do have an associated orbital angular momentum about the z-axis and a total angular momentum of 0.

EH $_m$ and *HE* $_m$ Mode Degeneracy

Recalling that the general characteristic equation for the modes is given by equation , one may notice that

the index m used to characterize the modes may assume any integer value (positive or negative) as well as zero. The modes that arise by solving equation will have a natural degeneracy in the choice of m. Both positive values of m (with the + sign in the characteristic equation) and negative values of m (with the − sign in the characteristic equation) will satisfy the characteristic equation, with the choice of m equal to zero being trivial. The resulting modes will propagate with the same propagation constant k_z. The choice of $m = 0$ in equation lead to the *TE/TM* modes, while the choice of m different from zero leads to the hybrid *EH/HE* modes. Equation is valid for all values of χ_0. For x rays, when the limit of small χ_0 is taken, a degeneracy will arise that will allow one to combine the hybrid circularly polarized modes into a set of linearly polarized modes.

EH and *HE* Mode Degeneracy as a consequence of Changing Indices From m to $-m$

The EH_m and the HE_{-m} modes will be ultimately be defined by the same characteristic equation, in the limit of small χ_0. It will be shown that equation for the EH_m modes will turn out, in the limit of small χ_0, to be identical to the characteristic equation, equation for the HE_{-m} modes. Thus, those modes will be called degenerate in the sense that EH_m and HE_{-m} modes will propagate with the same propagation constant k_z. To do this, one may recall equations for the *EH* modes and for the *HE* modes. Recall from equation the characteristic equation for the HE_m modes is given by

$$\frac{J_{m-1}(u)}{uJ_m(u)} - \frac{K_{m-1}(w)}{wK_m(w)} = 0.$$

If one makes the substitution of $m \to -m$ in equation , one finds

$$\frac{J_{-m-1}(u)}{uJ_{-m}(u)} - \frac{K_{-m-1}(w)}{wK_{-m}(w)} = 0.$$

Using the fact that $J_{-n}(x) = (-1)^n J_n(x)$ and that $K_{-n}(x) = K_n(x)$ one obtains the following relation

$$\frac{J_{m+1}(u)}{uJ_m(u)} + \frac{K_{m+1}(w)}{wK_m(w)} = 0,$$

which is equation , the characteristic equation for the EH_m modes. Thus the HE_{-m} and the EH_m modes are degenerate, that is they propagate with the same propagation constant k_z which is given by equation . Therefore one may write this degeneracy as

$$HE_{-m}^{\mathrm{RCP}} \overset{\mathrm{deg}}{=} EH_{m}^{\mathrm{LCP}}$$

Next, one may ask how the fields that describe the modes change as one makes the substitution $m \rightarrow -m$ in the characteristic equations. Recall that the radial and azimuthal electric and magnetic fields for the EH_{m}^{LCP} modes are given by equations through , while for the HE_{-m}^{RCP} modes they are given by equations through . Suppose, for example, that one examines the radial and azimuthal electric field of the EH_{m} mode, with the radial and azimuthal magnetic fields following by analogy. If one makes the substitution of $m \rightarrow -m$, the radial and azimuthal electric fields transforms from

$$EH_{m}^{\mathrm{LCP}}: \quad E_{\rho}^{m} = -\frac{ik_z a}{u} J_{m+1}\left(\frac{u}{a}\rho\right) E_{\mathrm{in}}^{+} e^{im\varphi} e^{ik_z z}$$

$$EH_{m}^{\mathrm{LCP}}: \quad E_{\varphi}^{m} = -\frac{ka}{u} J_{m+1}\left(\frac{u}{a}\rho\right) E_{\mathrm{in}}^{+} e^{im\varphi} e^{ik_z z}$$

to

$$E_{\rho}^{-m} = -(-1)^{m-1} \frac{ik_z a}{u} J_{m-1}\left(\frac{u}{a}\rho\right) E_{\mathrm{in}}^{+} e^{i(-m)\varphi} e^{ik_z z}$$

$$E_{\varphi}^{-m} = -(-1)^{m-1} \frac{ka}{u} J_{m-1}\left(\frac{u}{a}\rho\right) E_{\mathrm{in}}^{+} e^{i(-m)\varphi} e^{ik_z z}$$

Absorbing the factors of $(-1)^{m} E_{\mathrm{in}}^{+}$ into E_{in}^{-} and simplifying, one obtains:

$$\frac{ik_z a}{u} J_{m-1}\left(\frac{u}{a}\rho\right) E_{\mathrm{in}}^{-} e^{-im\varphi} e^{ik_z z} = E_{\rho}^{m} \quad : HE_{m}^{\mathrm{RCP}}$$

$$\frac{ka}{u} J_{m-1}\left(\frac{u}{a}\rho\right) E_{\mathrm{in}}^{-} e^{-im\varphi} e^{ik_z z} = E_{\varphi}^{m} \quad : HE_{m}^{\mathrm{RCP}}$$

Recall that the index m describes the orbital angular momentum. In making the substitution from $m \rightarrow -m$, the total angular momentum has flipped its sign and the mode has gone from a state of being LCP to being RCP. Further, notice that the spin angular momentum has gone from $+1$ in an *EH* mode to -1 in an *HE* mode while the mode continues to propagate in the $+z$-direction. An illustration of this degeneracy is shown in figure 3.7.

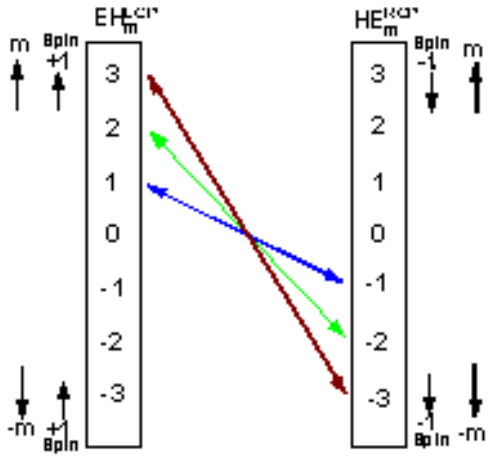

Illustration of the degeneracy that arises between the EH_m and HE_{-m} modes when the index is changed from $m \rightarrow -m$. This degeneracy was explored and used as a basis the eventual superpostion of the hybrid circularly polarized *EH/HE* to form the linearly polarized modes.

Behavior of modes for $\theta \ll \theta_c$

The behavior of the hybrid modes needs to be examined for angles of incidence that are much less than critical angle, or for the condition of near grazing incidence. Note, as the angle of incidence approaches the critical angle u gets larger (it is proportional to the angle of incidence), and w gets smaller, and the x rays penetrates farther into the glass capillary and are no longer confined in the vacuum channel. The behavior of the modes for angles of incidence much less than the critical angle is determined by the limit of $w \gg 1$. In this situation there is little penetration of the x rays into the glass capillary. For large w, the modified Bessel functions become, for angles of incidence much less than the critical angle:

$$K_m(w) \approx \left(\frac{\pi}{2w}\right)^{\frac{1}{2}} e^{-w},$$

such that

$$K_m'(w) = \frac{d}{dw}\left[\left(\frac{\pi}{2w}\right)^{\frac{1}{2}} e^{-w}\right] = -\left(1 + \frac{1}{2w}\right) K_m(w).$$

Since there exist different classes of modes, namely the *TE*, *TM*, and the hybrid EH_m and HE_m modes, it is instructive to look at each of these cases separately.

The *TE* and *TM* modes for $\theta \ll \theta_c$

Here one will examine the behavior of the *TE* and *TM* modes for angles of incidence that are much less than critical angle. Recall that the *TE* and *TM* modes are identical for $\chi_0 \ll 1$ and that the characteristic equation is given by either equation (for the *TE* modes) or equation (for the *TM* modes). For $m = 0$, the

characteristic equation for the *TE* or *TM* modes becomes, in the limit of large w,

$$\frac{J_0'(u)}{uJ_0(u)} = -\frac{K_0'(w)}{wK_0(w)} \approx \frac{-\left(1+\frac{1}{2w}\right)}{w} \approx 0.$$

Further, from the recurrence relations for the Bessel functions:

$$J_0'(u) = -J_1(u),$$

such that the left hand side of equation in the limit of large w, the behavior of the *TE* $_{m=0,p}$ or *TM* $_{m=0,p}$ modes are governed by

$$J_1(u) = 0,$$

where $u_{m=0,p}$ is the p^{th} zero of $J_1(u)$. The first five zeros of $J_1(u)$ are given in table 3.1 below

m	$J_1(u)$
1	3.832
2	7.016
3	10.173
4	13.324
5	16.471

\caption{The first five zeros of J_{1}(u).\label{key}}

The *EH* modes for $\theta \ll \theta_c$

Again to determine the behavior of the *EH* $_m$ modes one assumes that the incident wave vector makes a small angle of incidence, much smaller than the critical angle, and that χ_o is much less than unity. For the *EH* $_{m,p}$ modes far from the critical angle (in the limit of large w,) the modified Bessel functions are given again by equation . Recalling the *EH* $_{m,p}$ defined by equation , one seeks a representation of $K_{m+1}(w)$ in terms of $K_m(w)$. From the recurrence relations for the modified Bessel functions,

$$K_{m+1}(w) = \frac{2m}{w}K_m(w) + K_{m-1}(w),$$

and

$$K_{m-1}(w) = -2K_m'(w) - K_{m+1}(w),$$

where $K_m'(w)$ from equation will be utilized. Thus

$$K_{m+1}(w) = \left(\frac{m}{w} + 1 + \frac{1}{2w}\right)K_m(w).$$

Therefore equation becomes:

$$-\frac{J_{m+1}(u)}{uJ_m(u)} = \frac{K_{m+1}(w)}{wK_m(w)} \approx \frac{1}{w}.$$

In the limit that $w \to \infty$, the right hand side of equation vanishes and the behavior of the $EH_{m,p}$ modes is dictated by:

$$J_{m+1,p}(u) = 0.$$

The p^{th} zeros of $J_{m+1}(u)$ are given in the table 3.2 above.

m,p	1	2	3	4	5
0	3.832	7.016	10.173	13.324	16.471
1	5.136	8.417	11.620	14.796	17.960
2	6.380	9.761	13.015	16.224	19.409
3	7.588	11.065	14.373	17.616	20.827
4	8.771	12.339	15.700	19.980	22.218
5	9.936	13.589	17.004	20.321	23.586

\caption{The zeros of $J_{m+1} $(u). The values of m are labeled down the left most column.\label{key}}

The above analysis has $w \to \infty$. One could redo the analysis for w large, but not necessarily infinite. The radial Bessel function solution does not go to zero and vanish at the glass interface. In the glass, the solutions decay as a modified Bessel function. The u's that appear in the argument of the Bessel function will in general lie close to a zero of the Bessel function that describes the radial solution, in this case $J_{m+1}(u)$. To incorporate this fact, let

$$u = \hat{u} - \delta u.$$

Here $\hat{u}$ represents the p^{th} zero of $J_{m+1}(\hat{u})$ as $w \gg 1$ for the case where there is no penetration by the x-ray into the glass, and δu is a small first order correction to $\hat{u}$ which represents the amount of penetration of the x-ray into the glass. Taylor expanding $J_m(\hat{u})$ and $J_{m+1}(\hat{u})$ about u produces:

$$J_m(u) = J_m(\hat{u}) - \delta u J'_m(\hat{u})$$

$$J_{m+1}(u) = -\delta u J'_{m+1}(\hat{u}),$$

where $J_{m+1}(\hat{u}) = 0$. The derivatives of the Bessel functions are obtained through the use of the recurrence relations. Thus equations and become:

$$J_m(u) = \left(1 + \frac{m}{\hat{u}}\delta u\right) J_m(\hat{u})$$

$$J'_{m+1}(u) = J_m(\hat{u}),$$

and equation becomes for any w,

$$-\frac{J_{m+1}(u)}{uJ_m(u)} = \frac{-\delta u}{u\left(1 + \frac{m}{\hat{u}}\delta u\right)} \approx \frac{1}{w},$$

where:

$$w = \sqrt{V^2 - u^2} \approx V,$$

for the case that $V^2 \gg \hat{u}^2$. Therefore equation becomes

$$\frac{-\delta u}{(\hat{u} - \delta u)\left(1 + \frac{m}{\hat{u}}\delta u\right)} \approx \frac{1}{V}.$$

In this case, for any w,

$$\delta u \approx -\frac{\hat{u}}{V},$$

so that

$$u = \hat{u}\left(1 + \frac{1}{V}\right).$$

Recalling that since $V \sim 887$ and $\hat{u} \sim 2$, equation gives $u \sim \hat{u}$ and the real zeros of the Bessel function when the x-ray penetrates into the glass, u, may be approximated by the zeros of the Bessel functions when there is no penetration of the x-ray into the glass $\hat{u}$.

The *HE* modes for $\theta \ll \theta_c$

For $\theta \ll \theta_c$ and for large w, the modified Bessel functions are given again by equation . Recalling the *HE* $_{m,p}$ defined by equation , one seeks a representation of $K_{m-1}(w)$ in terms of $K_m(w)$. In an analogous fashion to the development of the *EH* $_{m,p}$ modes, the behavior of the mode is given by:

$$\frac{J_{m-1}(u)}{uJ_m(u)} = \frac{K_{m-1}(w)}{wK_m(w)} \approx \frac{1}{w}.$$

For $w \rightarrow \infty$, the behavior of the *HE* $_{m,p}$ is given by:

$$J_{m-1}(u) = 0.$$

and the p^{th} zeros of $J_{m-1}(u)$ are given in the table 3.3 below.

m,p	1	2	3	4	5
2	3.832	7.016	10.174	13.324	16.471
3	5.136	8.417	11.620	14.796	17.960
4	6.380	9.761	13.015	16.223	19.409
5	7.588	11.065	14.373	17.616	20.827
6	8.775	12.339	15.700	18.980	22.218

\caption{The zeros of J_{m-1}(u). \label{key}} The above analysis has $w \gg 1$. One could redo the analysis for w large, but not necessarily infinite. The radial Bessel function solution does not go to zero and vanish at the glass interface. In the glass, the solutions decay as a modified Bessel function. Thus the u's that appear in the argument of the Bessel function will in general lie between two successive zeros of the Bessel function that describes the radial solution, in this case $J_{m-1}(\hat{u})$. To incorporate this fact, again, let u be given again by equation and Taylor expand $J_{m-1}(\hat{u})$ and $J_m(\hat{u})$ about u in evaluating equation . In a completely analogous fashion to the development of the *EH* $_m$ modes, the *HE* $_m$ modes become:

$$u = \hat{u}\left(1 - \frac{1}{V}\right).$$

Recalling that since $V \sim 887$ and $\hat{u} \sim 2$, equation gives $u \sim \hat{u}$ and the real zeros of the Bessel function when the x-ray penetrates into the glass, u, may be approximated by the zeros of the Bessel functions when there is no penetration of the x-ray into the glass $\hat{u}$.

Linearly Polarized Modes

The degenerate circularly polarized *EH* $_m$ and *HE* $_m$ modes can be superposed to form linearly polarized or *LP* modes. These differ from the usual linearly polarized modes for x rays in vacuum in that these linearly polarized modes have total angular momentum denoted by the mode index m. In order to superpose the *EH* $_m$ and *HE* $_m$ modes with the same total angular momentum, one will transform both sets of modes from a cylindrical coordinate system to a rectangular coordinate system. In performing this transformation to a rectangular coordinate system, the rotating modes will be able to be superposed in a compact and easy manner. The linearly polarized modes will be the modes used in the remainder of the thesis.

Transformation of the EH_m modes from Cylindrical to Rectangular Coordinates

Since the hybrid EH_m or HE_m modes are degenerate, one would like to combine them together to form a linearly polarized mode. To do this it is advantageous to express the electric and magnetic fields in terms of Cartesian components rather than cylindrical components. To transform from the cylindrical coordinate system to the rectangular coordinate system, one applies the transformation matrix to the cylindrical field components. For the electric field, one has

$$\begin{bmatrix} E_x \\ E_y \end{bmatrix} = \begin{bmatrix} \cos\varphi & -\sin\varphi \\ \sin\varphi & \cos\varphi \end{bmatrix} \begin{bmatrix} E_\rho \\ E_\varphi \end{bmatrix},$$

with a similar transformation matrix for the magnetic field. To transform the EH_m modes, recall that the longitudinal electric and magnetic field components are given by equations and , while the transverse electric and magnetic field components are given by equations through in the vacuum channel. For brevity, the z-dependent term, $e^{ik_z z}$ will be suppressed the following derivation. Expanding the complex exponentials using Euler's result:

$$e^{im\varphi} = \cos(m\varphi) + i\sin(m\varphi)$$

it follows that the EH_m modes may be expressed as:

$$E_z = E_{\text{in}} J_m\left(\frac{u}{a}\rho\right)(\cos(m\varphi) + i\sin(m\varphi))$$

$$H_z = E_{\text{in}} J_m\left(\frac{u}{a}\rho\right)(-\sin(m\varphi) + i\cos(m\varphi))$$

$$E_\rho = \frac{k_z a}{u} E_{\text{in}} J_{m+1}\left(\frac{u}{a}\rho\right)(\sin(m\varphi) - i\cos(m\varphi))$$

$$B_\rho = \frac{k_z a}{u} E_{\text{in}} J_{m+1}\left(\frac{u}{a}\rho\right)(\cos(m\varphi) + i\sin(m\varphi))$$

$$E_\varphi = -\frac{ka}{u} E_{\text{in}} J_{m+1}\left(\frac{u}{a}\rho\right)(\cos(m\varphi) + i\sin(m\varphi))$$

$$B_\varphi = \frac{ka}{u} E_{\text{in}} J_{m+1}\left(\frac{u}{a}\rho\right)(\sin(m\varphi) - i\cos(m\varphi)).$$

Applying the transformation matrix and simplifying the resultant expressions for $\theta \ll \theta_c$, the electric fields yields:

$$E_x = \frac{k_z a}{u} E_{\text{in}} J_{m+1}\left(\frac{u}{a}\rho\right)[\sin(m\varphi)\cos(\varphi) - i\cos(m\varphi)\cos(\varphi)]$$
$$+ \frac{ka}{u} E_{\text{in}} J_{m+1}\left(\frac{u}{a}\rho\right)[\cos(m\varphi)\sin(\varphi) + i\sin(m\varphi)\sin(\varphi)]$$

$$E_y = \frac{k_z a}{u} E_{\text{in}} J_{m+1}\left(\frac{u}{a}\rho\right)[\sin(m\varphi)\sin(\varphi) - i\cos(m\phi)\sin(\varphi)]$$
$$- \frac{ka}{u} E_{\text{in}} J_{m+1}\left(\frac{u}{a}\rho\right)[\cos(m\varphi)\cos(\varphi) + i\sin(m\varphi)\cos(\varphi)]$$

$$B_x = \frac{k_z a}{u} E_{\text{in}} J_{m+1}\left(\frac{u}{a}\rho\right)[\cos(m\varphi)\cos(\varphi) + i\sin(m\varphi)\cos(\varphi)]$$
$$- \frac{ka}{u} E_{\text{in}} J_{m+1}\left(\frac{u}{a}\rho\right)[\sin(m\varphi)\sin(\varphi) - i\cos(m\varphi)\sin(\varphi)]$$

$$B_y = \frac{k_z a}{u} E_{\text{in}} J_{m+1}\left(\frac{u}{a}\rho\right)[\cos(m\varphi)\sin(\varphi) + i\sin(m\varphi)\sin(\varphi)]$$
$$+ \frac{ka}{u} E_{\text{in}} J_{m+1}\left(\frac{u}{a}\rho\right)[\sin(m\varphi)\cos(\varphi) - i\cos(m\varphi)\cos(\varphi)].$$

Next, one may simplify equations to by using the following identities:

$$\sin(m\varphi)\cos(\varphi) = \frac{1}{2}[-\sin((m-1)\varphi) + \sin((m+1)\varphi)]$$

$$\cos(m\varphi)\cos(\varphi) = \frac{1}{2}[\cos((m-1)\varphi) + \cos((m+1)\varphi)]$$

$$\sin(m\varphi)\sin(\varphi) = \frac{1}{2}[\cos((m-1)\varphi) - \cos((m+1)\varphi)]$$

$$\cos(m\varphi)\sin(\varphi) = \frac{1}{2}[\sin((m-1)\varphi) + \sin((m+1)\varphi)].$$

Thus for the EH_m modes the transformed electric and magnetic fields are given by:

$$E_x = \frac{ka}{u} E_{\text{in}} J_{m+1}\left(\frac{u}{a}\rho\right)[\sin((m+1)\varphi) - i\cos((m+1)\varphi)]$$

$$E_y = -\frac{ka}{u} E_{\text{in}} J_{m+1}\left(\frac{u}{a}\rho\right)[\cos((m+1)\varphi) + i\sin((m+1)\varphi)]$$

$$B_x = \frac{ka}{u} E_{in} J_{m+1}\left(\frac{u}{a}\rho\right)[\cos((m+1)\varphi) + i\sin((m+1)\varphi)]$$

$$B_y = \frac{ka}{u} E_{in} J_{m+1}\left(\frac{u}{a}\rho\right)[\sin((m+1)\varphi) - i\cos((m+1)\varphi)].$$

This accomplishes the first task. The EH_m modes have been transformed from a cylindrical coordinate system to a rectangular coordinate system.

Transformation of the HE_m modes from Cylindrical to Rectangular Coordinates

Having transformed the EH_m modes, the HE_m modes need to be transformed in order to fashion the *LP* modes. In order to transform the fields of the HE_m modes, one follows the same procedure given for the EH_m modes, and the results are given by

$$E_x = \frac{ka}{u} E_{in} J_{m-1}\left(\frac{u}{a}\rho\right)[\sin((m-1)\varphi) + i\cos((m-1)\varphi)]$$

$$E_y = -\frac{ka}{u} E_{in} J_{m-1}\left(\frac{u}{a}\rho\right)[\cos((m-1)\varphi) - i\sin((m-1)\varphi)]$$

$$B_x = \frac{ka}{u} E_{in} J_{m-1}\left(\frac{u}{a}\rho\right)[\cos((m-1)\varphi) - i\sin((m-1)\varphi)]$$

$$B_y = \frac{ka}{u} E_{in} J_{m-1}\left(\frac{u}{a}\rho\right)[\sin((m-1)\varphi) + i\cos((m-1)\varphi)],$$

where the EH_m and HE_m transformed components, (equations through), are valid in the limit of $\chi_0 \ll 1$ and for $\theta \ll \theta_c$. This accomplishes the second task. The HE_m modes have been transformed from a cylindrical coordinate system to a rectangular coordinate system. Further, equations through , may be rewritten in terms of complex exponentials rather than the in a form that uses the sine and cosine function. Thus, in summary, replacing the sines and cosines by their complex exponential representation yields:

$$E_x = \mp iE_{in} J_{m\pm1}\left(\frac{u}{a}\rho\right) e^{\pm i(m\pm1)\varphi}$$

$$E_y = -E_{in} J_{m\pm1}\left(\frac{u}{a}\rho\right) e^{\pm i(m\pm1)\varphi}$$

$$E_z = \frac{ka}{u} E_{in} J_m\left(\frac{u}{a}\rho\right) e^{im\varphi}$$

$$B_x = E_{in} J_{m\pm1}\left(\frac{u}{a}\rho\right) e^{\pm i(m\pm1)\varphi}$$

$$B_y = \mp i E_{in} J_{m\pm1}\left(\frac{u}{a}\rho\right) e^{\pm i(m\pm1)\varphi}$$

$$B_z = \pm i \frac{ka}{u} E_{in} J_m\left(\frac{u}{a}\rho\right) e^{im\varphi}$$

where the upper sign is for the $EH_{m,p}$ modes and lower sign is for the $HE_{m,p}$ modes respectively.

Superposition of the hybrid modes to form the *LP* modes

The circularly polarized degenerate modes EH_m and HE_{-m} can be superposed to form a set of linearly polarized, *LP* modes. Recall that the transformed electric and magnetic fields for the EH_m and HE_m modes are given by equations through and the recipe for transforming to the *LP* modes will now be given. Write the transverse electric field components of the EH_m and HE_m modes (with analogous expressions for the transverse magnetic field components omitted for brevity)

$$EH_m: \quad \left\{ \begin{array}{l} E_x = -iE_{in}^{+} J_{m+1}\left(\frac{u}{a}\rho\right) e^{i(m+1)\varphi} \\ E_y = -E_{in}^{+} J_{m+1}\left(\frac{u}{a}\rho\right) e^{i(m+1)\varphi} \end{array} \right\}$$

$$HE_m: \quad \left\{ \begin{array}{l} E_x = +iE_{in}^{-} J_{m-1}\left(\frac{u}{a}\rho\right) e^{-i(m-1)\varphi} \\ E_y = -E_{in}^{-} J_{m-1}\left(\frac{u}{a}\rho\right) e^{-i(m-1)\varphi} \end{array} \right\},$$

where one has defined the undetermined constant amplitudes E_{in}^{+} for the EH_m modes and E_{in}^{-} for the HE_m modes. Next, using the fact that the EH_m modes are degenerate with the HE_{-m} modes, and using a reoccurrence relation for Bessel functions, $J_{-m-1} = (-1)^{m+1} J_{m+1}$, one one can write the transverse electric field components of the HE_{-m} modes as (with analogous expressions for the transverse magnetic field components omitted for brevity)

$$HE_{-m}: \quad \left\{ \begin{array}{l} E_x = -i(-1)^m E_{in}^{-} J_{m+1}\left(\frac{u}{a}\rho\right) e^{i(m+1)\varphi} \\ E_y = +(-1)^m E_{in}^{-} J_{m+1}\left(\frac{u}{a}\rho\right) e^{i(m+1)\varphi} \end{array} \right\}.$$

Next, absorbing the factors of $(-1)^m$ into the amplitude E_{in}^{-} by defining $(-1)^m E_{in}^{-} \stackrel{def}{=} E_{in}^{+}$ one is able to form linear combinations of modes with the same azimuthal variation, m by additions and subtractions of various transverse field components. Thus one can define the linearly polarized modes as

$$LP_m^{\pm} \stackrel{\text{def}}{=} \frac{1}{2}\left(EH_m \pm HE_{-m}\right).$$

Now, using equation with the upper sign, one can form the electric and magnetic fields of the LP^{x} modes by superposing the appropriate electric and magnetic fields of the degenerate hybrid HE_{-m} and EH_{m} modes with the same azimuthal variation, and thus the same propagation constant, k_z.

$$E_x = \frac{1}{2}\left(E_{x(HE_{-m})} + E_{x(EH_m)}\right) = -iE_{\text{in}}J_{m+1}\left(\frac{u}{a}\rho\right)e^{i(m+1)\varphi}$$

$$E_y = \frac{1}{2}\left(E_{y(HE_{-m})} + E_{y(EH_m)}\right) = 0$$

$$E_z = \frac{1}{2}\left(E_{z(HE_{-m})} + E_{z(EH_m)}\right) = \frac{ka}{u}E_{\text{in}}J_m\left(\frac{u}{a}\rho\right)\cos m\varphi$$

$$B_x = \frac{1}{2}\left(B_{x(HE_{-m})} + B_{x(EH_m)}\right) = 0$$

$$B_y = \frac{1}{2}\left(B_{y(HE_{-m})} + B_{y(EH_m)}\right) = -iE_{\text{in}}J_{m+1}\left(\frac{u}{a}\rho\right)e^{i(m+1)\varphi}$$

$$B_z = \frac{1}{2}\left(B_{z(HE_{-m})} + B_{z(EH_m)}\right) = \frac{ka}{u}E_{\text{in}}J_m\left(\frac{u}{a}\rho\right)\sin m\varphi$$

Now one can form the electric and magnetic fields of the LP^{y} modes by superposing the appropriate electric and magnetic fields of the degenerate hybrid HE_{-m} and EH_{m} modes with the same azimuthal variation, and thus the same propagation constant, k_z, by using equation with the lower sign

$$E_x = \frac{E_{x(HE_{-m})} - E_{x(EH_m)}}{2} = 0$$

$$E_y = \frac{E_{y(HE_{-m})} - E_{y(EH_m)}}{2} = -E_{\text{in}}J_{m+1}\left(\frac{u}{a}\rho\right)e^{i(m+1)\varphi}$$

$$E_z = \frac{E_{z(HE_{-m})} + E_{z(EH_m)}}{2} = -i\frac{ka}{u}E_{\text{in}}J_m\left(\frac{u}{a}\rho\right)\sin m\varphi$$

$$B_x = \frac{B_{x(HE_{-m})} - B_{x(EH_m)}}{2} = E_{in} J_{m+1}\left(\frac{u}{a}\rho\right) e^{i(m+1)\varphi}$$

$$B_y = \frac{B_{y(HE_{-m})} - B_{y(EH_m)}}{2} = 0$$

$$B_z = \frac{B_{z(HE_{-m})} + B_{z(EH_m)}}{2} = i\frac{ka}{u} E_{in} J_m\left(\frac{u}{a}\rho\right) \cos m\varphi.$$

Next, one may notice that the LP^{x} contain $m+1$ and the LP^{y} modes contain $m-1$. To simplify the notation for the *LP* modes define $l = m+1$ for the LP^{x} and $l = m-1$ for the LP^{y}.

The index for the various *LP* modes can assume all values $l \geq 0$. For example, choosing the upper sign in the definition of l, for $l = 0$, $m = +1$, and the $LP_{0,1}$ modes is thus called the fundamental mode, while for $l > 0$ the modes are called higher order. Next, one may ask where are the $m = 0$ *TE/TM* modes? For $m = 0$ this gives $l = 1$ and the *TE/TM* modes are thus not fundamental modes, but actually are higher order modes. To see this what this implies, recall that the propagation constants, k_z are obtained from equation . The values of u_l (the zeros of the Bessel function) increase for increasing values of the index l. This produces for an x-ray incident with wave vector k, a smaller magnitude for the longitudinal wave vector k_z. Since the energy carried in the mode is proportional to the longitudinal wave vector, this gives lower order modes a lower energy. In other words the fundamental mode is the mode in the lowest energy state and higher order modes are consequently in higher energy states.

To summarize, the electric and magnetic fields associated with these LP_{l}^{x} modes have the following form

$$LP_l^x : \left\{ \begin{array}{c} E_x = -iE_{in} J_l(\frac{u}{a}\rho) e^{il\varphi} \\ E_y = 0 \\ E_z = E_{in} J_{l-1}(\frac{u}{a}\rho)\cos(l-1)\varphi \\ B_x = 0 \\ B_y = -iE_{in} J_l(\frac{u}{a}\rho) e^{il\varphi} \\ B_z = E_{in} J_{l-1}(\frac{u}{a}\rho)\sin(l-1)\varphi \end{array} \right\}$$

while the electric and magnetic fields associated with these LP_{l}^{y} modes have the following form

$$LP_l^y : \left\{ \begin{array}{c} E_x = 0 \\ E_y = -E_{in} J_l(\frac{u}{a}\rho) e^{il\varphi} \\ E_z = -iE_{in} J_{l+1}(\frac{u}{a}\rho) \sin(l+1)\varphi \\ B_x = -E_{in} J_l(\frac{u}{a}\rho) e^{il\varphi} \\ B_y = 0 \\ B_z = iE_{in} J_{l+1}(\frac{u}{a}\rho) \cos(l+1)\varphi \end{array} \right\}$$

Next, one may notice that the the *LP* modes form a degenerate set. The LP_l^x modes are simply a 90^o rotation of the LP_l^y modes. Thus the LP_l^x modes look like

$$E_x = -iE_{in} J_l\left(\frac{u}{a}\rho\right) e^{il\varphi}$$
$$B_y = -iE_{in} J_l\left(\frac{u}{a}\rho\right) e^{il\varphi}$$
$$E_z = E_{in} J_{l+1}\left(\frac{u}{a}\rho\right) \cos(l+1)\varphi$$
$$B_z = E_{in} J_{l+1}\left(\frac{u}{a}\rho\right) \sin(l+1)\varphi$$

while the LP_l^y modes are thus

$$E_y = -E_{in} J_l\left(\frac{u}{a}\rho\right) e^{il\varphi}$$
$$B_x = -E_{in} J_l\left(\frac{u}{a}\rho\right) e^{il\varphi}$$
$$E_z = iE_{in} J_{l-1}\left(\frac{u}{a}\rho\right) \sin(l-1)\varphi$$
$$B_z = iE_{in} J_{l-1}\left(\frac{u}{a}\rho\right) \cos(l-1)\varphi$$

The electric field patterns associated with an *LP* mode, say the LP_l^y mode are shown in the following section.

LP Mode Electric Field Patterns

In the accompanying figures the first few of the low order $LP_{l,p}$ modes are shown, where p represents the p th zero of $J_l(u)$. The real part of the electric field for one combination of the $LP_{l,p}$ modes, namely the y-polarized $LP_{l,p}^y$ modes, is plotted according to equation , (the other set of fields, equation is simply the same as equation , rotated by 90°.) In the following the magnetic fields are omitted for clarity as well as the z-components of the electric and magnetic fields.

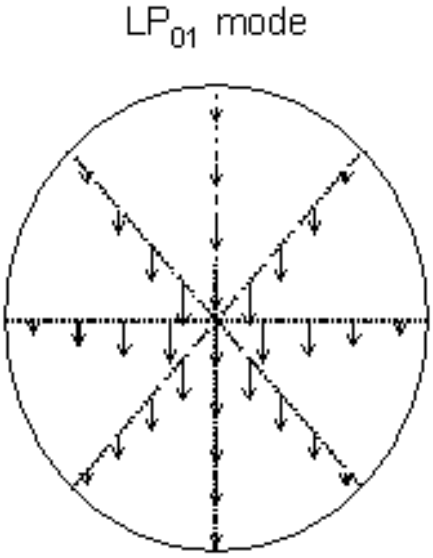

Plot of the electric field in the $LP_{0,1}^{y}$ mode in an x-ray waveguide. The electric field vectors are obtained by taking the real part of the complex electric field of the associated $LP_{0,1}^{y}$ mode. The real part of the electric field follows $E_{in}J_l(\frac{u}{a}\rho)\cos l\varphi = E_{in}J_0(\frac{u}{a}\rho)$ and the plot is for a waveguide whose radius has been normalized to 1.

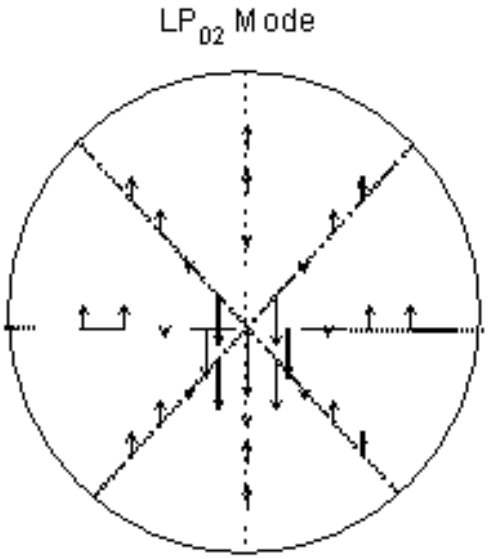

Plot of the electric field in the $LP_{0,2}$ mode in an x-ray waveguide. The electric field vectors are obtained by taking the real part of the complex electric field of the associated $LP_{0,2}^{y}$ mode. The real part of the electric field follows $E_{in}J_l(\frac{u}{a}\rho)\cos l\varphi = E_{in}J_0(\frac{u}{a}\rho)$ and the plot is for a waveguide whose radius has been normalized to 1..

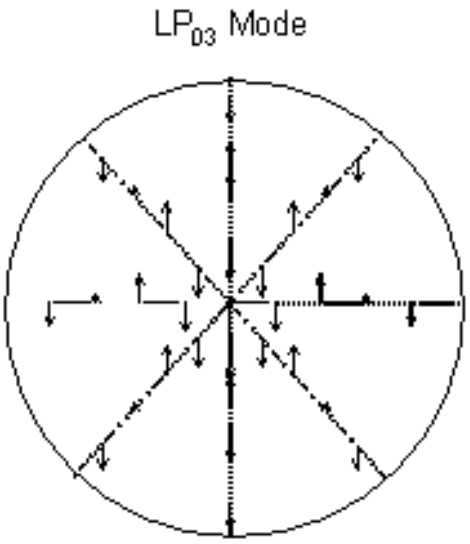

Plot of the electric field in the $LP_{0,3}$ mode in an x-ray waveguide. The electric field vectors are obtained by taking the real part of the complex electric field of the associated $LP^{y}_{0,3}$ mode. The real part of the electric field follows $E_{in}J_l(\frac{u}{a}\rho)\cos l\varphi = E_{in}J_0(\frac{u}{a}\rho)$ and the plot is for a waveguide whose radius has been normalized to 1.

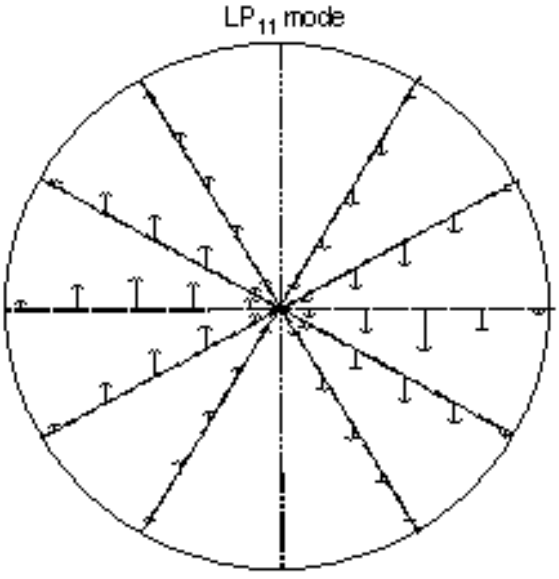

Plot of the electric field in the $LP_{1,1}$ mode in an x-ray waveguide. The electric field vectors are obtained by taking the real part of the complex electric field of the associated $LP^{y}_{1,1}$ mode. The real part of the electric field follows $E_{in}J_l(\frac{u}{a}\rho)\cos l\varphi = E_{in}J_1(\frac{u}{a}\rho)\cos\varphi$ and the plot is for a waveguide whose radius has been normalized to 1.

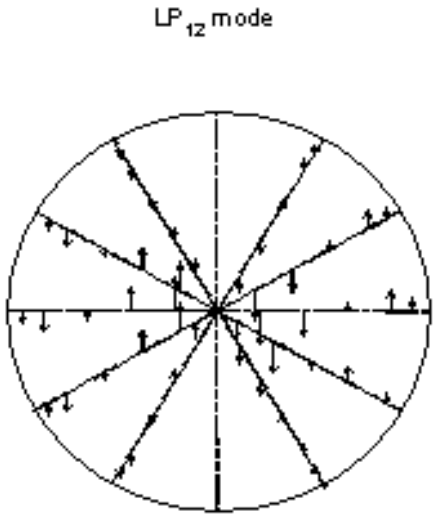

Plot of the electric field in the $LP_{1,2}$ mode in an x-ray waveguide. The electric field vectors are obtained by taking the real part of the complex electric field of the associated $LP^{y}_{1,2}$ mode. The real part of the electric field follows $E_{in}J_l(\frac{u}{a}\rho)\cos l\varphi = E_{in}J_1(\frac{u}{a}\rho)\cos\varphi$ and the plot is for a waveguide whose radius has been normalized to 1.

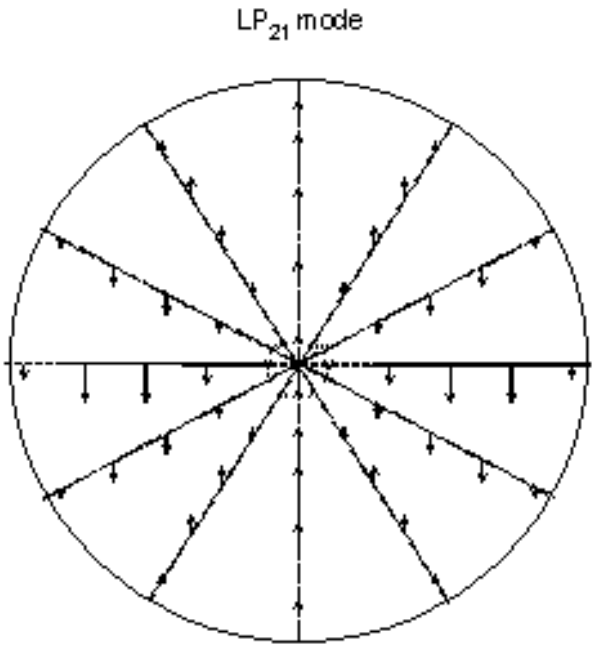

Plot of the electric field in the $LP_{2,1}$ mode in an x-ray waveguide. The electric field vectors are obtained by taking the real part of the complex electric field of the associated $LP^{y}_{2,1}$ mode. The real part of the electric field follows $E_{in}J_l(\frac{u}{a}\rho)\cos l\varphi = E_{in}J_2(\frac{u}{a}\rho)\cos 2\varphi$ and the plot is for a waveguide whose radius has been normalized to 1.

In the following figures the real part of the electric field is plotted for various $LP^{y}_{l,p}$ modes. Recall that the y-polarized electric field is given by equation and the associated real part is obtained by taking

$\mathrm{Re}(E_y) \propto \mathrm{Re}\left(-J_l(\frac{u}{a}\rho)e^{il\varphi}\right) \propto -J_l(\frac{u}{a}\rho)\cos l\varphi$. In figure 3.8, for example, notice that the field is that of an y-polarized $LP_{0,1}$ mode, whose real part of the electric field in the y-direction is proportional to $-J_0(\frac{u}{a}\rho)$. The real part of the electric field follows a Bessel function in the radial direction and has a maximum at the center of the guide and decreases to a small value at the glass boundary. Around the axis of the guide the mode follows a cosine pattern, given by $\cos(l\varphi)$. Here, $l = 0$ and $\cos(l\varphi) = 1$, thus the magnitude of the electric field around the axis of the waveguide is constant in the y-direction for a given radius, ρ, from the center of the waveguide. Further the electric field decreases from its maximum value to nearly zero along any radial direction as described by the Bessel function.
Next one could ask where the energy is contained in the waveguide. Since the energy carried by an x-ray is proportional to the square of the electric field, examination of figure 3.8 for the $LP_{0,1}$ mode, shows that the energy is most nearly contained along the axis of the waveguide. As one moves toward the outer edges of the waveguide the energy flowing there decreases. Since the electric field, which is proportional to $J_0(\frac{u}{a}\rho)$

decreases, thus the energy contained near the edges of the waveguide is very small.

Figures 3.9 and 3.10 show a $LP_{0,2}$ and a $LP_{0,3}$ mode respectively. These figures show patterns similar to those of figure 3.8 Again the electric fields vary as $-J_0(\frac{u}{a}\rho)$ in the radial direction and in the azimuthal direction for a given radius from the origin, the electric field is constant in magnitude. Further the electric field oscillates from the center of the waveguide toward the glass boundary. Thus the energy contained in the waveguide is most nearly contained close to the axis of the waveguide and decreases as one moves along any radial direction toward the glass boundary.

In figures 3.11 and 3.12 the the electric and magnetic field variation is with the cosine of φ while figure 3.13 varies with cosine 2φ. Further the fields vary in the radial direction as a Bessel function, $-J_l(\frac{u}{a}\rho)$, and the electric fields increase from zero to a maximum halfway from center of the waveguide and then decreases back to zero along any radial direction described by the Bessel function. In figure 3.11, for example, most of the energy is flowing where the electric field is a maximum, which by inspection, occurs roughly halfway between the center and glass capillary walls of the waveguide. Similar features can be seen in figures 3.11 and 3.12.
Further, not shown in the figures are places where the electric field vanishes. These places are called nodes. One set of nodes are radial and are given where the radial variation of the field vanishes. These radial nodes described by $J_l(\frac{u}{a}\rho) = 0$, are fixed. The other set of nodes are obtained from where the azimuthal variation of the electric fields ($\cos l\varphi$) vanishes and these rotate in time around the z-axis of the waveguide.
Although it cannot be seen in figures 3.8 through 3.13, the radial solution does not vanish at the vacuum-glass boundary. In the glass the electric and magnetic fields are described by a modified Bessel function and the fields exponentially tail-off.

Photoelectric Absorption of the LP_l Modes Along the Waveguide

The photoelectric absorption of a waveguide mode as it travels down the guide is due mainly to penetration of the mode into the glass. Modes for which $\theta \ll \theta_c$ penetrate less and thus experience less absorption.

Absorption coefficients are calculated from the imaginary part of the longitudinal wave vector, k_z. Since the susceptibility has both a real and an imaginary component given by

$$\chi_0 = \chi_r + i\chi_i,$$

V becomes

$$V = ak\sqrt{-\chi_r - i\chi_i} = ak\sqrt{-\chi_r}(1 + i\delta)^{\frac{1}{i}}$$

where δ is defined as

$$\delta = \frac{\chi_i}{\chi_r}.$$

Next using the definition for u^2 (equation) with the condition that $k^2 \left(= \frac{\omega^2}{c^2}\right)$ must be real, one can write:

$$\frac{1}{a^2}\left(u_{lr}^2 - u_{li}^2\right) + \frac{2i}{a^2}(u_{lr}u_{li}) + \left(k_{zr}^2 - k_{zi}^2\right) + 2i(k_{zr}k_{zi}) = k^2.$$

Since $k^2 \left(= \frac{\omega^2}{c^2}\right)$must be real, the imaginary part of equation must vanish identically. Thus

$$\frac{2i}{a^2}(u_{lr}u_{li}) + 2i(k_{zr}k_{zi}) = 0,$$

or,

$$k_{zi} = -\frac{1}{a^2}\frac{u_{lr}}{k_{zr}}u_{li}.$$

For modes in which $\theta \ll \theta_c$, recall that $\bar{u}_l$ for the $LP_{l,p}$ modes are given by equation and the imaginary part of $\bar{u}_{l,p}$, $\mathrm{Im}\,\bar{u}_{l,p} = \bar{u}_{l,p,i}$, is then for the $LP_{l,p}$ modes:

$$\bar{u}_{l,p,i} = \frac{u_{l,p}}{2i}\left(\frac{V - V^*}{V_r^2}\right),$$

Since χ_r is typically larger than χ_i, δ is small. Thus equation may be approximated by:

$$V \approx ak\sqrt{-\chi_r}\left(1 + \frac{i}{2}\delta\right).$$

Therefore, the imaginary part of the longitudinal wave vector can be written:

$$k_{zi} = -\frac{1}{a^2}\frac{u_{lr}}{k_{zr}}u_{li} \approx -\frac{u_{lr}^2}{2a^2k_{zr}}\frac{\chi_i}{V_r\chi_r}$$

where δ has been replaced by its definition, equation . Furthermore equation , with $V^2 \propto \chi$, becomes for the $LP_{l,p}$ modes:

$$u_{li} \approx -\frac{u_{l,p}}{2i}\left(\frac{V_r i\delta}{V_r^2 + V_i^2}\right) \approx -\frac{u_{l,p}}{2}\left(\frac{\delta}{V_r}\right).$$

If one further approximates $k_{zr} \approx k$ which is approximately valid for small χ, and further recalling that $V_r \approx ak\sqrt{-\chi_r}$, one obtains for the $LP_{l,p}$ modes:

$$k_{zi} \approx \frac{k}{2}u_{l,p}^2\frac{\chi_i}{V_r^3} = \frac{k\chi_i}{2}\frac{u_{l,p}^2}{V_r^3}.$$

Defining the effective linear absorption coefficient for glass to be $\mu = k\chi_i$ and since $\mu_{l,p} = 2k_{zi}$, one

obtains the effective linear absorption coefficient for each mode for $\theta \ll \theta_c$:

$$\mu_{l,p} = 2k_{zi} \approx \mu \frac{u_{l,p}^2}{V_r^3}.$$

The $\mu_{l,p}$s that appear in equation depend on the x-ray energy. For Cu K_α x rays with an energy of 8 keV in borosilicate glass, μ_{Cu} =72.16 cm^{-1}, while for oxygen x rays with an energy of 522 eV, μ_O =9331.4 cm^{-1}. Since the x-ray intensity varies as $e^{-\mu t}$, where t is the penetration depth in the material, the $\frac{1}{e}$ decay length is the distance that the x ray travels before before its intensity decreases by a factor of $\frac{1}{e}$. This decay length is proportional to $\frac{1}{2k_{zi}}$ which is simply $\frac{1}{\mu}$. The effective linear absorption coefficients (in m^{-1}) and the $\frac{1}{e}$ decay lengths (in m) for several modes of Cu K_α x rays in a 5 micron waveguide are calculated in the tables 3.4 and 3.4 above (while for O x rays the effective linear absorption coefficients and $\frac{1}{e}$ decay lengths in a 5 micron waveguide are given in tables 3.6 and 3.7 respectively, below.)

$\mu_{l,p}$	$p = 1$	$p = 2$	$p = 3$
$l = 0$	6.0×10^{-5}	3.2×10^{-4}	7.7×10^{-4}
$l = 1$	1.5×10^{-4}	5.1×10^{-4}	1.1×10^{-3}
$l = 2$	2.7×10^{-4}	7.3×10^{-4}	1.4×10^{-3}

\caption{Effective linear absorption coefficients (in m{-1}) for copper x rays.\label{key}}

L	1	2	3
0	16667	3175	1299
1	6667	1961	909
2	3704	1370	714

\caption{(1/e) decay lengths (in m) for the copper x rays.\label{key} }

$\mu_{l,p}$	$p = 1$	$p = 2$	$p = 3$
$l = 0$	7.7×10^{-3}	4.1×10^{-2}	1.0×10^{-1}
$l = 1$	2.0×10^{-2}	6.5×10^{-2}	1.4×10^{-1}

$l = 2$	3.5×10^{-2}	9.4×10^{-2}	1.8×10^{-1}

\caption{Effective linear absorption coefficients (in m{-1}) for oxygen x rays.\label{key}}

L	1	2	3
0	130	25	10
1	51	15	7
2	29	11	6

\caption{(1/e) decay lengths (in m) for oxygen x rays.\label{key}}

Let's consider for example, the $LP_{2,1}$ mode for the Cu K_α x rays. The $\frac{1}{e}$ decay length for the $LP_{2,1}$ mode, from table 3.6, is approximately 3700 meters. This is a very large propagation distance for the x-ray to travel. This striking result is probably not a realizable result in a practical x-ray waveguide. Further, equation

has $\mu_{l,p}$ proportional to $\frac{1}{a^3}$, for a waveguide of radius *a*. This could be a potentially dangerous result. The waveguides would need to be very narrow in order for waveguide effects to be relevant. These large propagation distances are most likely due to the low order modes being contained almost entirely within the waveguide, and thus the low order modes experiences very little penetration into the glass. As the mode number increases, so too do the absorptive losses of the x-ray to the glass capillary walls. The x rays strike the glass walls at larger angles and thus are more likely to be absorbed by the glass capillary.
Another important energy loss mechanism that the x-ray experiences is loss due to rough surfaces. Thus far, the waveguide has been assumed to be perfectly smooth. In a real x-ray waveguide, the walls of the waveguide are most likely going to be rather rough. The effects of surface roughness on the propagation of the x-ray needs to be studied and will be revisited in chapter 6 where a model for surface roughness will be proposed. Chapter 6 will incorporate the effects of surface roughness effects and new $\frac{1}{e}$ decay lengths will be calculated and compared to the $\frac{1}{e}$decay lengths calculated above.

Conclusion

For the circular dielectric waveguide, the modes were obtained by solving Maxwell's equations. The transverse fields were expressed in terms of the longitudinal fields and wave equations for the longitudinal electric and magnetic fields were solved by separation of variables. Next boundary conditions on the wave function solutions were imposed and the characteristic equation for the modes was derived. For the $m = 0$ case the modes were found to exhibit properties of the *TE* and *TM*. The modes ($m \neq 0$) are neither *TE* or *TM* but are termed hybrid and denoted by EH_m and HE_m.
The propagating modes were obtained by solving Maxwell's equations. Thus, polarization effects are fully taken into account. The transverse fields were expressed in terms of the longitudinal fields and wave equations for the longitudinal electric and magnetic fields were solved by separation of variables. Next boundary conditions on the wave function solutions were imposed and the characteristic equation for the

modes was derived.

In the limit that χ_o is much smaller than unity, the hybrid EH_m and HE_m modes were found to obey the same characteristic equation for the change of indices $m \rightarrow -m$. This degeneracy was exploited and used to superpose the hybrid circular modes to form a set of nearly linearly polarized or LP_l modes. There were found two sets of *LP* modes denoted respectively LP^x and LP^y. Only the LP^y modes were investigated since the LP^x modes are simply a 90^0 rotation of the LP^y modes. One could associate with the modes an orbital angular momentum (the φ-dependence of the electric and magnetic fields) and a spin. The modes have a total angular momentum of m. The right or left circular polarization (the rotation of the electric fields at a given point in space) is associated with the helicity or spin of the photons. Spin is usually associated with quantum mechanics. Here one has a purely classical example that involves spin.

The real part of the electric field for various LP_l^y modes was plotted for a waveguide of an arbitrary radius.

For the low order $LP_{0,p}$ family of modes it was found that the energy flow was at the center of the waveguide and decreased as one moved from the center of the waveguide toward the glass boundary along any radial direction. For the higher order modes, $l > 0$, it was found that the energy flow was not near the center of the waveguide. It was found by inspection that most of the energy was flowing at increasing radial distances from the center of the waveguide and ultimately decreased as one approached the glass boundary along any radial direction.

There are two energy loss mechanisms that the x-ray experiences. Photoelectric absorption effects were investigated and losses due to photoelectric absorption were calculated. This was done by calculating the imaginary part of the dielectric susceptibility. The imaginary part of the wave vector was then calculated and used to calculate the $\frac{1}{e}$ decay lengths for the x rays as they travel down the fiber. It was found that the lowest order modes (the $LP_{0,p}$) propagate on the order of 10 kilometers for higher energy x rays, while for lower energy x rays the propagation distances were on the order of hundreds of meters. While these propagation distances may be a shocking result, in practical x-ray fibers this is probably not a realizable feature.

The second energy loss mechanism is due to surface roughness. It has been assumed thus far that the glass capillary fibers have perfectly smooth walls. A more realistic treatment of the x-ray capillary needs to include losses to the x-ray energy from the x-ray striking a rough glass surface. A model of surface roughness needs to be developed (chapter 6) and new $\frac{1}{e}$ decay lengths for the x rays as they travel down the fiber need to be calculated and compared to the results stated above.

Excitation at the Waveguide Entrance

Introduction

Having derived and calculated the modes that can propagate along the waveguide, one wants in this chapter

to investigate the extent to which the various modes are excited by an externally incident plane wave. In particular, one is interested in finding under what conditions can one selectively excite a subset of the modes, or perhaps a single mode. This amounts to coupling at the waveguide entrance the incident plane wave, directed at an arbitrary angle of incidence, to the launching of the LP_l field modes that propagate in the waveguide. In order to accomplish the task coupling the plane wave incident at the waveguide entrance and the LP_l modes launched, the modes must be first normalized.

Normalization of the Incident Plane Wave and the LP_l Modes

Normalization of the Incident Plane Wave

In order to couple the incident plane to the modes launched at the waveguide entrance the plane wave solutions as well as the electric and magnetic fields that describe the modes need to be normalized. For the plane wave in free space, one can assume the electric and magnetic fields are given by:

$$\vec{E}(\vec{r},t) = \vec{E}e^{i\left(\vec{k}\vec{r}-\omega t\right)},$$

$$\vec{B}(\vec{r},t) = \vec{B}e^{i\left(\vec{k}\vec{r}-\omega t\right)}.$$

For small θ, $k_z = k\cos\theta \approx k\,(= \frac{\omega}{c})$, $\vec{E} = \hat{\epsilon}_1 E_0$, $\vec{B} = \hat{\epsilon}_2 E_0 = \hat{n} \times \vec{E}$, where $\hat{\epsilon}_1$, $\hat{\epsilon}_2$, and $\hat{n}$ are three mutually perpendicular unit vectors and E_0 is a constant. The time averaged flux of energy is given by the Poynting vector S and may be written as:

$$\vec{S}(\vec{r}) = \frac{c}{8\pi}\mathrm{Re}\left[\vec{E}(\vec{r}) \times \vec{B}^*(\vec{r})\right],$$

which can be simplified, in the case of a plane wave, by using equations and , to read:

$$\vec{S} = S_z\hat{n} = \frac{c}{8\pi}\left|E_0\right|^2\hat{n}.$$

To fix the constant E_0 one imposes a normalization condition. Here, the normalization condition is chosen such that the flow of energy is 1 photon of energy $\hbar\omega$ per unit time into the area πa^2 of the capillary. Performing the normalization for the incident plane wave produces,

$$1\frac{\text{photon}}{\text{sec}} = \int \vec{S}(\vec{r}) \cdot d\vec{a} = \frac{1}{\hbar\omega}\int_0^{2\pi}\int_0^a \frac{c}{8\pi}|E_0|^2\hat{n} \cdot d\vec{a} = \frac{1}{\hbar\omega}\frac{c|E_0|^2}{8\pi}\pi a^2\cos\theta.$$

Since for small angles θ, $\cos\theta \sim 1$, equation yields,

$$|E_0| = \sqrt{\frac{8\hbar\omega}{ca^2}}.$$

The incident plane wave energy density, given by the Poynting vector, is

$$\vec{S} = S_z \hat{n} = \frac{\hbar\omega}{\pi a^2}\hat{k}.$$

Normalization of the LP_l^y Mode Solutions

This section describes the normalization procedure for the LP_l modes. One needs only to consider the LP_l^y polarizations of the modes since the analysis of the LP_l^x polarizations is analogous. Thus in what follows, the superscript y of the LP mode polarization will be omitted. Up to now, there has been an overall constant that describes the amplitude of the modes, E_{in}. To fix this constant, one also normalizes the LP_l mode solutions to a fixed, but arbitrary, flux of 1 $\frac{\text{photon}}{\text{sec}}$. The Poynting vector, using the electric and magnetic fields for the LP_l modes, equation , can be simplified to

Performing the normalization for the LP_l modes over the aperture of the waveguide gives:

$$E_{\text{in}} = \sqrt{\frac{\hbar\omega}{ca^2}}\frac{1}{J_{l+1,p}(u_{l,p})}.$$

Excitation by an Externally Directed Plane Wave at the Waveguide Entrance

Having the electric and magnetic fields of the LP_l modes normalized, one may now calculate the excitations of the waveguide modes by directing, at some angle θ with respect to the normal to the waveguide entrance, an externally directed plane wave of frequency ω. The extent to which various modes are excited will be investigated as a function of the incident angle θ.

Here it is assumed that the only portion of the incident plane wave that contributes to the LP_l mode's excitation will be that which is incident on the waveguide aperture. Since the susceptibility is small ($\chi \sim 10^{-5}$), the contribution of the portion incident on the glass can therefore be neglected. Without loss of generality, one may assume that the incident plane wave lies in the $y-z$ plane, $(k_x = 0)$, and where the waveguide opening is taken to be at $z = 0$. In other words,

$$E_0 e^{i\left(\vec{K}\cdot\vec{r}-\omega t\right)} = E_0 e^{i(k_x x+k_y y+k_z z-\omega t)} = \sqrt{\frac{8\hbar\omega}{ca^2}}\, e^{i(k_y y-\omega t)},$$

where E_0 has been replaced by equation .

Recall that the electromagnetic boundary conditions used in chapter 3 were that the tangential components of $\vec{E}$ and $\vec{H}$ (along with the normal components of $\vec{D}$ and $\vec{B}$) must be continuous across the boundary. This requirement gives the tangential components of $\vec{E}_{\parallel} = E_y\hat{y}$ and $\vec{H}_{\parallel} = B_x\hat{x}$ for non-magnetic media, while the normal components are given as $\vec{D}_{\perp} = (1+\chi_0)E_z\hat{z}$ and $\vec{B}_{\perp} = B_z\hat{z}$. At the $z = 0$ boundary there will be both a reflected as well as a transmitted wave. The transmitted wave will be that used to excite the various *LP* modes. Since the susceptibly is small ($\chi \sim 10^{-5}$) the reflected waves at the boundary as well as the evanescent waves in the glass are negligible hence will be neglected in the present study. In other words the modes will propagate with nearly the same propagation constant as the plane wave.

In order to determine the extent to which various *LP* modes are excited, one sets the electric field of the incident plane wave equal to the sum of the linearly polarized modes wavefunctions weighted by their respective excitation coefficients, $C_{l,p}$, at $z = 0$. Equating electric field of the incident plane wave to the electric field of the linearly polarized modes launched the waveguide entrance, produces:

$$\sqrt{\frac{8\hbar\omega}{ca^2}}\, e^{i\eta\frac{\rho}{a}} = \sqrt{\frac{8\hbar\omega}{ca^2}}\, e^{i\frac{\eta}{a}\rho\sin\varphi} = \sum_{l,p} C_{l,p}E_y^{l,p} =$$

$$\sum_{l,p} 2\sqrt{\frac{\hbar\omega}{ca^2}}\,\frac{1}{J_{l+1,p}(u_{l,p})}C_{l,p}J_{l,p}\left(\frac{u_{l,p}}{a}\rho\right)e^{il\varphi},$$

where $\eta \overset{\text{def}}{=} k_y a = ka\sin\theta$ for the plane wave incident at angle θ, and the excitation coefficients need to be extracted. The left hand side of equation can be expanded in a Bessel Series. From Arfken,

$$e^{ix\sin\varphi} = \sum_{l'=-\infty}^{\infty} J_{l'}(x)e^{il'\varphi}.$$

Therefore, one has

$$\sqrt{\frac{8\hbar\omega}{ca^2}}\sum_{l'=-\infty}^{\infty} J_{l'}\left(\frac{\eta}{a}\rho\right)e^{il'\varphi} = \sum_{l=-\infty}^{\infty}\sum_{p=-\infty}^{\infty} 2\left(\sqrt{\frac{\hbar\omega}{ca^2}}\,\frac{1}{J_{l+1}(u_l)}\right)C_{l,p}J_{l,p}\left(\frac{u_{l,p}}{a}\rho\right)e^{il\varphi}.$$

The excitation of a *LP* $_l$ mode is defined as the square of the coefficients $C_{l,p}$. To extract the excitation coefficients one multiplies the right and left hand sides (denoted by RHS and LHS respectively) of equation by the complex conjugate and integrates over the cross sectional area of the waveguide. This produces for the right hand side of equation ,

$$\mathrm{RHS} = 2\sqrt{\frac{\hbar\omega}{ca^2}}\frac{1}{J_{l+1,p}(u_{l,p})}\sum_{l,p}\sum_{l',p'}C_{l,p}\int_0^a J_{l,p}\left(\frac{u_{l,p}}{a}\rho\right)J_l\left(\frac{u_{l',p'}}{a}\rho\right)\rho d\rho\int_0^{2\pi}e^{i(l-l')\varphi}.$$

The integral over φ gives $2\pi\delta_{l,l'}$. Equation now may be expressed as after performing the integral over ρ,

$$\mathrm{RHS} = 2\pi a^2\sqrt{\frac{\hbar\omega}{ca^2}}\frac{1}{J_{l+1}(u_l)}C_l J_{l+1}^2(u_l)$$

In a similar manner after some algebra, produces for the left hand side:

$$\mathrm{LHS} = 2\pi a^2\sqrt{\frac{8\hbar\omega}{ca^2}}\int_0^1 J_l(\eta r)J_l(u_l r)rdr,$$

where $\frac{\rho}{a} = r$. Equating the LHS and the RHS (equations and) one obtains an equation for the excitation coefficients $C_{l,p}$:

$$C_{l,p} = \frac{2}{J_{l+1,p}(u_{l,p})}\int_0^1 J_l(\eta r)J_l(u_{l,p}r)rdr.$$

For Cu K_α x-rays, the excitation coefficients in equation is computed for input angles θ ranging from -50 μrad to 50 μrad, and the excitation, $C_{l,p}^2$, is plotted in the figures 4.1 and 4.2 below. These figures demonstrate the extent to which the LP_{l} modes may be preferentially excited by the incident plane wave. For example, for Cu K_α x rays, with an energy of 8 keV, incident at an angle of 0 μrad, one can see that from figure 4.1, about 70% of the wave will appear in the $LP_{0,1}$ mode, 13% of the wave will appear in the $LP_{0,2}$ mode, 6% of the wave will appear in the $LP_{0,3}$ mode, 3% of the wave will appear in the $LP_{0,4}$ mode, and 1% of the wave will appear in the $LP_{0,5}$ mode.
In terms of the flow of energy along the longitudinal axis of the waveguide, the majority of energy flow for the $LP_{0,p}$ family of modes is contained near the center of the waveguide. The energy flow can be calculated, as a function of waveguide radius, by evaluating equation . Since the energy flow is given by the Poynting vector, equation , is proportional to the square of the electric field, and thus where the electric field is larger, more energy will be flowing. Figures 3.8 through 3.10 corroborate this result, namely that most of the energy in the $LP_{0,p}$ family of modes is flowing along the longitudinal axis of the waveguide for small values of ρ. As one moves toward larger radii, the electric field vectors are smaller and thus the energy flowing at these larger radii is smaller.

At exactly 0 μrad none of the higher l modes will be excited by the incident plane wave. To excite the higher order modes, one needs to change the angle of incidence of the incident plane wave. From figures 4.1

and 4.2, at say an angle of incidence of 5 μrad, the energy contained in the modes is shared primarily between the LP_{01} mode and the higher order $LP_{1,1}$, $LP_{1,2}$, and $LP_{1,3}$ modes. Again, most of the energy carried in these *LP* modes finds itself flowing again near the center of the waveguide. As one moves to the outer edges, the higher modes have a lower excitation and the energy these modes carries decreases rapidly. This can be corroborated by examining figures 3.11 through 3.13.

Of course, one does not have to use Cu K_α x rays. In figure 4.3 the x-ray energy is varied as a function of input angle. In this figure, the excitation of the fundamental $LP_{0,1}$ mode is plotted versus input angle for various x-ray energies ranging from 0.5 keV (soft x-rays) to 8 keV (hard x-rays). The x-ray energy enters the calculation of the excitation $|C_{l,p}|^2$ through the dimensionless parameter, $\eta = ka\sin\theta$. By changing the wave vector k, one in essence changes the x-ray energy. Here one finds that the individual excitations of the modes remain unchanged. In other words, the $LP_{0,1}$ mode has an excitation of approximately 70% independent of the x-ray energy used to excite the $LP_{0,1}$ mode. However, there is a larger input angle cone as the energy of the x-ray is lowered because the critical angle, which is inversely proportional to the x-ray energy (see for example equations and), is much larger. Thus for lower energy x rays, incident at an angle θ, the input cone is much larger. This larger input cone produces the broad spreading of the excitation curve for lower energy x rays and the narrow excitation curve for higher energy x rays.

Next one could ask, how many modes can be excited at a given angle of incidence? In order to answer this question, one can plot, for example, several of the lowest order family of modes, the $LP_{0,p}$ modes versus input angle as shown in figure 4.4 below.

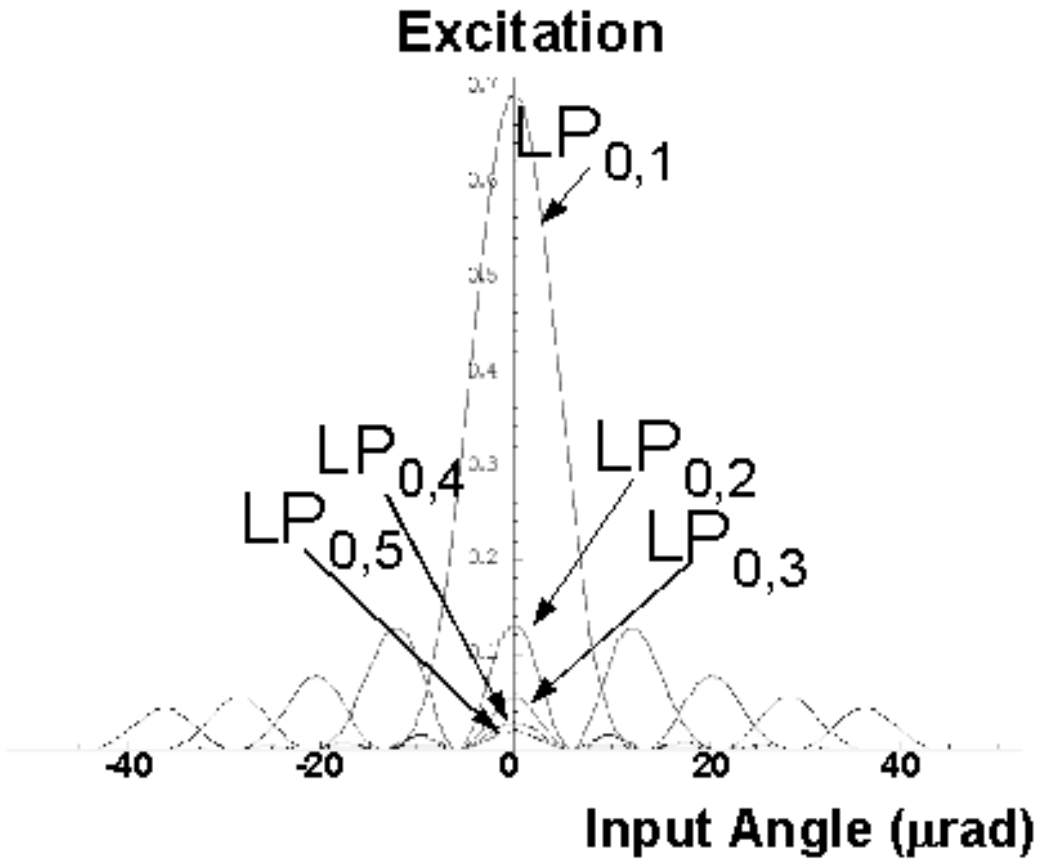

Excitation of the zeroth order linearly polarized modes $LP_{0,1}$, $LP_{0,2}$, $LP_{0,3}$, $LP_{0,4}$, and $LP_{0,5}$ versus input angle in μradians. The excitations are $|C_{0,p}|^2$ from equation .

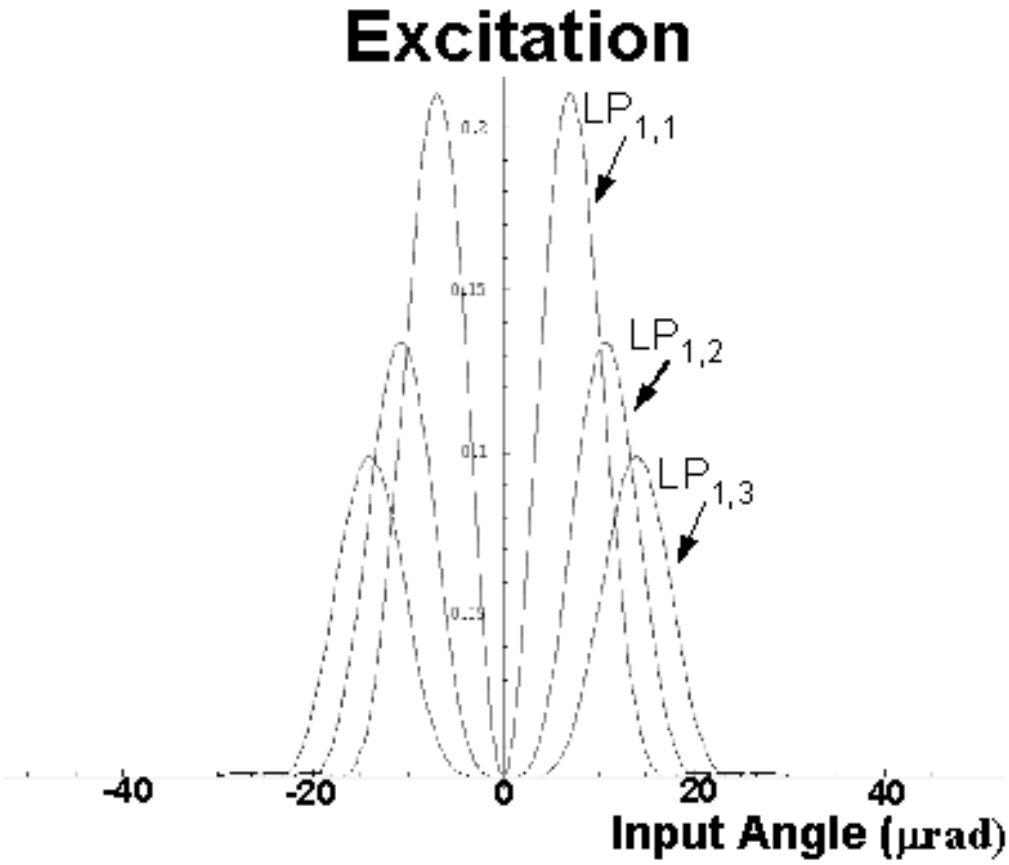

Excitation of the first order linearly polarized modes $LP_{1,1}$, $LP_{1,2}$, and $LP_{1,3}$ versus input angle in μradians. The excitations are $|C_{1,p}|^2$ from equation .

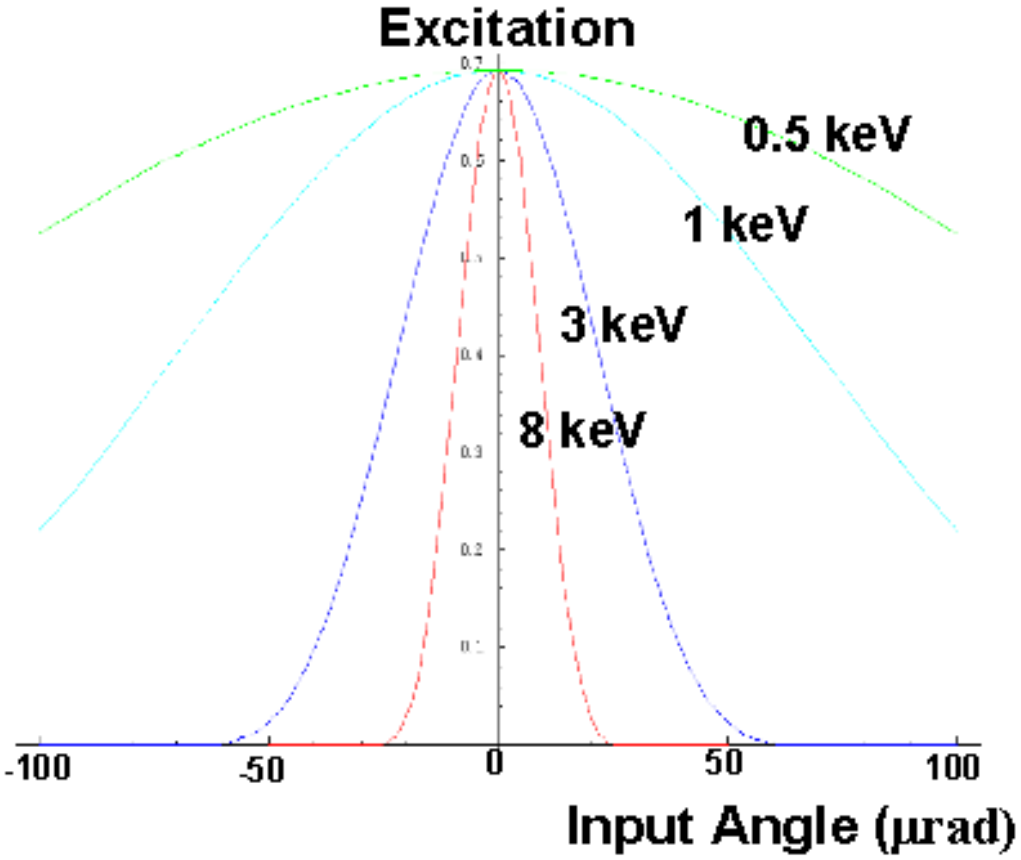

Excitation $|C_{0,1}|^2$ of the zeroth order linearly polarized mode $LP_{0,1}$ versus input angle in μradians for various x-ray energies in keV.

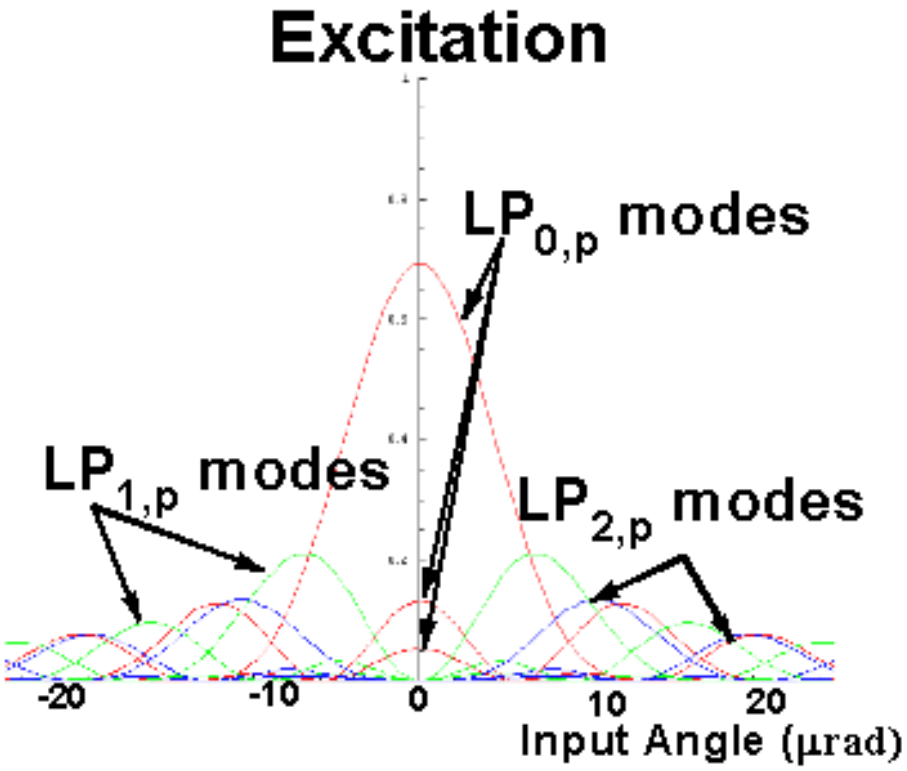

Plot of the excitation of a LP_{l} mode versus input angle in μradians for Cu K_{α} x rays. This plot is used to determine the approximate number of modes that propagate at a given input angle. It should be noted here that exept for the horizontal scale this plot is valid for any energy x-ray.

Examination of figure 4.4 shows that at an angle 0 μradians, the x rays are shot directly down the center of the waveguide. Here, for example, one can excite with an excitation greater than 1%, 6 modes, namely $LP_{0,1}$ through $LP_{0,6}$. However, no x-ray source is perfectly collimated. There will be some angular divergence inherent in the x-ray beam. Thus some mode mixing is bound to happen. As one can see from examining figure 4.4, at say an angle of 5 microradians, the $LP_{0,1}$ mode is excited with a probability of about 40%, the $LP_{1,1}$ mode is excited with a probability of about 15%, the $LP_{0,2}$ and $LP_{1,2}$ modes are excited with almost equal probabilities, namely 3%, along with some higher order modes, namely those of the $LP_{2,p}$ family.

Conclusion

The excitation of various *LP* modes that were excited by an external incident plane wave were calculated. In order to calculate the excitation, the *LP* modes and incident plane wave were normalized to an flux of energy of 1 $\frac{\text{photon}}{\text{sec}}$ into the cross sectional area of the waveguide.

The x-ray energy was varied for the lowest order, $LP_{0,1}$ mode. Here it was found that the excitation of the $LP_{0,1}$ mode is 70% and is independent of the x-ray energy. Since the critical angle increases with decreasing x-ray energy, one finds for soft x rays the input angle cone is larger than the input angle cone for hard x rays.

The number of modes that are excited was also investigated for the case of the lowest order $LP_{0,p}$ modes. It was found that for an arbitrary value of the excitation, namely greater than 1%, 6 modes propagate at exactly 0 μradians. At increasing angles of incidence higher order modes are also excited and thus propagate down the waveguide. In this thesis the x-ray beam is highly collimated and in practice the x-ray beam has an angular divergence and some mode mixing is bound to occur.

Diffraction at the Waveguide Exit: A New Approach to Vector Diffraction Theory

Introduction

Having launched modes into the waveguide, one is interested in how those modes that reach the waveguide end couple to the outside world. This amounts to calculating the diffraction pattern produced on a "detector"

at a point *P* far from the waveguide. The diffraction pattern, which is a Fraunhofer diffraction pattern, is similar to that of a diffraction pattern produced by a plane wave incident on a circular aperture. The calculation of the vector diffracted fields based on the vector analogue of the Kirchhoff diffraction formula is very difficult in all but the simplest geometries. This difficulty has induced one to seek an alternative approach to diffraction. The approach used in this chapter follows a logic similar to the asymptotic reciprocity theorem (ART) to calculate the diffracted fields.

The usual form of the principle of reciprocity states that everything else being equal, the amplitude of a wave at some point *A* due to a source located at another point *B* is equal to the amplitude of a wave at point *B* due to a source located at a point *A*. In other words there is a symmetry between the source and field points. In terms of waveguide terminology, reciprocity can be stated in the following manner: the diffracted fields produced on a detector at a point *P* due to a source located at the waveguide exit will be equal to the amplitudes of the fields at the waveguide exit due to a source located at the point *P*. The drawback is that the usual form of the reciprocity theorem refers to the exchange between the source and field points. In other words, usually one has a source of spherical waves, perhaps in a medium, and one is interested in the fields at some distance far away from the source where at these far distances the fields are typically plane wave. The result Caticha [Caticha] obtains is an asymptotic form of the reciprocity theorem that gives the asymptotic radiation fields directly in terms of the source. The approach taken here (section 5.2) allows computation of the asymptotic diffracted fields directly in terms of the fields at the exit opening of the waveguide. The source is effectively being replaced by the fields at the waveguide exit. The net result is a formalism that is equivalent to the Kirchhoff vector diffraction formula and is considerably more convenient because it is better suited to plane wave geometry.

As a first pedagogical example one calculates the diffracted fields for a well known case, namely that of a plane wave incident on a circular aperture (section 5.3). The result for the diffracted fields due to a plane wave incident on a circular aperture will coincide with the well known result given in, for example, Jackson. This is a very a remarkable result. Historically, calculations involving standard vector diffraction has been very labor intensive and difficult to apply in all but a few special circumstances. The ART reproduces the classic far field results for vector diffraction of a plane wave by a circular aperture in just a couple of lines of calculations rather than pages of calculations using standard vector diffraction theory. Being able to reproduce these results using the asymptotic reciprocity theorem, as opposed to the standard vector theory of diffraction used in Jackson or Born and Wolf, provides a new and very powerful techniques for calculating the far field diffracted fields. The asymptotic reciprocity theorem provides a clean and easy to follow recipe for calculating these diffracted fields for the classic textbook cases as well as for calculating diffracted fields for highly non-trivial fields in arbitrarily shaped guiding structures and geometries, such Bessel waves incident in cylindrical waveguides.

Derivation of the Asymptotic Reciprocity Theorem

The reciprocity theorem in physics states that under optimized conditions, the power flow from a wave at a point A due to a source at a point B is equal to the power flow at B due to a source at A. Reciprocity theorems find their way into all sorts of fields of physics. In electrodynamics, reciprocity is usually attributed to Lorentz who made extensive use of it in studying antennae. In this thesis the reciprocity theorem will be used to study vector x-ray diffraction from the end of a waveguide.

Starting from Maxwell's equations

$$\vec{\nabla} \times \vec{E} = ik\mu\vec{H}$$

$$\vec{\nabla} \times \vec{H} = ik\vec{D} + \frac{4\pi}{c}\vec{J},$$

where $k = \frac{\omega}{c}$. Equations and govern the fields generated by the sources J. The method relies on introducing the auxiliary fields called connecting fields generated by the sources J_c and are found in an analogous way from Maxwell's equations

$$\vec{\nabla} \times \vec{E}_c = ik\mu\vec{H}_c$$

$$\vec{\nabla} \times \vec{H}_c = ik\vec{D}_c + \frac{4\pi}{c}\vec{J}_c.$$

The source J generates the fields $\vec{E}$ and $\vec{H}$ and a source J_c of the same frequency gives rise to the fields $\vec{E}_c$ and $\vec{H}_c$. Next use the identity

$$\vec{\nabla} \cdot \left(\vec{E} \times \vec{H}_c\right) = \vec{H}_c \cdot \left(\vec{\nabla} \times \vec{E}\right) - \vec{E} \cdot \left(\vec{\nabla} \times \vec{H}_c\right).$$

Since $\vec{D} = \varepsilon\vec{E}$ and $\vec{H} = \vec{B}$ (for non-magnetic media, $\mu = 1$), insertion of equations and into equation yields:

$$\vec{\nabla} \cdot \left(\vec{E} \times \vec{H}_c\right) = ik\vec{H}_c \cdot \vec{H} - ik\varepsilon\vec{E} \cdot \vec{E}_c - \frac{4\pi}{c}\vec{E} \cdot \vec{J}_c.$$

Rearranging equation exploiting the commutativity of the dot product, one obtains:

$$\frac{4\pi}{c}\vec{E} \cdot \vec{J}_c + \vec{\nabla} \cdot \left(\vec{E} \times \vec{H}_c\right) = ik\vec{B} \cdot \vec{B}_c - ik\varepsilon\vec{E}_c \cdot \vec{E}.$$

A similar treatment of $\nabla \cdot \left(\vec{E}_c \times \vec{H}\right)$ gives

$$\frac{4\pi}{c}\vec{E}_c \cdot \vec{J} + \vec{\nabla} \cdot \left(\vec{E}_c \times \vec{H}\right) = ik\vec{B} \cdot \vec{B}_c - ik\varepsilon\vec{E}_c \cdot \vec{E}.$$

Subtracting equations and produces the reciprocity theorem in differential form:

$$\frac{4\pi}{c}\left(\vec{E}_c \cdot \vec{J} - \vec{E} \cdot \vec{J}_c\right) = \vec{\nabla} \cdot \left(\vec{E} \times \vec{H}_c - \vec{E}_c \times \vec{H}\right).$$

Integrating equation over a large volume V bounded by a surface S, one can express the reciprocity theorem in integral form. It follows that

$$\frac{4\pi}{c}\int_V \left(\vec{E}_c \cdot \vec{J} - \vec{E} \cdot \vec{J}_c\right) dV = \int_V \vec{\nabla} \cdot \left(\vec{E} \times \vec{H}_c - \vec{E}_c \times \vec{H}\right) dV,$$

and by the divergence theorem, the right hand side of equation may be transformed to an integral over the surface S which bounds the volume V. Therefore,

$$\frac{4\pi}{c}\int_V \left(\vec{E}_c \cdot \vec{J} - \vec{E} \cdot \vec{J}_c\right) dV = \oint_S \vec{\nabla} \cdot \left(\vec{E} \times \vec{H}_c - \vec{E}_c \times \vec{H}\right) \cdot \hat{n} dA,$$

where $\hat{n}$ is a unit vector normal to a patch of surface area described by dA, such that $\hat{n}dA = d\vec{s}$.

The LP_{l} Modes at the Waveguide Exit and Vector Diffraction Theory

Having excited modes and propagated them down the waveguide, one will now study how the modes leave the waveguide and couple to the outside world. This amounts to calculating the diffraction pattern produced on a "detector" far from the waveguide. The diffraction pattern, is a Fraunhoffer diffraction pattern, similar to the diffraction pattern produced by a plane wave incident on a circular aperture. Knowing the electric field at the exit of the waveguide and using the asymptotic reciprocity theorem (ART) derived in section 5.2, equation , the diffracted fields will be calculated. The intensity of radiation for a plane wave incident on the waveguide exit will also be calculated using the asymptotic reciprocity theorem and compared to the well known result given in such texts as Jackson [Jackson], Arfken [Arfken], or Born and Wolf [Born and Wolf]. Being able to reproduce these results using the asymptotic reciprocity theorem, as opposed to the classic vector theory of diffraction used by Jackson, Arfken, and Born and Wolf, provides a new and very powerful techniques for calculating the vector diffraction fields at a distant point on a detector. The vector theory of diffraction is very difficult to apply in all but a few specialized circumstances. The asymptotic reciprocity theorem provides a clean and easy to follow recipe for calculating these diffracted fields.
Recalling that the asymptotic reciprocity theorem is given by ,

$$\int_S \left(\vec{E}\times\vec{H}_c - \vec{E}_c\times\vec{H}\right)\cdot d\vec{s} = \frac{4\pi}{c}\int_V \left(\vec{E}_c\cdot\vec{J} - \vec{E}\cdot\vec{J}_c\right)dV.$$

For source free regions, $J = 0$, and thus the right hand side of equation vanishes. Thus the ART becomes:

$$\int_S \left(\vec{E}\times\vec{H}_c - \vec{E}_c\times\vec{H}\right)\cdot d\vec{s} = 0.$$

Consider a surface S. Let the length, from $z = 0$, to the detector be given as $L \to \infty$ (with l_w being the length of the waveguide and where $L \gg l_w$.) Let the surface S_1 be located at the waveguide exit, surface S_2 be located at a distance $L \to \infty$ away from the waveguide entrance, and the remaining surfaces (shown in dashed lines) be surfaces at infinity as shown in figure 5.1.

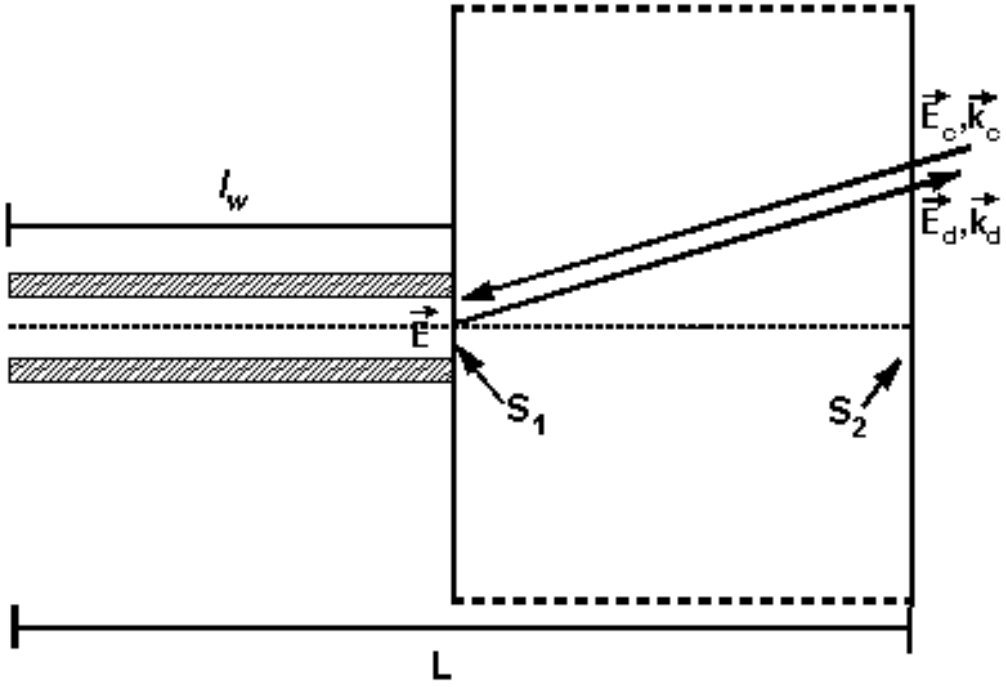

The surfaces S_1 (at the waveguide exit) and S_2 (at infinity) used to calculate the Fraunhoffer diffracted fields at a detector at a distance $L \to \infty$ from the waveguide exit. The waveguide has a length $l_w \ll L$, and at the waveguide exit are superpositions of *LP* mode fields. The connecting fields ($\vec{E}_c$) are used determine the diffracted fields through equation .

The diffracted fields will propagate in the forward direction in space. The remaining surfaces will see a zero net power flow. Since the plane wave has a some spacial extent these other surfaces are located at infinity and there is no net flow of energy through them. The integral equation may be split into two pieces, one over S_1 and one over S_2. Thus,

$$\int_{S_1} \left(\vec{E} \times \vec{H}_c - \vec{E}_c \times \vec{H}\right) \cdot d\vec{s}_1 = -\int_{S_2} \left(\vec{E}_d \times \vec{H}_c - \vec{E}_c \times \vec{H}_d\right) \cdot d\vec{s}_2.$$

Letting $\vec{E}$ be the electric field at the waveguide exit, that is, one (or a superposition) of the $LP_{l,p}$ modes and $\vec{E}_d$ be the diffracted electric field that needs to be calculated. Further, one lets $\vec{E}_c$ be the connecting field that will be used to connect the electric field at the waveguide exit to the diffracted electric field at $L \to \infty$. The choice of the connecting field is dictated purely by convenience. A good choice for the connecting field is a plane wave of unit amplitude and wave vector k_c where k_{cz} (the z-component of the connecting field wave vector) is negative. Thus one has for the connecting field,

$$\vec{E}_c = \hat{e}_c e^{i\vec{k}_c \cdot \vec{r}},$$

and without loss of generality, let the connecting field wave vector lie in the $y - z$ plane. Hence,

$$\vec{k}_c \cdot \vec{r} = k_{cy}y + k_{cz}z.$$

Next, one expands the connecting field in terms of Bessel functions, since the fields at the waveguide exit are in terms of the $LP_{l,p}$ Bessel modes. For $y = \rho \sin\varphi$, the connecting field takes on the following form (evaluating the field at $z = l_w$):

$$\vec{E}_c = \hat{e}_c e^{i\vec{k}_c \vec{r}} = \hat{e}_c e^{ik_{cz}l_w} e^{-i\eta \frac{\rho}{a} \sin\varphi},$$

where $\eta = k_{cy}a$ is a dimensionless parameter proportional to k_c. Recognizing that $e^{-ix\sin\varphi}$ can be expanded as a Bessel series, one obtains

$$\vec{E}_c = \hat{e}_c e^{ik_{cz}z} e^{-i\eta \frac{\rho}{a} \sin\varphi} = \hat{e}_c e^{ik_{cz}l_w} \sum_j J_j\left(\eta \frac{\rho}{a}\right) e^{-ij\varphi}.$$

Equation is the form of the connecting field that will be used to calculate the diffracted electric field at the surface S_2.

The electric field at the waveguide exit is needed in order to calculate the surface integral over the surface S_1 on the left hand side of equation . Recall from equation that the electric field at the waveguide end is given by a superposition of $LP_{l,p}$ modes evaluated at $z = l_w$:

$$E_y = -E_{\text{in}} \sum_l C_{l,p} J_l\left(\frac{u_l}{a}\rho\right) e^{il\varphi} e^{ik_z^{l,p} l_w}.$$

The magnetic field at the waveguide exit (as well as the analogous connecting magnetic field) are obtained from Maxwell's equations. To calculate equation , one can proceed by first noting that $\nabla \times \vec{E}_y = ik\vec{B}_x$ and $\nabla \times \vec{E}_c = ik_c\vec{B}_c$. Rewriting equation as

$$\int_{S_1} \left(\vec{E}_y \times \left(\vec{\nabla} \times \vec{E}_c\right) - \vec{E}_c \times \left(\vec{\nabla} \times \vec{E}_y\right)\right) \cdot d\vec{s}_1 =$$
$$-\int_{S_2} \left(\vec{E}_d \times \left(\vec{\nabla} \times \vec{E}_c\right) - \vec{E}_c \times \left(\vec{\nabla} \times \vec{E}_d\right)\right) \cdot d\vec{s}_2$$

and from equation ,

$$\vec{\nabla} \times \vec{E}_y = -ikE_{\text{in}} \sum_l C_{l,p} J_l\left(\frac{u_l}{a}\rho\right) e^{il\varphi} e^{ik_z^{l,p} l_w} \hat{e}_x.$$

This allows one to express $\nabla \times \vec{E}_c$ as, using equation ,

$$\vec{\nabla} \times \vec{E}_c = \left[ik_c \sum_j J_j\left(\eta \frac{\rho}{a}\right) e^{-ij\varphi} e^{-ik_{cz}l_w} \right] \hat{e}_x.$$

Splitting the left hand side of equation into two parts calling them I_I and I_{II} respectively, one has

$$I_I = \int_{S_1} \left(\vec{E}_y \times \vec{B}_c \right) \cdot d\vec{s}_1 ,$$

and

$$I_{II} = -\int_{S_1} \left(\vec{E}_c \times \vec{B}_x \right) \cdot d\vec{s}_1 .$$

Substitution of the expressions for the field at the exit of the waveguide, equation , and the connecting magnetic field, equation , allows one to express I_I as

$$I_I = \int_{S_1} ik_c E_{in} \left[\sum_l C_{l,p} J_l \left(\frac{u_l}{a} \rho \right) e^{il\varphi} e^{ik_z^{l,p} l_w} \sum_j J_j \left(\eta \frac{\rho}{a} \right) e^{-ij\varphi} e^{-ik_{cz} l_w} \right] \rho d\rho d\varphi .$$

Correspondingly, I_{II} can be expressed as

$$I_{II} = -\int_{S_1} ikE_{in} \left[\sum_j J_j \left(\eta \frac{\rho}{a} \right) e^{-ij\varphi} e^{-ik_{cz} l_w} \sum_l C_{l,p} J_l \left(\frac{u_l}{a} \rho \right) e^{il\varphi} e^{ik_z^{l,p} l_w} \right] \rho d\rho d\varphi .$$

Therefore the left hand side of equation becomes after substitution and integration,

$$= i \left[\int_0^a \sum_l 2k C_{l,p} e^{2ik_z l_w} E_{in} J_l \left(\frac{u_l}{a} \rho \right) J_l \left(\eta \frac{\rho}{a} \right) \rho d\rho \right]$$

where the φ integral has been evaluated using the following

$$\int_0^{2\pi} e^{i(l-j)\varphi} d\varphi = \begin{cases} 0 & \text{for } l \neq j \\ 2\pi & l = j \end{cases}$$

and the fact that $k_z = -k_{cz}$. Thus equation becomes after rewriting $\rho d\rho = a^2 r dr$, over the exit of the waveguide

$$4\pi i E_{in} k a^2 \int_0^1 \sum_l C_{l,p} e^{2ik_z^{l,p} l_w} J_l(u_l r) J_l(\eta r) r dr .$$

Returning to equation , the right hand side can now be evaluated. Again, the connecting field is dictated purely by convenience, so why not choose it to be a superposition of plane waves with unit amplitude at infinity. Carrying out the necessary algebra and integration in an analogous manner to that described above, produces for the right hand side of equation

$$2ik_c \hat{e}_c \cdot \vec{E}_d \left(-\vec{k}_c \right) = 2ik_c \hat{e}_c \cdot \vec{E}_d e^{i\vec{k}\cdot\vec{r}} ,$$

where the only non-vanishing contributions arise only when $k = -\vec{k}_c$. Equating equations and produces the

diffracted fields that one was seeking.

$$\vec{E}_{\mathrm{d}}\left(-\vec{k}_c\right) = 2\pi E_{\mathrm{in}} ka^2 \int_0^1 \sum_l e^{2ik_z^{l_p} l_w} C_{l,p} J_l(u_l r) J_l(\eta r) r dr,$$

where one can recall that E_{in} was evaluated as in equation . This concludes the goal of this section, namely finding an expression for the amplitude of the diffracted electric field.

Diffraction of a Plane Wave by a Circular Aperture using the ART

In this section one checks that the ART approach to vector diffraction theory yields results in agreement with the standard theory. Thus one calculates the diffracted fields for a plane wave incident on a circular aperture.

Consider a plane wave incident on a conducting screen with a circular aperture of radius a. Using standard vector diffraction theory one arrives at (from Jackson [Jackson]):

$$\vec{E}_{\mathrm{d}}^{\mathrm{SVDT}}(\vec{x}) = \frac{1}{2\pi}\vec{\nabla} \times \int_{\mathrm{apertures}} \left(\hat{n} \times \vec{E}\right) \frac{e^{ikR}}{R} da',$$

where the integration is performed only over the aperture(s) in the screen and $\vec{E}$ is the total tangential electric field in the aperture(s). In performing this integration it is customary to use the approximation that the exact field in the surface integrals may be replaced by the incident field. Evaluating equation , using standard vector diffraction theory, one finds:

$$\vec{E}_{\mathrm{d}}^{\mathrm{SVDT}}(\vec{r}) = \frac{ie^{ikr}}{r} a^2 E_0 \left(\vec{k} \times \hat{e}_2\right) \frac{J_1(ka\sin\theta)}{ka\sin\theta}.$$

The term $\frac{e^{ikr}}{r}$ is a spherical wave in free space. It is modified by a constant unit amplitude E_0. The intensity of the diffracted radiation $I \propto \left|E_{\mathrm{d}}^{\mathrm{SVDT}}\right|^2 \propto \frac{J_1^2(ka\sin\theta)}{k^2 a^2 \sin^2\theta}$, where θ is the exit angle that the x-ray makes with the normal to the aperture. Lastly the factor $\left(\vec{k} \times \hat{e}_2\right)$ gives the direction of the diffracted field.

Next one the diffracted field intensity using the ART approach. Consider the plane wave given by equation

$$\vec{E} = \vec{E}_0 e^{i\left(\vec{k}\vec{r} - \omega t\right)},$$

where normalization to 1 $\frac{photon}{\sec}$ produces from before, equations for E_0 with the flow of energy given by the Poynting vector, equation . Without loss of generality let $k_x = 0$ and let the aperture be located at $z = 0$. It follows that the electric field is given as:

$$\vec{E} = E_0 e^{ik_y y} e^{-i\omega t} \hat{e}_y$$

and this is the form of the electric field used in order to evaluate the left hand side of equation . Again, choosing the connecting field to be given as a plane wave with unit amplitude E_c as shown in equation .

$$\vec{E}_c = E_c e^{i\left(\vec{k}_c \cdot \vec{r} - \omega t\right)} \hat{e}_c,$$

where again without loss of generality, one can assume that $k_{cx} = 0$. Thus the connecting electric field takes the form

$$\vec{E}_c = E_c e^{-ik_{cy}y} e^{-ik_{cz}z} e^{i\omega t} \hat{e}_c.$$

Recalling that the left hand side of equation may be split into two parts, calling them I_I and I_{II} in an analogous fashion to equations and respectively. Performing the necessary curls of the electric field at the waveguide exit and of the connecting electric field produces the following integral over the exit surface of the waveguide

$$\mathrm{I} = -ikE_0E_c \int_0^a \int_0^{2\pi} e^{-2ik_z z} e^{2ik_\rho \rho \sin\varphi} \rho d\rho d\varphi,$$

where the fact that $-\vec{k}_{cz} = \vec{k}_z$ and $-\vec{k}_{cy} = \vec{k}_y$ has been used. The integrals over ρ and φ produce

$$\mathrm{I}_\mathrm{I} = -ia^2\pi E_0 E_c e^{ik_z z} \frac{J_1(ak\sin\theta)}{a\sin\theta}.$$

In an analogous fashion I_{II} can be evaluated to give

$$\mathrm{I}_\mathrm{II} = ia^2\pi E_0 E_c \frac{J_1(ak\sin\theta)}{ak\sin\theta}.$$

so that the left hand side of the ART, equation becomes for a plane wave incident on a circular aperture of radius a,

$$\mathrm{I} = \mathrm{I}_\mathrm{I} + \mathrm{I}_\mathrm{II} = -2ia^2\pi E_0 E_c \frac{J_1(ak\sin\theta)}{ak\sin\theta}.$$

In exactly the same manner, the right hand side of equation can be evaluated to give:

$$2ik_c \hat{e}_c \cdot \vec{E}_\mathrm{d}\left(-\vec{k}_c\right).$$

Equating equation to equation yields the amplitude of the diffracted field using the ART:

$$E_\mathrm{d}^\mathrm{ART} = a^2 \tilde{E}_d \frac{J_1(ak\sin\theta)}{ak\sin\theta}.$$

$\tilde{E}_\mathrm{d}$ is a constant that has the following form:

$$\tilde{E}_\mathrm{d} = \pi E_0 e^{i2k_z z},$$

where $|E_c| = 1$ (the connecting field has unit amplitude.) Comparing equation to the results obtained in

equation , one can see some remarkable results. Recalling equation gives the diffracted electric field for a plane wave incident on a circular aperture as

$$E_{\mathrm{d}}^{\mathrm{SVDT}} = a^2 E_0 \frac{J_1(ka\sin\theta)}{ka\sin\theta}.$$

Using the ART, the amplitude of the diffracted field is given by equation

$$E_{\mathrm{d}}^{\mathrm{ART}} = a^2 \tilde{E}_{\mathrm{d}} \frac{J_1(ak\sin\theta)}{ak\sin\theta}.$$

Here one should note that there is an overall normalization constant between the two results that depends on how the normalization was performed.
Here is the remarkable result, namely that standard vector diffraction theory and the ART yield the exact same result for the intensity of the diffracted fields (recalling that the intensity $I \propto \left|E_{\mathrm{d}}\right|^2$). The diffracted field, using vector diffraction theory, is very difficult and cumbersome to apply except in highly idealized conditions, for example a plane wave incident on a circular aperture . The ART is very easy and general enough to apply to highly idealized (plane waves incident on circular apertures) as well as very non-idealized conditions, namely those of Bessel wave fields incident on a circular aperture at the waveguide exit. The ART provides a clean and quick method to calculate these diffracted fields.

Diffraction Patterns of the LP Modes

Having determined in the last section that the ART approach agrees with standard vector diffraction theory, the next step is to return to equation and plot the Bessel diffracted fields. In order to determine the diffraction patterns for the *LP* modes, one must first determine whether the modes will be coherent when they reach the end of the waveguide. The individual modes will be coherent across the waveguide exit. The interesting question is whether the various modes superposed remain coherent as they propagate down the waveguide. Whether the *LP* modes remain coherent depends on the coherence length Δz. Assuming a wave packet given by the uncertainty relation

$$\Delta z \cdot \Delta k_z \geq \frac{1}{2},$$

where $\Delta k_z \approx \Delta k$, which is true for $\theta \ll \theta_c$. For a characteristic x-ray, $k = \frac{\omega}{c}$, and therefore $\Delta k = \frac{\Delta\omega}{c}$ and thus

$$\Delta z = \frac{1}{2\Delta k} = \frac{c}{2\Delta\omega} = \frac{\hbar c}{2\Delta E} \approx \frac{9.87 \times 10^{-6}\,\mathrm{cm}}{\Delta E(\mathrm{eV})}.$$

For a spread in energy of say $\Delta E \approx 1$ eV, the wave packet will have a longitudinal spread of about 1000Å. If two modes become separated by more than this amount they can be considered incoherent. Not only does the coherence length depend on ΔE, but also on the group velocity of the modes as they propagate down the waveguide. The group velocity differs for different $LP_{l,p}$ modes. Since the *LP* modes propagate with approximately the same k_z, one can assume that the group velocity will not vary appreciably provided the

waveguides are very short. Thus for a short waveguide, the *LP* modes are expected to remain coherent when they reach the end of the waveguide.

In figure 5.2, the intensity profile for a single diffracted $LP_{0,1}$ mode (weighted by its excitation) is shown, while figure 5.3 shows the intensity profile for the first five $LP_{0,p}$ modes. These was calculated by evaluating versus output angle. The intensity is proportional to the square of the diffracted field. For an input angle of 0 μradians, the beam essentially travels down the length of the waveguide and thus the diffraction pattern should be peaked at an output angle of 0 μradians. The diffraction peaks from the end of the waveguide are correlated to the angle of incidence of the plane wave at the waveguide entrance for short waveguides since the axially excited *LP* modes propagate with few reflections. This is not true for long waveguides.

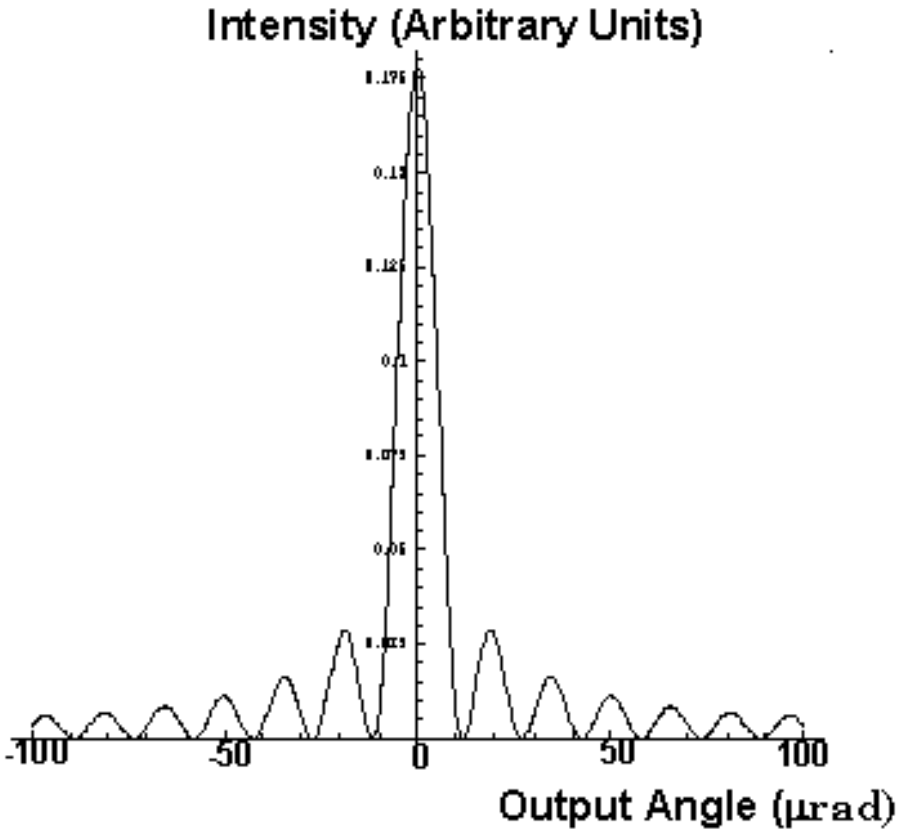

Intensity profile for an 8 keV Cu K_α x-ray versus the output angle (in μrad) for a the first $LP_{0,1}$ mode (weighted by its excitation of 70% at 0 μrad) incident at the waveguide exit, from equation .

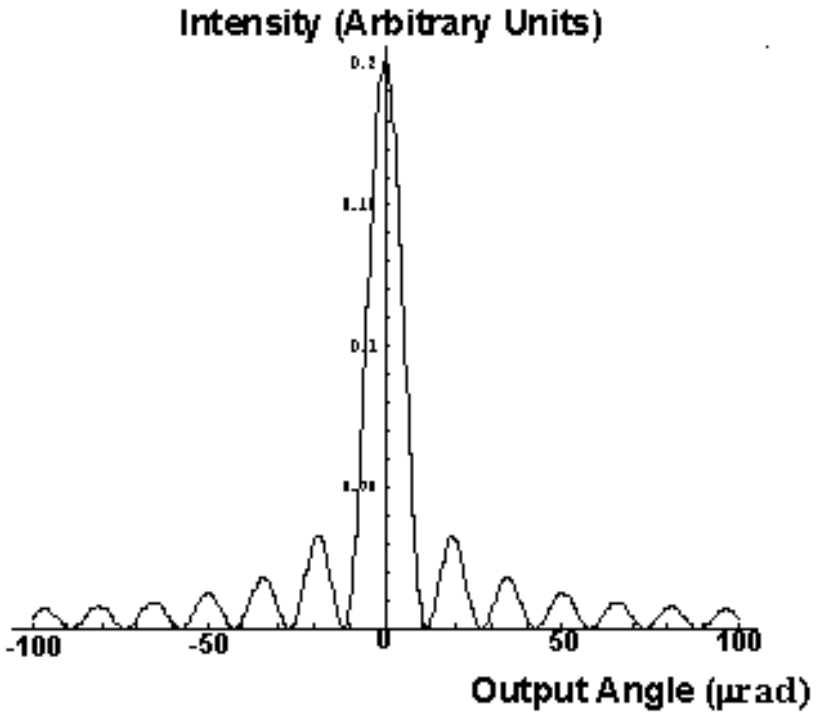

Intensity profile for an 8 keV Cu K_α x-ray versus the output angle (in μrad) for a the first five $LP_{0,p}$ modes (weighted by their respective excitations obtained from figure 4.1 at 0 μrad) incident at the waveguide exit, from equation .

Conclusion

The *LP* modes that make it to the end of the waveguide are considered coherent. Standard vector diffraction theory is the general approach to calculation of the diffracted fields. However, results in the literature refer to special cases (incident plane waves, spherical waves, etc.) and not to Bessel modes. The *LP* modes are neither plane nor spherical waves, but Bessel waves. Thus the standard results do not apply and modifications to the standard vector diffraction theory are needed.
An approach to vector diffraction theory inspired by the ART was therefore used as a viable alternative to the using standard vector diffraction theory. The vector Bessel diffracted fields were calculated. Further as the number of $LP_{0,p}$ modes increased the diffraction seen had a larger angular spread. This was attributed to the mixing of the higher order modes with the low order modes that were excited by the externally directed plane wave.
To ensure that the method was accurate, standard vector diffraction theory and the ART were both used to test a special case, namely that of a plane wave incident on a circular aperture. The results using both standard vector diffraction theory and the ART. Here, one has new approach to calculating the vector diffraction fields.

The Effect of Surface Roughness on the Propagation of X Rays

Introduction

The versatility of the x-ray waveguide depends in part, on how rough the glass surface is, on average. The rougher the surface, the smaller the distance the x rays will propagate in the waveguide. Ideally, one would like to have a perfectly smooth surface, as has been assumed thus far. In practice however, there is no surface that is perfectly smooth. Some variation of the surface height always exists. From a materials science standpoint, one would like to gather surface structural information from thin film deposition techniques. To do this, one may utilize many different techniques, one of them being x-ray scattering at grazing incidences. The scattering of x rays from a real (non-ideal or rough) interface naturally separates the waves into specular (coherent) and non-specular (diffuse) components. The effect of surface roughness is to decrease the reflectivity into the specularly reflected beam. There is extensive literature (sources to be listed) on specular and non-specular scattering from rough surfaces, that the reader may wish to consult. In all of these sources, the calculations of the reflectivities are done for plane surfaces. The waveguides in this thesis are glass capillary or cylindrical glass tubes. For these fibers there are no roughness studies. Here one will resort to an approximation, which is motivated by the observation that the effect of x-ray intensity loss into the specularly reflected beam can be described by an effective absorption of the x-ray by the waveguide [Caticha]. In other words, surface roughness will be modeled as an effective addition to the imaginary part of the susceptibility. To calculate the loss of x-ray intensity due to photoelectric absorption alone, one calculates the imaginary part of the susceptibility and the result of this calculation is used to determine the $\frac{1}{\varepsilon}$ decay lengths. This is what was done in chapter 3 section 6. Section 3.6 made no reference to the actual roughness of the glass surface. Both mechanisms, photoelectric absorption and surface roughness contribute to the decrease in x-ray intensity. To model the losses due to surface roughness an additional term will be added to the imaginary part of the susceptibility.

For the purpose of this thesis it will be shown that the surface roughness effects on the x rays can be taken into account using the Rayleigh approximation for long lateral correlation lengths for the scattering of x rays off of plane glass surfaces when the x rays are incident far below the critical angle. Long correlation lengths seem more natural since these glass fibers are produced by drawing out a piece of soft glass to form a fiber. This would tend to produce long correlation lengths, rather than short. For short correlation lengths there are other approximations that may be utilized, such as those of Nevot and Croce [Nevot and Croce].

The effects of surface roughness will be introduced as a first order correction to the effect of photoelectric absorption explored in chapter 3.6. In this chapter the Rayleigh reflectivity will be introduced and calculated, assuming no surface roughness of the glass waveguide. The correction to the imaginary part of the susceptibility will be numerically evaluated by comparing the decrease in the reflectivity curve in the absence of surface roughness to the reflectivity curve with a known surface roughness contribution. In other words, the reflectivity curves for a known amount of surface roughness and for no surface roughness will be produced and to the reflectivity curve with no surface roughness, a small correction term to the imaginary part of the x-ray susceptibility will be added. This correction term will be numerically varied until the known surface roughness reflectivity curve is reproduced. This will give the correction to the imaginary part of the x-ray susceptibility due to surface roughness and from this value, new $\frac{1}{\varepsilon}$ decay lengths may be calculated and compared to those in section 3.6.

Lastly, it will be shown that the results using a correction term in the imaginary part of the susceptibility will coincide with the results of Kimball and Bittel[Kimball and Bittel] using the Rayleigh reflectivity of an x-ray off of a plane glass surface. From this approximation one will make predictions on the applicability to

the cylindrical waveguides studied in this thesis.

Rayleigh Reflectivity of X Rays From Plane Surfaces

The photoelectric absorption of a waveguide mode as it travels down the guide is due mainly to penetration of the mode into the glass. Modes for which $\theta \ll \theta_c$ penetrate less and thus experience less absorption as was shown in chapter 3. Recall that the absorption coefficients are calculated from the imaginary part of the longitudinal wave vector, k_z. From section 3.6 the susceptibility has both a real and an imaginary component given by equation

$$\chi_0 = \chi_r + i\chi_i.$$

The imaginary part of the longitudinal wave vector k_z is given by equation as

$$k_{zi} \approx \frac{k}{2} u_{l,p}^2 \frac{\chi_i}{V_\gamma^3} = \frac{k\chi_i}{2} \frac{u_{l,p}^2}{V_\gamma^3}.$$

This lead to the effective linear absorption coefficient for the $LP_{l,p}$ modes, equation

$$\mu_{l,p} = 2k_{zi} \approx \mu \frac{u_{l,p}^2}{V_\gamma^3}.$$

Absorptive losses in the intensity of the x-ray as it travels down the waveguide were calculated in this manner, with no regard to the actual roughness of the surface. Rough surfaces also contribute to the loss of x-ray intensity as the wave travels down the waveguide. Both mechanisms, photoelectric absorption and surface roughness contribute to the decrease in x-ray intensity. Therefore, as a first approximation, consider surface roughness as a correction to photoelectric absorption. This will amount to recalculating the imaginary part of the x-ray susceptibility due to roughness scattering of the x-ray by the plane glass surface, using equation , and then calculating the corresponding $\frac{1}{e}$ decay lengths, which are given as the inverse of equation .

Rayleigh Approximation for Long Lateral Correlation Lengths

Since the waveguides are normally produced by drawing out a piece of soft glass to form a fiber, long correlation lengths seem more natural. Therefore, surface roughness effects on the x rays may be taken into account using the Rayleigh approximation for long lateral correlation lengths for x rays incident far below the critical angle. Using the Rayleigh approximation,

$$r \approx r_s e^{-2q^2\sigma^2},$$

where r_s is the Fresnel reflection coefficient for a sharp smooth planar surface, q is the normal component of the incident wave vector, and σ^2 is the mean square surface height distribution, or the roughness. The Fresnel reflection coefficient is given by

$$r_s = \frac{q - \overline{q}}{q + \overline{q}},$$

where $q = k\sin\theta$ is the component of the wave vector normal to the surface, and $\overline{q} = \left(q^2 + k^2\chi_0\right)^{\frac{1}{2}}$ is the component of the transmitted wave vector deep into the medium, $k = \frac{\omega}{c}$, and χ_0 is the x-ray susceptibility. Clearly the reflectivity, $|r|^2$, is dependant on the angle of incidence. Thus, the reflectivity is given by

$$|r|^2 = \left(\frac{q - \overline{q}}{q + \overline{q}}\right)\left(\frac{q - \overline{q}}{q + \overline{q}}\right)^* e^{-4q^2\sigma^2}.$$

Expanding equation , and substituting the expressions for q and $\overline{q}$, one obtains

$$|r|^2 = \left[\frac{k\sin\theta - \left(k^2\sin^2\theta + k^2(\chi_r + i\chi_i)\right)^{\frac{1}{2}}}{k\sin\theta + \left(k^2\sin^2\theta + k^2(\chi_r + i\chi_i)\right)^{\frac{1}{2}}}\right]$$
$$\left[\frac{k\sin\theta - \left(k^2\sin^2\theta + k^2(\chi_r - i\chi_i)\right)^{\frac{1}{2}}}{k\sin\theta + \left(k^2\sin^2\theta + k^2(\chi_r - i\chi_i)\right)^{\frac{1}{2}}}\right] e^{-4q^2\sigma^2}.$$

Equation is the reflectivity of an x-ray off of a plane glass surface. One can plot equation for x rays of varying energies versus angle of incidence as shown in figures 6.1 through 6.4.
Also included in figures 6.1 through 6.4 are the effects of varying the amount of surface roughness for these different energies. From figure 6.1, for example, shows Cu K_α x rays (with energy 8 keV) incident on a glass surface with increasing roughness. One can see that as the surface roughness increases (from 0Å to 20Å) the net affect is to decrease the surface reflectivity for fixed energy. One could vary both the x-ray energy and the amount of surface roughness. In figure 6.2 potassium x rays (with energy 3 keV) are incident and again the same pattern is noticeable. As the amount of surface roughness is increased the reflectivity decreases. In figures 6.3 and 6.4 sodium (1 keV) and oxygen (0.5 keV) x rays respectively are used. The same trend is again shown, namely that for a fixed energy, as the surface roughness increases the surface reflectivity decreases. It should also be noted that the critical angle for the x rays incident on the glass surface depends on the x-ray susceptibility (equation) as well as the x-ray energy. For hard (Cu K_α) x rays the critical angle is approximately 4.4 mrad (0.25 degrees), while for soft (O) x rays the critical angle is approximately 67.2 mrad (3.85 degrees). These critical angles could also have been inferred by inspection from figures 6.1 through 6.4, where the reflectivity goes to zero.

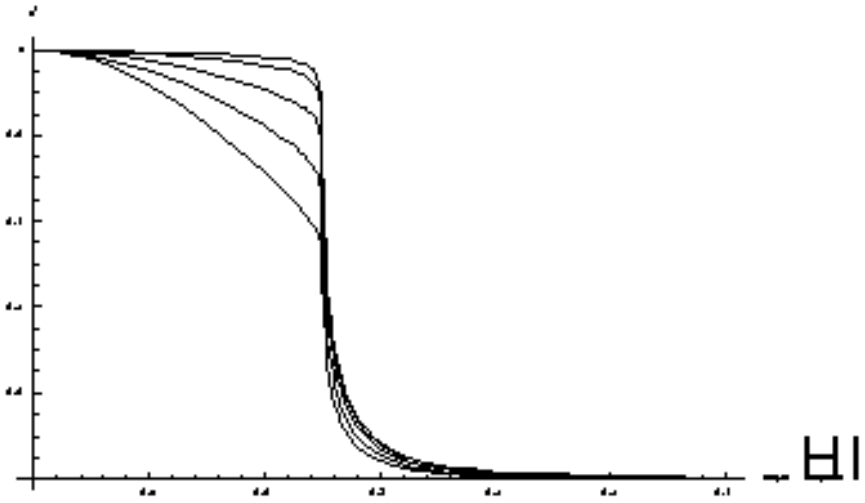

Reflectivity versus angle for mean square surface height distributions ranging from $\sigma = 0$Å to $\sigma = 20$Å, in steps of 5Å for Cu K_α x rays with energy 8 keV. These reflectivity curves were generated by evaluation of equation for varying angle of incidence of the x-ray beam on the plane glass surface.

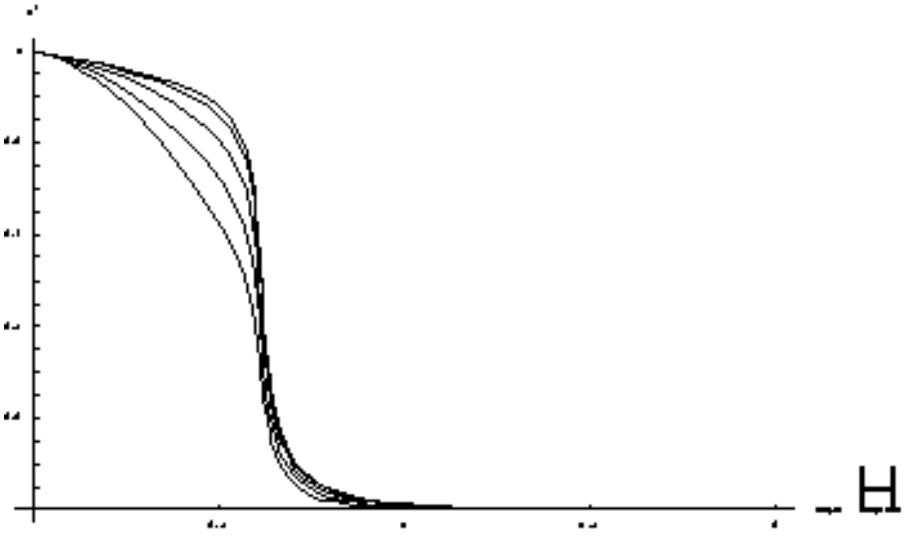

Reflectivity versus angle for mean square surface height distributions ranging from $\sigma = 0$Å to $\sigma = 20$Å, in steps of 5Å for potassium x rays with energy 5 keV. These reflectivity curves were generated by evaluation of equation for varying angle of incidence of the x-ray beam on the plane glass surface.

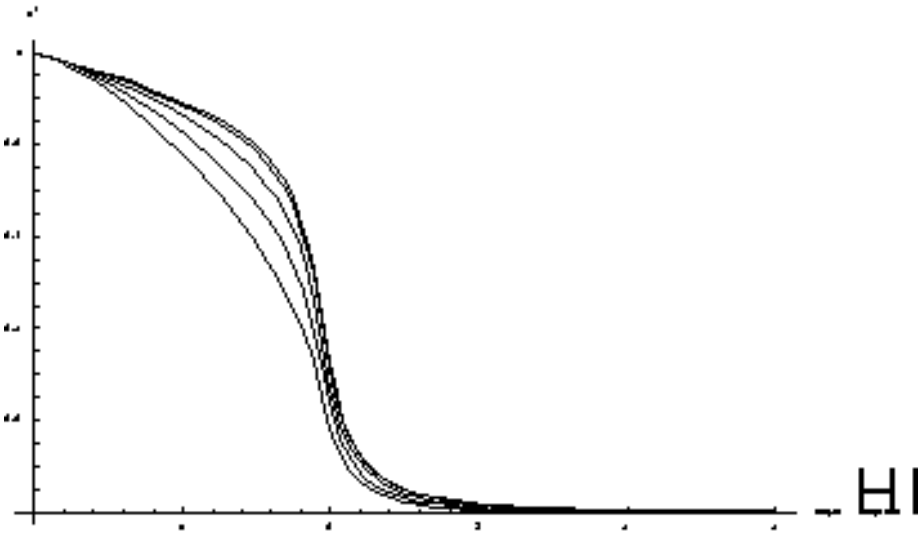

Reflectivity versus angle for mean square surface height distributions ranging from $\sigma = 0$Å to $\sigma = 20$Å, in steps of 5Å for sodium x rays with energy 1 keV. These reflectivity curves were generated by evaluation of equation for varying angle of incidence of the x-ray beam on the plane glass surface.

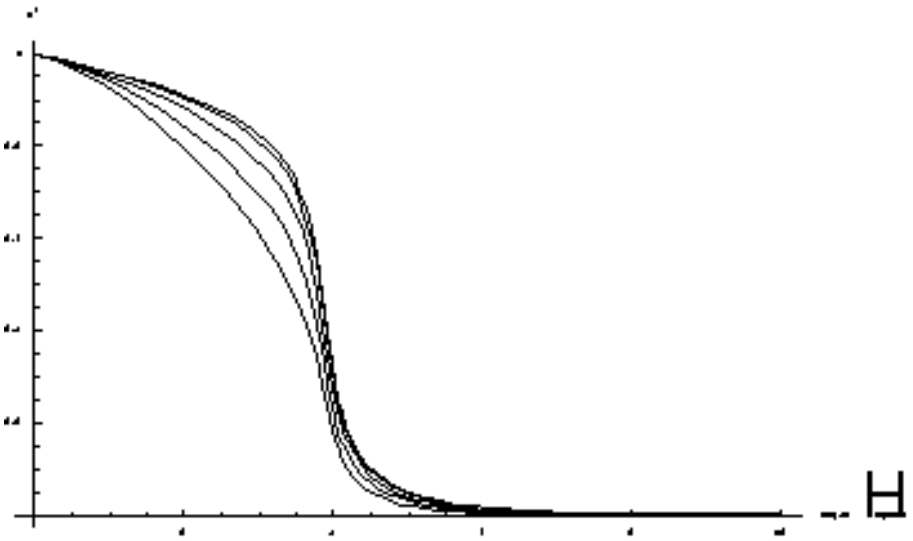

Reflectivity versus angle for mean square surface height distributions ranging from $\sigma = 0$Å to $\sigma = 20$Å, in steps of 5Å for oxygen x rays with energy 522 eV. These reflectivity curves were generated by evaluation of equation for varying angle of incidence of the x-ray beam on the plane glass surface.

Addition to Photoelectric Absorption, Method of Effective Susceptibility

Since the effect of surface roughness is to decrease the surface reflectivity, by virtue of the small imaginary part of the x-ray susceptibility, one can assume that this is akin to the decrease in surface reflectivity due to photoelectric absorption. Thus, to calculate the $\frac{1}{e}$ decay lengths of the x rays one starts by assuming that the

linear absorption coefficient contains two terms, one due to photoelectric absorption and due to surface roughness. Recalling the definition of the linear absorption coefficient for glass, $\mu = k\chi_i$, one can now define an effective χ_i which contains a contribution from the effect of photoelectric absorption and a contribution from the effect of surface roughness.

$$\chi_i = \chi_{iPA} + \chi_{iSR},$$

where χ_{iPA} is the contribution from photoelectric absorption and χ_{iSR} is the contribution from surface roughness. Following, in a completely analogous manner to the derivation of equation of chapter 3, the imaginary part of the longitudinal component of the wave vector may be written in terms of the contributions due to photoelectric absorption and surface roughness. Thus the imaginary part of the longitudinal component of the wave vector is given as:

$$k_{zi} = \frac{k}{2}(\chi_{iPA} + \chi_{iSR})\frac{u_{l,p}^2}{V_\gamma^3}.$$

Since, by definition, the linear absorption coefficient for the $LP_{l,p}$ modes in the glass due to photoelectric absorption is $\mu_{l,p,PA} = 2k_{zi,PA} = k\chi_{iPA}$, one can define the linear absorption coefficient for the $LP_{l,p}$ modes in the glass due to surface roughness as $\mu_{l,p,SR} = 2k_{zi,SR} = k\chi_{iSR}$. This produces

$$\mu_{l,p} = (\mu_{l,p,PA} + \mu_{l,p,SR})\frac{u_{l,p}^2}{V_\gamma^3}.$$

In order to include the effects of surface roughness, one needs to calculate $\mu_{l,p,SR}$ from equation . First, one starts by plotting the reflectivity (versus angle) for two cases. The first case is for 0Å of surface roughness and the second is for a known amount of surface roughness, for example, 5Å. Here, Cu K_α x rays are used for the example and the reflectivities are calculated according to equation . In order to calculate the effective susceptibility and thus the linear absorption coefficient for an $LP_{l,p}$ mode, through equation , one varies the imaginary part of the susceptibility in a known manner. If the assumption that surface roughness effects can be modeled as an addition to the effects of photoelectric absorption, then as one varies the imaginary part of the susceptibility the reflectivity curve for the known amount of surface roughness should be reproduced. In other words, from the reflectivity curve with 0Å of surface roughness, a value for the imaginary part of the susceptibility was chosen and the decrease in the reflectivity was calculated (and plotted according to equation). If the value of the susceptibility chosen was correctly then the reflectivity curve with 0Å of surface roughness should decrease towards the reflectivity curve with the known amount of surface roughness. At a particular value for the susceptibility the curve with a known amount of surface roughness should be reproduced. The χ_i that made the 0Å reflectivity curve match the 5Å is the contribution to photoelectric absorption that was being sought. In figures 6.5 and 6.6, numerical methods were used to vary

the imaginary part of the susceptibility until the reflectivity with known amount of surface roughness was obtained from the curve with no surface roughness. Once the contribution to the imaginary part of the susceptibility is known, the new linear absorption coefficients, $\mu_{l,p,SR}$, may be calculated. From equation the effective linear absorption coefficients can be calculated and thus new $\frac{1}{e}$ x-ray decay lengths.

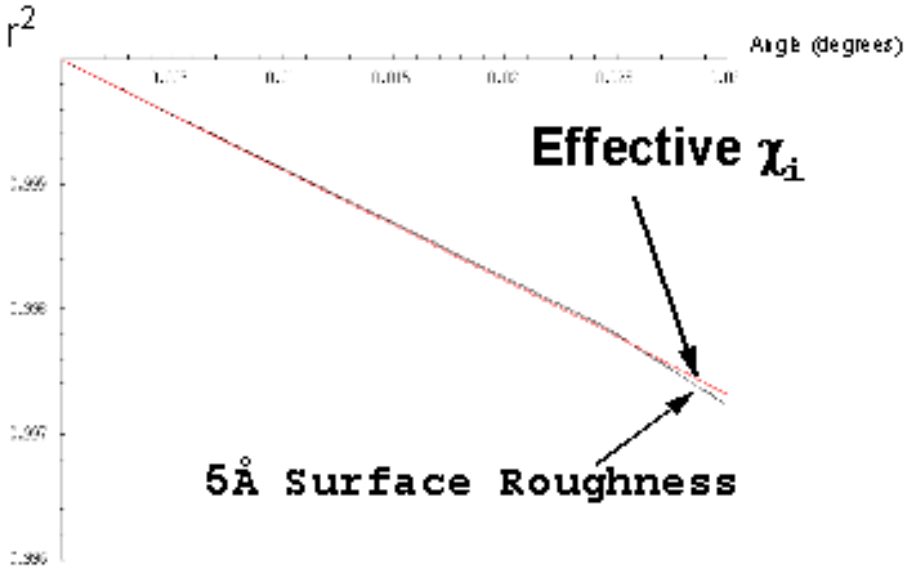

Surface reflectivity for 5Å surface roughness for copper K_α x rays versus angle (in degrees). Also included is the surface reflectivity for 0Å of surface roughness. This curve has been produced by successive iterations of the variable imaginary part of the x-ray susceptibility. The overlap of the two curves for $\theta \ll \theta_c$ produces the desired result, namely the desired contribution of surface roughness to the decrease in reflectivity. From this effective χ_i one This allows one to recalculate the $\frac{1}{e}$ decay lengths based on equation .

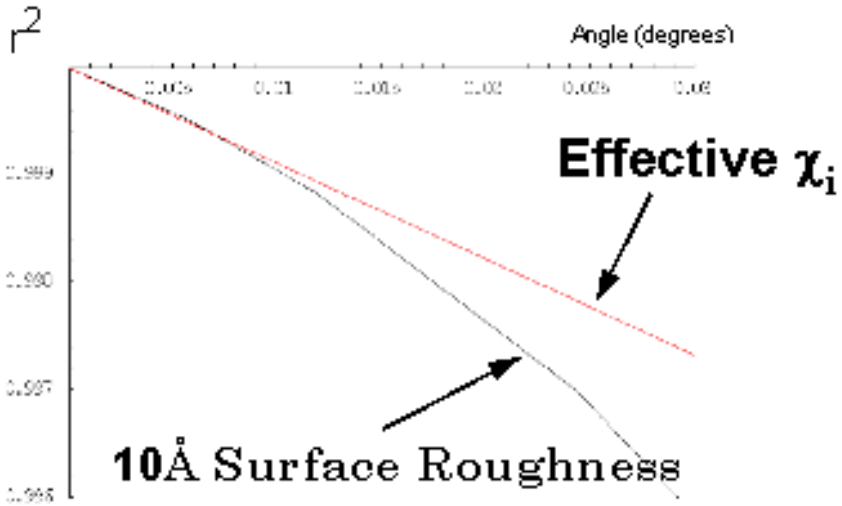

Surface reflectivity for 10Å surface roughness for copper K_α x rays versus angle (in degrees). Also included is the surface reflectivity for 0Å of surface roughness. This curve has been produced by successive iterations of the variable imaginary part of the x-ray susceptibility. The overlap of the two curves for $\theta \ll \theta_c$ produces the desired result, namely the desired contribution of surface roughness to the decrease in reflectivity. From this effective χ_i one This allows one to recalculate the $\frac{1}{e}$ decay lengths based on equation .

From figures 6.5 and 6.6, for $\theta \ll \theta_c$ and for Cu K_α x rays with an energy of 8 keV, the contribution due to surface roughness through the imaginary part of the x-ray susceptibility may be calculated. This gives a value of $\chi_{i,SR,Cu} = 2.5 \times 10^{-8}$ for 5 and 10Å of surface roughness. For x rays in borosilicate glass, one finds $\mu_{Cu,SR}$ =9.97 cm^{-1} and $\mu_{Cu,PA}$ =72.16 cm^{-1} (from chapter 3.6). Therefore equation may be evaluated and the new $\frac{1}{e}$ decay lengths with surface roughness and photoelectric absorption effects included, for several modes of Cu K_α x rays may be calculated as is shown in tables 6.1 and 6.2.

$\mu_{l,p}\ (m^{-1})$	$p = 1$	$p = 2$	$p = 3$
$l = 0$	7.1×10^{-5}	3.7×10^{-4}	9.1×10^{-4}
$l = 1$	1.8×10^{-4}	6.0×10^{-4}	1.3×10^{-3}
$l = 2$	3.2×10^{-4}	8.6×10^{-4}	1.7×10^{-3}

\caption{Linear absorption coefficients for copper x rays of energy 8 keV due to 5 angstroms of surface roughness and photoelectric absorption.\label{key} }

L (m)	1	2	3
0	14173	2690	1095
1	5583	1665	792
2	3108	1157	607

\caption{New (1/e) decay lengths for copper x rays due to 5 angstroms of surface roughness and photoelectric absorption.\label{key} } Table 6.2 shows the propagation lengths for 5Å of surface roughness for Cu K_α x rays incident in a glass capillary. These propagation lengths may be compared with pure photoelectric absorption, that was calculated in chapter 3. From section 3.6 with pure photoelectric

absorption one calculated the $\frac{1}{e}$ decay lengths, and these are shown again in table 6.3.

L (m)	1	2	3
0	16667	3175	1299
1	6667	1961	909
2	3704	1370	714

\caption{(1/e) decay lengths for copper x rays due to photoelectric absorption only.\label{key} }
Comparison of tables 6.2 and 6.3 show that when surface roughness effects are taken into account, the x-ray does not propagate as far as it would if there were a smooth waveguide surface. Let's consider again for example, the $LP_{2,1}$ mode for the Cu K_α x rays. The $\frac{1}{e}$ decay length for the $LP_{2,1}$ mode, from table 6.3, is approximately 3700 meters for pure photoelectric absorption. This is a very large propagation distance for the x-ray to travel. Incorporating the effects of photoelectric absorption and surface roughness, the $\frac{1}{e}$ decay length for the $LP_{2,1}$ mode, from table 6.2 is approximately 3100 meters. This too is a striking result and is probably not a realizable result in a practical x-ray waveguide. It does show that surface roughness does affect the propagation of the x-ray. However, surface roughness probably is not a significant effect in these waveguides. These large propagation distances are most likely due to the low order modes being contained entirely within the waveguide, and thus the low order modes experiences very little penetration into the glass and see very little of the rough surfaces since they undergo very few reflections. Whereas the higher order modes do not propagates as far since they undergo more reflections off of the glass surface. The more reflections the x-ray undergoes the more likely it is to be lost due to absorption by the glass or diffuse scattering by the rough surface.

Photoelectric Absorption and Surface Reflectivity, Method of Kimball and Bittel

Following the procedure outlined in the paper by Kimball and Bittel [Kimball and Bittel], one can examine the effects of rough surfaces by using the Fresnel reflectivity. The Fresnel reflectivity can be derived in the same manner as section 5.2, but with out the exponential decay term. Again, let r_s be the refection coefficient for a sharp smooth surface, q be the normal component of the incident wave vector, and let σ^2 is the mean square surface height distribution, or the roughness. The Fresnel reflection coefficient is given by equation :

$$r_s = \frac{q - \overline{q}}{q + \overline{q}},$$

where $q = k\sin(\theta)$ is the component of the wave vector normal to the surface, and $\overline{q} = \left(q^2 + k^2\chi_0\right)^{\frac{1}{2}}$ is the component of the transmitted wave vector deep into the medium, $k = \frac{w}{c}$, and χ_0 is the x-ray

susceptibility. Clearly the reflectivity, $|r|^2$, is dependant on the angle of incidence. The Fresnel reflectivity is given by:

$$|r|^2 = \left(\frac{q-\overline{q}}{q+\overline{q}}\right)\left(\frac{q-\overline{q}}{q+\overline{q}}\right)^*.$$

Expanding equation , and substituting the expressions for q and $\overline{q}$, one obtains:

$$|r|^2 = \left[\frac{k\sin(\theta) - \left(k^2\sin^2(\theta) + k^2(\chi_r + i\chi_i)\right)^{\frac{1}{2}}}{k\sin(\theta) + \left(k^2\sin^2(\theta) + k^2(\chi_r + i\chi_i)\right)^{\frac{1}{2}}}\right]$$
$$\left[\frac{k\sin(\theta) - \left(k^2\sin^2(\theta) + k^2(\chi_r - i\chi_i)\right)^{\frac{1}{2}}}{k\sin(\theta) + \left(k^2\sin^2(\theta) + k^2(\chi_r - i\chi_i)\right)^{\frac{1}{2}}}\right].$$

Surface roughness decreases the specular reflection coefficient, R^0 by $\Delta\ r$. Thus the specular reflection coefficient is given by:

$$R^0 = |r|^2 - \Delta\ r,$$

where $\Delta\ r$ needs to be evaluated. Kimball and Bittel give the results for $\Delta\ r$ by the following expression:

$$\Delta\ r = 4\eta\pounds^2\left[\sqrt{r_a}\cos\left(\frac{\xi_a}{2}\right) - \sqrt{r_b}\sin\left(\frac{\xi_b}{2}\right)\right].$$

The dimensionless parameters r_a and r_b are proportional to the range of the roughness and given by the expressions:

$$r_a = \sqrt{\frac{1}{\phi^2} + \eta^4}$$

$$r_b = \sqrt{\frac{1}{\phi^2} + \left(1-\eta^2\right)^2},$$

where ϕ characterizes the roughness range and is related to the lateral correlation length of the roughness and the lateral distance P, the x-ray travels in the medium while it is being reflected. Furthermore, several parameters pertinent to the geometry of the fiber need to be introduced and defined. The ratio of the input angle to the critical angle is defined as η, while $\pounds^2$ is defined as the ratio of the mean square surface height distribution σ to the glancing angle penetration depth, D (how far into the glass fiber the x-ray travels into the surface perpendicularly while it is being reflected.) Further, the glancing angle penetration depth D can related to the speed of light in vacuum and to the plasma frequency for borosilicate glass. Thus $\pounds^2$ becomes:

$$\pounds^2 = \frac{\sigma^2}{D^2} = \frac{\sigma^2}{c^2}\omega_p^2,$$

where the plasma frequency for borosilicate glass was found, in chapter 2, to be 35.1 eV and thus $D = 56.1$ Å. Therefore using equation for $|r|^2$ and equation for the surface roughness correction, equation may be plotted for various x-ray energies as shown in figures 6.7 and 6.8. Figures 6.7 and 6.8 are for Cu K_α x rays with an energy of 8 keV. Figure 6.7 is for no surface roughness and 5Å of surface roughness, while figure 6.8 is for 10Å of surface roughness. Here one can notice that as the height of the rough surface increases the specular reflection coefficient decreases from unity as is expected. This effect is not very dramatic. Further, as the magnitude of the surface roughness increases from 5Å to 10Å more of the x-ray is scattered in random directions and thus the reflection coefficient suffers a greater decrease for increased surface roughness.

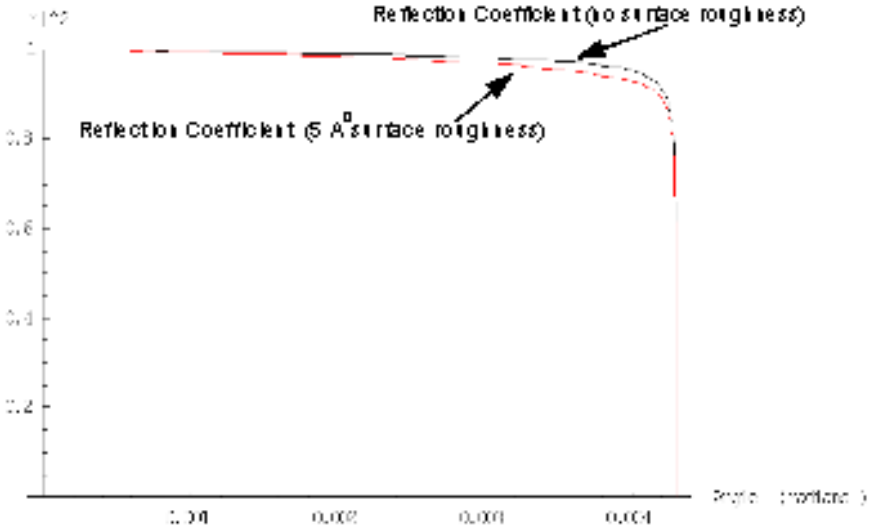

Plot of the specular reflection coefficient following the method of Kimball and Bittel for 0Å and 5Å of surface roughness for copper K_α x rays. The upper curve (no surface roughness) was generated by plotting equation versus angle of incidence. The lower curve was generated by plotting equation versus angle of incidence using equations for the reflectivity and for the surface roughness correction. Surface roughness decreases the specular reflection coefficient as expected.

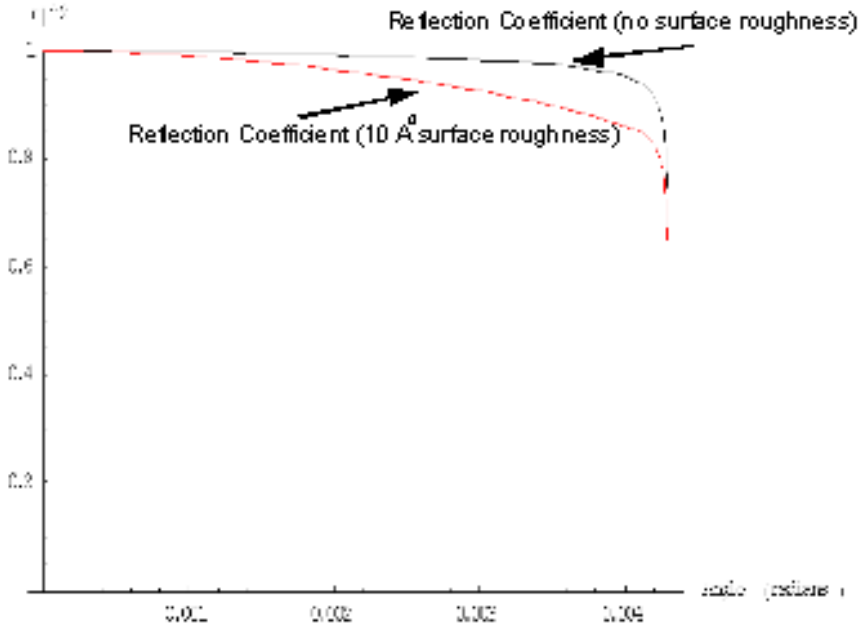

Plot of the specular reflection coefficient following the method of Kimball and Bittel for 0Å and 10Å of surface roughness for copper K_α x rays. The upper curve (no surface roughness) was generated by plotting equation versus angle of incidence. The lower curve was generated by plotting equation versus angle of incidence using equations for the reflectivity and for the surface roughness correction. Surface roughness decreases the specular reflection coefficient as expected.

Comparison of Variable X-ray Susceptibility Method to the Method of Kimball and Bittel

Next, one would like to compare the methods of calculating the surface roughness as a correction to the imaginary part of the x-ray susceptibility from section 6.2 and the decrease in the specular reflection coefficients due to surface roughness following the method of Kimball and Bittel. In figure 6.9 a mean surface height distribution of 5Å was used for Cu K_α x rays incident in borosilicate glass. The upper two curves in figure 6.9 were obtained by plotting equation (effective susceptibility method) and equation (method of Kimball/Bittel). Both of the upper two overlaid reflectivity curves are for 0Å of surface roughness. To compare the two methods of effective susceptibility and of Kimball/Bittel, equations and were both evaluated for various angles of incidence. The lower curve (method of Kimball/Bittel) was obtained by plotting equation for 5Å of surface roughness versus angle of incidence of the x-ray beam according to equation with the surface roughness correction given by . The second, lower curve (effective susceptibility) was obtained by numerically varying the susceptibility, using equation , until the reflectivity of a known amount of surface roughness was obtained, in this case 5Å. This curve, the 5Å of surface roughness produced by varying the x-ray susceptibility, was shown previously in figure 6.5. Here it is overlaid against the curve produced by the method of Kimball/Bittel. One can notice the agreement between the two methods. For a known amount of roughness, it seems that modeling the effect of surface roughness as a correction to the effect of photoelectric absorption is valid. The discrepancy between the two methods may be attributed to the precision in the numerical approximation of the imaginary part of the susceptibility. This needs to be addressed with further studies.

Of course, one does not have to use hard Cu K_α x rays. One could decrease the x-ray energy from say hard

Cu K_α x rays with energy 8 keV to soft O x rays with energy 0.5 keV and see if the two methods are still equivalent. This is what is shown in figures 6.10 to 6.12. From figures 6.10 through 6.12 one can see that again the two methods yield exactly the same results. By the method of Kimball/Bittel one calculates the decrease in the specular reflection coefficient due to surface roughness by evaluating equation . The Fresnel reflection coefficient, equation , is evaluated for a known amount of surface roughness. For perfectly smooth surfaces, Δr is zero and equation is equivalent to equation . For a known amount of surface roughness, the reflectivity is decreased and this decrease is calculated by evaluating equations and .
The assumption that the rough surface contributes to an affective absorption seems to be valid. In both instances one can conclude that whether the x-ray is scattered (reflected) by the rough surface and this specular reflectance calculated (as shown by Kimball and Bittel) or lost (scattered) and simply treated as another instance of loss due to absorption, one arrives at the same result.

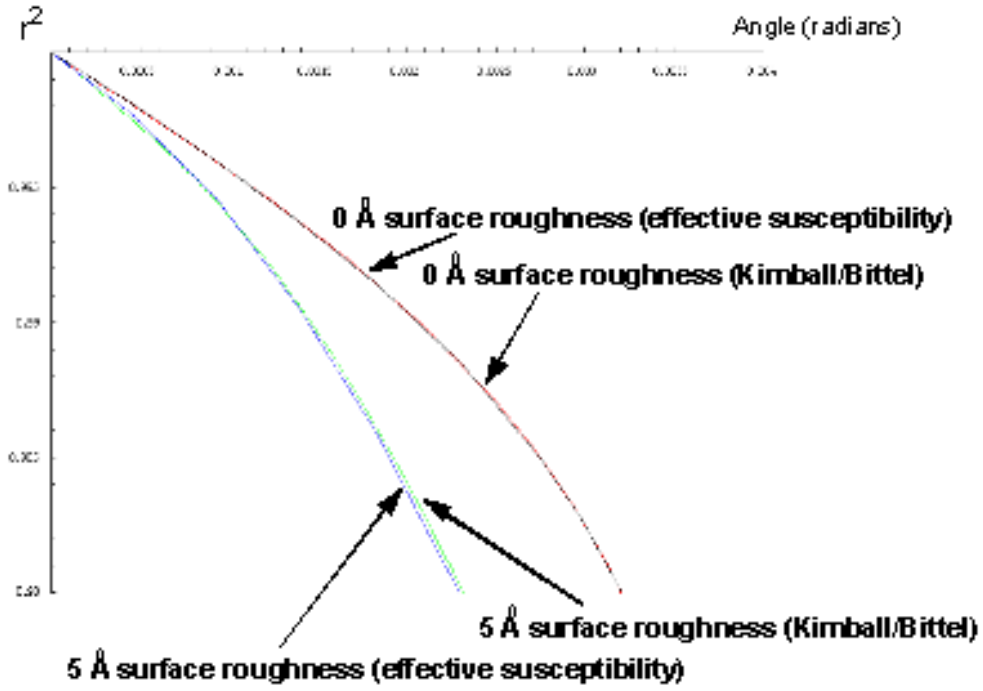

Plot of the reflectivity versus angle of incidence for Cu K_α x rays with energy 8 keV. The upper two curves were obtained by plotting equation (effective susceptibility method) and equation (method of Kimball/ Bittel). Both of the upper two overlayed reflecticity curves are for 0Å of surface roughness. The lower curve (method of Kimball/Bittel) was obtained by plotting equation for 5Å of surface roughness versus angle of incidence of the x-ray beam. The other lower curve (effective susceptibility) was obtained by numerically varying the susceptibility, using equation , until the reflectivity of a known amount of surface roughness was obtained. This curve was shown previously in figure 6.5. Here it is overlayed against the curve produced by the method of Kimball/Bittel. One can see the agreement between the two methods.

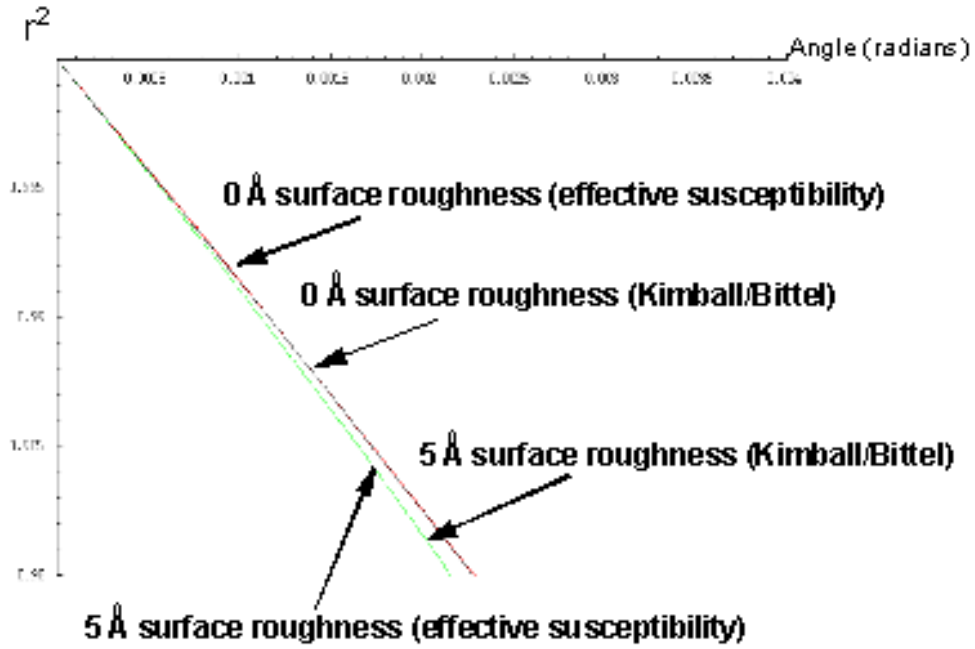

Plot of the reflectivity versus angle of incidence for potassium x rays with energy 3 keV. The upper two curves were obtained by plotting equation (effective susceptibility method) and equation (method of Kimball/Bittel). Both of the upper two overlayed reflecticity curves are for 0Å of surface roughness. The lower curve (method of Kimball/Bittel) was obtained by plotting equation for 5Å of surface roughness versus angle of incidence of the x-ray beam. The other lower curve (effective susceptibility) was obtained by numerically varying the susceptibility, using equation , until the reflectivity of a known amount of surface roughness was obtained. One can see the agreement between the two methods for an energy between those of hard and soft x rays.

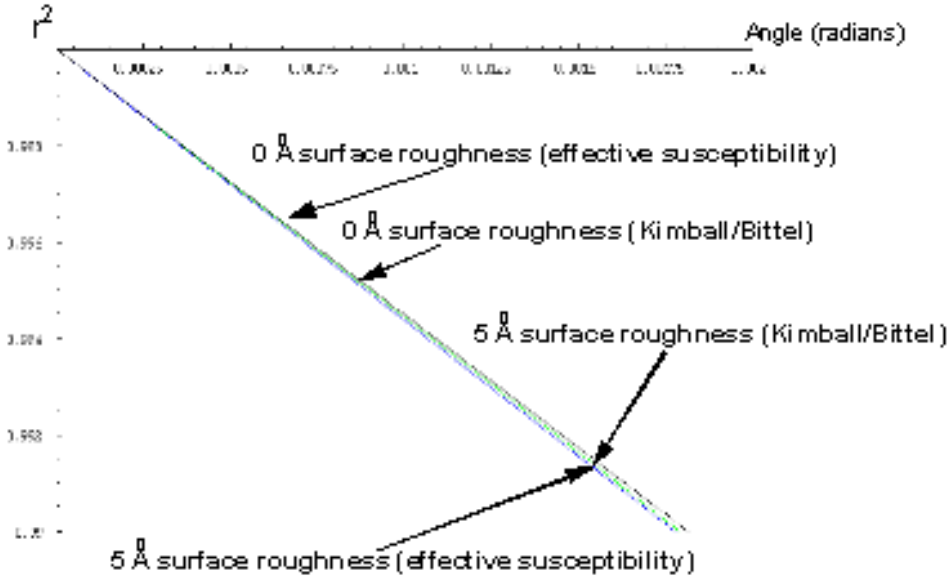

Plot of the reflectivity versus angle of incidence for sodium x rays with energy 1 keV. The upper two curves were obtained by plotting equation (effective susceptibility method) and equation (method of Kimball/Bittel). Both of the upper two overlayed reflecticity curves are for 0Å of surface roughness. The lower curve (method of Kimball/Bittel) was obtained by plotting equation for 5Å of surface roughness versus angle of incidence of the x-ray beam. The other lower curve (effective susceptibility) was obtained by numerically varying the susceptibility, using equation , until the reflectivity of a known amount of surface roughness was obtained. One can see the agreement between the two methods for soft x rays.

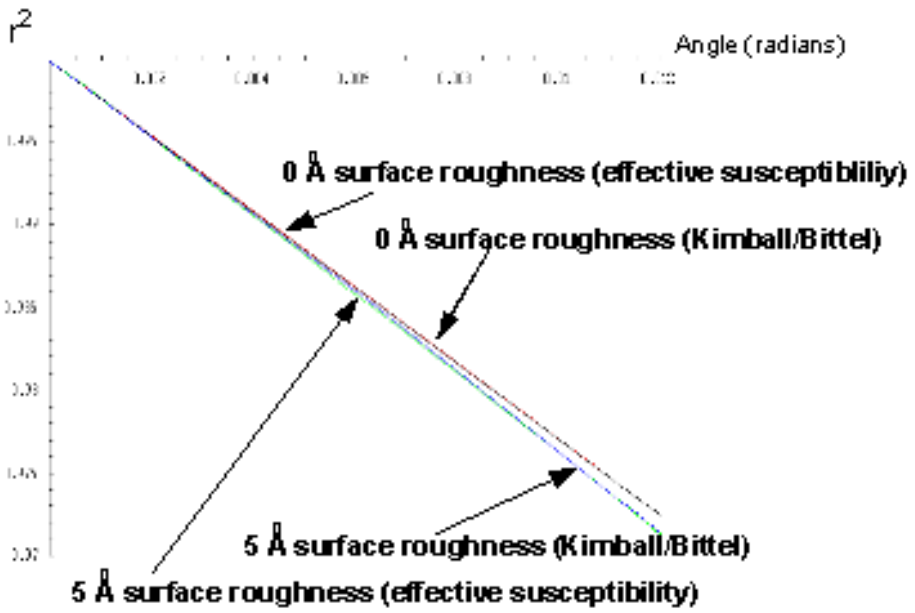

Plot of the reflectivity versus angle of incidence for soft oxygen x rays with energy 0.5 keV. The upper two curves were obtained by plotting equation (effective susceptibility method) and equation (method of Kimball/Bittel). Both of the upper two overlayed reflecticity curves are for 0Å of surface roughness. The lower curve (method of Kimball/Bittel) was obtained by plotting equation for 5Å of surface roughness versus angle of incidence of the x-ray beam. The other lower curve (effective susceptibility) was obtained by numerically varying the susceptibility, using equation , until the reflectivity of a known amount of surface roughness was obtained. One can see the agreement between the two methods for soft x rays.

Conclusion

The waveguides in this thesis were glass capillary tubes. One resorted to an approximation, which was motivated by the observation that the effect of x-ray intensity loss into the specularly reflected beam could be described by an effective absorption of the x-ray by the waveguide. In other words, surface roughness was modeled as an effective addition to the imaginary part of the susceptibility It seems reasonable that the Rayleigh reflectivity is an adequate approach for long lateral correlation lengths in these pulled fibers. Further one finds that as the mean surface height distribution of the surface increases the x-ray intensity decreases and this decrease can be modeled as a correction to the imaginary part of the x-ray susceptibility. This correction was added to the previously determined effect of photoelectric absorption and the two effects contribute to the loss of x-ray intensity as the x-ray propagates in the waveguide. It can also be concluded

that for small angles of incidence, $\theta \ll \theta_c$, surface roughness does not seem to have much of an effect on the propagation of the x-ray. The assumption that the rough surface contributes to an affective absorption seems to be valid. In both instances one can conclude that whether the x-ray is scattered (reflected) by the rough surface and the specular reflectance calculated (as shown by Kimball and Bittel) or lost (scattered) and simply treated as another instance of loss due to absorption, one arrives at the same result.

Summary and Conclusions

Summary of Conclusions

The purpose of this thesis was to develop the theory for describing the performance of cylindrical glass capillaries as waveguides for x rays. The propagating modes were obtained by solving Maxwell's equations. Thus, polarization effects are fully taken into account. The transverse fields were expressed in terms of the longitudinal fields and wave equations for the longitudinal electric and magnetic fields were solved by separation of variables. Next boundary conditions on the wave function solutions were imposed and the characteristic equation for the modes was derived. For the $m = 0$ case the modes were found to exhibit properties of the *TE* and *TM* modes in the limit of small angles of incidence and for all values of χ_o. The higher order modes ($m \neq 0$) are neither *TE* or *TM* but are termed hybrid and denoted by EH_m and HE_m. In the limit that χ_o is much smaller than unity, the hybrid EH_m and HE_m modes were found to obey the same characteristic equation for the change of indices $m \rightarrow -m$. This degeneracy was exploited and used to superpose the hybrid circular modes to form a set of linearly polarized modes. One could associate with the modes an orbital angular momentum (the φ-dependence of the electric and magnetic fields) and a spin. The modes have a total angular momentum of $m \pm 1$. The right or left circular polarization (the rotation of the electric fields at a given point in space) is associated with the helicity or spin of the photons. Spin is usually associated with quantum mechanics. Here one has a purely classical example that involves spin. The circularly polarized hybrid EH_m and HE_{-m} modes were superposed to form a set of linearly polarized or LP_l modes. There were found two sets of *LP* modes denoted respectively LP^x and LP^y. Only the LP^y modes were investigated since the LP^x modes are simply a 90^0 rotation of the LP^y modes.

The real part of the electric field for various LP_l^y modes was plotted for a waveguide of an arbitrary radius. For the low order $LP_{0,p}$ family of modes it was found that the energy flow was at the center of the waveguide and decreased as one moved from the center of the waveguide toward the glass boundary along any radial direction. For the higher order modes, $l > 0$, it was found that the energy flow was not near the center of the waveguide. It was found by inspection that most of the energy was flowing at increasing radial distances from the center of the waveguide and ultimately decreased as one approached the glass boundary along any radial direction.

There are two energy loss mechanisms that were studied. Photoelectric absorption effects were investigated and losses due to photoelectric absorption were calculated. This was done by calculating the imaginary part of the dielectric susceptibility. The imaginary part of the wave vector was then calculated and used to calculate the $\frac{1}{e}$ decay lengths for the x rays as they travel down the fiber. It was found that the lowest order modes (the $LP_{0,p}$) propagate on the order of 10 kilometers for higher energy x rays, while for lower energy x rays the propagation distances were on the order of hundreds of meters. Thus for typical values of the roughness these losses are minimal. However, localized defects such as obstructions in the waveguide, waviness over long scales, bending, etc., can actually be more dominant. While these propagation distances may be a shocking result, in practical x-ray fibers this is probably not a realizable feature.
The excitation of various *LP* modes that were excited by an externally directed plane wave were calculated. In order to calculate the excitation, the *LP* modes and the externally directed plane wave used to excite these modes needed to be normalized to an arbitrary flux of energy of 1 $\frac{\text{photon}}{\text{sec}}$ into the cross sectional area of the waveguide. The x-ray energy was varied for the lowest order, $LP_{0,1}$ mode. Here it was found that the excitation of the $LP_{0,1}$ mode is 70% and is independent of the x-ray energy. Since the critical angle increases with decreasing x-ray energy, one finds for soft x rays the input angle cone is larger than the input angle cone for hard x rays. As one approaches the critical angle for a given x-ray energy, the x-ray undergoes more reflections and has a higher probability of being absorbed by the glass capillary.

The number of modes that are excited was also investigated for the case of the lowest order $LP_{0,1}$ mode. It was found that for an arbitrary value of the excitation, namely greater than 1%, 6 modes propagate at exactly 0 μradians. At increasing angles of incidence higher order modes are also excited and thus propagate down the waveguide. In this thesis the x-ray beam is highly collimated and in practice the x-ray beam has an angular divergence some mode mixing is bound to occur.
In chapter 5, the *LP* modes that make it to the end of a short waveguide were considered coherent. Standard vector diffraction theory is the general approach to the calculation of the diffracted fields. However, results in the literature refer to special cases (incident plane waves, spherical waves, etc.) and not to Bessel modes. The *LP* modes are neither plane nor spherical waves, but Bessel waves. Thus the standard results do not apply and modifications to the standard vector diffraction theory were needed. An approach to vector diffraction theory inspired by the ART was therefore used as a viable alternative to the using standard vector diffraction theory. The vector Bessel diffracted fields were calculated. One finds that the Fraunhoffer diffraction patterns produced are intimately tied to how the modes were excited at the waveguide entrance for very short waveguides. In other words, if the modes were excited by an externally directed plane wave at 0 μradian angle of incidence then the diffraction patters produced at the waveguide exit were peaked in the forward direction at the same angle. Further, if one used, say an incident plane wave directed at 20 μradians, the peak of the diffraction pattern would be in the forward direction and peaked at 20 μradians. Further as the number of $LP_{0,p}$ modes increased the diffraction seen had a larger angular spread. This was attributed to the mixing of the higher order modes with the low order modes that were excited by the externally directed plane wave.

To ensure that the method was accurate, standard vector diffraction theory and the ART were both used to test a special case, namely that of a plane wave incident on a circular aperture. The results using both standard vector diffraction theory and the ART were identical. Here, one has new approach to calculating the vector diffraction fields.
Chapter 6 investigated the effects of rough surfaces on the transmission of the x rays down the cylindrical glass capillaries. One resorted to an approximation, motivated by the observation that the effect of x-ray intensity loss into the specularly reflected beam is described by an effective absorption of the x-ray by the waveguide. In other words, surface roughness can be modeled as an effective addition to the imaginary part of the susceptibility It seems reasonable that the Rayleigh reflectivity is an adequate approach for long lateral correlation lengths in these pulled fibers. Further one finds that as the mean surface height distribution of the surface increases the x-ray intensity decreases and this decrease can be modeled as a correction to the imaginary part of the x-ray susceptibility. This correction was added to the previously determined effect of photoelectric absorption and the two effects contribute to the loss of x-ray intensity as the x-ray propagates in the waveguide. It can also be concluded that for small angles of incidence, $\theta \ll \theta_c$, surface roughness does not seem to have much of an effect on the propagation of the x-ray. The assumption that the rough surface contributes to an affective absorption seems to be valid. In both instances one can conclude that whether the x-ray is scattered (reflected) by the rough surface and the specular reflectance calculated (as shown by Kimball and Bittel) or lost (scattered) and simply treated as another instance of loss due to absorption, one arrives at the same result.

Future Directions

From chapter 4 orbital angular momentum of the *LP* modes was investigated. Orbital angular momentum being displayed by optical beams have been know for about a decade there has been recent interest in these light beams. Galvez et al [Galvez] have recently been working on optical beams possessing orbital angular momentum as possible systems for N-bit quantum computing. Still others, in particular astronomers [Musser], are interested in this property of light. Natural astrophysical processes such as lenslike density variations in interstellar gas or perhaps the warped space-time around rotating black holes may twist light producing a beam of light with orbital angular momentum. These capillary fibers offer the possibility of being able to generate similarly interesting light beams in the x-ray part of the spectrum.
As seen in Chapter 5 there is a distinct possibility for the existence of a diffractionless Bessel Beam. Non-diffacting beams, introduced by Durnin in 1987, have seen considerable study in past years [Durnin], [Bouchal]. Using the ART one can now focus not on Fraunhoffer diffraction but on Fresnel diffraction. If one can generate, by choosing the entrance, propagation and exit conditions appropriately, namely exciting a $LP_{0,1}$ mode by a plane wave incident at 0 μradians on a short waveguide, a non-diffracting single mode Bessel Beam may be produced. This may have very important technological and theoretical implications. For example, one may be interested in how far this single mode Bessel Beam will propagate in free space before it begins to diverge and spread, the Fresnel diffraction limit. This is a highly non trivial process. In order to attempt a solution to this problem, one will have to study vector Fresnel diffraction. Here the current use of standard vector diffraction theory would prove to difficult to apply and therefore a solution would be hard to generate. The ART may provide a solution to this problem with minimal approximations and calculations.
Next, one could observe that the geometry of the fibers used in this thesis were strictly cylindrical and very close to ideal. Other waveguiding structures are possible such as waveguides with hexagonal cross-sections.

An investigation of how edges and non-cylindrical structures will effect the reflection of the x-rays and ultimately their propagation down the longitudinal axis of the waveguide. This would be an interesting question that this thesis has set the stage to answer.
From here, one could envision other interesting scenarios. Effects such as waveguide curvature (both purposeful and accidental) and waveguide tapering (thinning of the waveguide in the direction of x-ray propagation) have on the x-ray as it propagates down the waveguide. Purposeful sources of bending and tapering the waveguide include the study of focusing many capillaries to one spot.
It is possible to excite the *LP* modes in the waveguide with something other than a plane wave. Since the *LP* modes were constructed by a superposition of circularly polarized modes, one could try to excite modes with a circularly polarized wave at the waveguide opening. Thus one could attempt to preferentially excite say, the left circularly polarized modes rather than the right circularly polarized modes. Instead of a straight capillary waveguide what would happen if one were to twist the fiber around its longitudinal axis?
\bibliographystyle{AMS} %\bibliography{bibfile_name}

- B.E.A. Saleh, M.C. Teich, Fundamentals of Photonics, 274 (1991)
- Lord Rayleigh, Phil. Mag. S. 5 Vol. 43 (261) 125 (1897)
-
- D. Hadros and P. Debye, Ann. Phys. Vol. 32, 465 (1910).
- G.C. Southworth, Bell Systems Technical Journal, Vol. 15, 284 (1936).
- J.R. Carson, S.P. Mead, and S.A. Schelkunoff, Bell Systems Technical Journal, Vol. 15, 310 (1936)
- C. H. Chandler, J. Appl. Phys. Vol. 20, 1188 (1949)
- N.S. Kapany and J.J. Burke "Optical Waveguides" 2 (1972)
- D. Gloge, "Weakly Guiding Fibers," Applied Optics Vol. 10, 2252-2258 (1971)
- D. Marcuse, *Theory of Dielectric Optical Waveguides* , (Second Edition, Academic Press, Boston 1991)
- M.A. Kumakhov, Nucl. Instrum. Methods B, Vol. 48, 283 (1990)
- Lei Wang, B.K. Rath, W.M. Gibson, J.C. Kimball, and C.A. MacDonald, J. Appl. Phys., Vol. 80 (7) 3628 (1996)
- J.C. Kimball and D. Bittel, J. Appl. Phys., Vol. 74 887 (1993)
- A.V. Vinogradov, N.N. Zorev, I.V. Kozhevnikov, and I.G. Yakushkin, Sov. Phys. JETP, Vol. 62 (6), 1225 (1985)
- Liu, C. and Golovchenko, J., "Surface Trapped X Rays: Whispering-Galley Modes at $\lambda = 0.7\mathring{A}$," Phys. Rev. Letters Vol 79 (5) 788 (1997)
- Liu, C. and Golovchenko, J., "Deflection and diffraction of x rays bound to curved surfaces," Optics Letters, Vol 24 (9) 587 (1999)
- Y.P. Feng, S.K. Sinha, H.W. Deckman, J.B. Hastings, and D.P. Siddons, Phys. Rev. Letters Vol. 71 (4), 537 (1993)
- Y.P. Feng, H.W. Deckman, and S.K. Sinha, Appl. Phys. Letters Vol. 64 (7), 930 (1994)
- Y.P. Feng, S.K. Sinha, E.E. Fullerton, G. Grubel, D. Abernathy, D.P. Siddons, and J.B. Hastings, Appl. Phys. Letters Vol. 67 (24) 3647 (1995)
- Zheludeva, S.I., Kovalchuk, M.V., Novikova, N.N., Sosphenov, A.N., Malysheva, N.E., Salashenko, N. N., Akhsakhalyan, A.D., and Platonov, Y.Y., J. Phys. III France Vol. 4, 1581 (1994)
- Lagomarsino, S., Jark, W., Di Fonzo, S., Cedola, A, Mueller, B., Engstrom, P., and Riekel, C., J. Appl. Phys. Vol 79 (8), 4471 (1996)
- Jark, W., Di Fonzo, S., Lagomarsino, S., Cedola, A., di Fabrizio, E., Bram, A., and Riekel, C., J. Appl. Phys. Vol 80 (9), 4831 (1996)

- Lord Rayleigh, *The Theory of Sound*, American Ed. (Dover, New York, 1945)
- Braud, J.P., and Hagelstein, P.L., "Whispering-Galley Laser Resonators-Part I: Diffractio nof whispering-Galley Modes," IEEE Journal of Quantum Electronics Vol. 27 (4) 1069 (1991)
- Braud, J.P., and Hagelstein, P.L., "Whispering-Galley Laser Resonators-Part II: Analysis of Mirrors with Nonuniform Curvature," IEEE Journal of Quantum Electronics Vol. 28 (1) 254 (1992)
- Vinogradov, A.V., Kovalev, V.F., Kozhevnikov, I.V., and Pustovalov, V.V., "Diffraction theory for grazing modes in concave mirrors and resonators at x-ray wavelengths: II," Sov. Phys. - Tech. Phys. Vol 30 (3) 335 (1985)
- Barcomb, F, "Waveguides for X Rays and Neutrons: A Scalar Model," Ph.D. Thesis, University at Albany (1999)
- J.D. Jackson, *Classical Electrodynamics* (Second Edition, J. Wiley & Sons, New York,1975)
- Born, M. and Wold, E. *Principles of Optics*, 6^{th} corr. edition, Pergamon Press, New York (1989)
- A. Caticha, "Asymptotic form of the reciprocity theorem with applications in x-ray scattering" Phys. Rev. B, Vol. 62(6), 3639 (2000)
- Arfken, G. and Weber, H.J., *Mathematical Methods for Physicists*, 4^{th} edition, Academic Press, New York (1995)
- E. Snitzer, J. Opt. Soc. Am. Vol. 51, (5) 491 (1961)
- M. Abramowitz and I.A. Stegun, *Handbook of Mathematical Functions*, (National Bureau of Standards, 1972)
- Caticha, A., Gordon Conference presentation (unpublished)
- Nevot, L. and Croce, P., Rev. Phys. Appl., Vol. 15, 761 (1980)
- Bass, F.G., and Fuks, I.M. *Wave Scattering from Statistically Rough Surfaces*, Pergamon Press, NY (1979)
- Bennett, J.M., Mattsson, L., *Introduction to Surface Roughness and Scattering*, Opt. Soc. Am. (1989)
- Galvez, E.J., Crawford, P.R., Sztul, H.I., Pysher, M.J., Haglin, P.J., and Williams, R.E., "*Geometric Phase Associated with Mode Transformations of Optical Beams Bearing Orbital Angular Momentum*," Phys. Rev. Lett. Vol 90 (20) 203901 (2003)
- Musser, G., "*All Screwed Up*," Scientific American, November 2003, 22 (2003)
- Durnin, J., Journal of the Opt. Soc. of America, A4, 651, (1987)
- Bouchal, Z., J. Mod. Opt. Vol. 40, 1325 (1993)

This document created by Scientific WorkPlace 4.1.

Dr. Scott LaBrake

Digitally signed by Dr. Scott LaBrake
DN: CN = Dr. Scott LaBrake, C = US
Reason: I am the author of this document
Date: 2004.09.09 09:51:34 -04'00'